Analysis and modelling of immune cell behaviour in lymph nodes based on multi-photon imaging

Dan Erben

BSc MSc MRes

Submitted in fulfilment of the requirements for
the degree of PhD

Institute of Biodiversity, Animal Health
and Comparative Medicine

College of Medicine, Veterinary and Life Sciences

University of Glasgow

March 2016

0.1 Abstract

This thesis presents quantitative studies of T cell and dendritic cell (DC) behaviour in mouse lymph nodes (LNs) in the naive state and following immunisation. These processes are of importance and interest in basic immunology, and better understanding could improve both diagnostic capacity and therapeutic manipulations, potentially helping in producing more effective vaccines or developing treatments for autoimmune diseases. The problem is also interesting conceptually as it is relevant to other fields where 3D movement of objects is tracked with a discrete scanning interval. A general immunology introduction is presented in chapter 1. In chapter 2, I apply quantitative methods to multi-photon imaging data to measure how T cells and DCs are spatially arranged in LNs. This has been previously studied to describe differences between the naive and immunised state and as an indicator of the magnitude of the immune response in LNs, but previous analyses have been generally descriptive. The quantitative analysis shows that some of the previous conclusions may have been premature. In chapter 3, I use Bayesian state-space models to test some hypotheses about the mode of T cell search for DCs. A two-state mode of movement where T cells can be classified as either interacting to a DC or freely migrating is supported over a model where T cells would home in on DCs at distance through for example the action of chemokines. In chapter 4, I study whether T cell migration is linked to the geometric structure of the fibroblast reticular network (FRC). I find support for the hypothesis that the movement is constrained to the fibroblast reticular cell (FRC) network over an alternative 'random walk with persistence time' model where cells would move randomly, with a short-term persistence driven by a hypothetical T cell intrinsic 'clock'. I also present unexpected results on the FRC network geometry. Finally, a quantitative method is presented for addressing some measurement biases inherent to multi-photon imaging. In all three chapters, novel findings are made, and the methods developed have the potential for further use to address important problems in the field. In chapter 5, I present a summary and synthesis of results from chapters 3-4 and a more speculative discussion of these results and potential future directions.

Contents

0.2 Acknowledgements

My foremost thanks goes to my supervisor Professor Dan Haydon for his guidance, support and patience. Dan has always been positive and encouraging, even in times when I was full of doubt and when I was perhaps making things harder than necessary. I feel very lucky to have had Dan as a supervisor and to have had the chance to learn from his unique approach to problem solving.

I also wish to thank my other supervisors, Professors Paul Garside and Jim Brewer, who supervised the immunological side of my project and provided the support, lab space and resources needed to collect the data. I am also grateful to Doctors Bob Benson and Agi Patakas for helping me through the lab-based part of my work, for sharing some of their data, and for their friendly attitude.

I am grateful to Professor Andrew Yates for hosting my visit at the Albert Einstein College of Medicine, and to him and his then postdoc Dr Ulrich Kadolsky for a very warm welcome to New York. My PhD experience was also enriched by some enlightening and fun discussions with Andrew both during my visit to New York and later when he moved to the University of Glasgow.

I also wish to thank Dr Paul Johnson for some useful suggestions on spatial analysis.

My PhD was funded by a generous Wellcome Trust studentship, which made it possible for me to make the most of this very special time at the University of Glasgow and in Scotland generally. I am very grateful for this support.

Working in an office with some great people to share ideas, inevitable frustrations and occasional excitements (and cake) with, made the whole experience much more positive and enjoyable. The Graham Kerr Building was a great environment to work in, thanks to all the staff and students who helped to make it such a special place.

My partner Pavla, the most important person in my life, has always been there to love and support me, even through times that were difficult for both of us.

I am where I am thanks to the many people who influenced and supported me – in the last 4 years and throughout my whole life – my family, friends, teachers, supervisors and colleagues.

My late father Jan always supported my interest in the wonderful world of science, and taught me so much. I dedicate this thesis to his memory.

0.3 Author's declaration

I declare that this thesis and the research it represents are my own work, carried out under the supervision of Professors Dan Haydon, Paul Garside, Jim Brewer and with the advice from Professor Andrew Yates on some aspects of chapter 4. None of this work has been submitted for another degree or professional qualification. Where I have discussed or cited the work of others, this is always attributed and the source is given.

Dan Erben

Chapter 1

Introduction

1.1 Basic immunology introduction

This section provides a very general necessary immunological background. More specific questions and technical points will be discussed in the individual results chapters.

The immune system consists of numerous types of cells performing specific functions, cooperating to mount the immune response to a range of potentially harmful substances, while avoiding reaction to the organism's own building blocks and incoming nutrients. Their action has to be well orchestrated, which is accomplished by a number of direct or indirect interactions [1, 2, 3]. When pathogens enter the body, or when tumour cells form, some of their components (antigens) picked up and processed by dendritic cells (DCs), carried into lymph nodes (LNs), and displayed on the surface of the DCs [4]. Then these antigens have to be located and recognised by naive T cells which carry corresponding antigen-specific receptors in a process called antigen-presentation [1]. The T cell receptors are generated through a pseudo-random process, resulting in a very heterogeneous T cell population where only a very few cells in the whole organism are specific to one given antigen – therefore, the effective antigen search and antigen presentation in the LNs are critical steps in the establishment of a successful immune response [1, 5]. This activation of naive T cells in support of a defensive response is called priming, and results in T cell proliferation, exit of lymph nodes, and further participation in the immune response towards the pathogen. In vertebrates, previous exposure to antigen increases the rapidity and magnitude of response to a subsequent exposure, in the so-called adaptive immune response. T cells are essential for this as upon primary antigen-presentation, they become more efficient with repeated exposure at recognising and destroying specific pathogens, infected cells or tumour cells. T cells also orchestrate other cells participating in the secondary response. At the same time, tolerance towards the body's own antigenic components and harmless antigens in food must be maintained. The same processes which initiate the immune response to pathogens participate in the development of autoimmune diseases, where the immune system wrongly reacts to the body's own antigens (breach of tolerance).

Fig. 1.1 shows a simplified diagram of the steps leading to the initiation of the adaptive immune response. Although a number of other cell types participate in the immune response, the initial contacts between naive T cells and dendritic cells are one of the most important determinants of programming the subsequent T cell response towards priming or tolerance [6, 7]. Consequently, there is a continued interest in studying the mechanisms underlying the initiation of immune responses [8, 9]. Understanding the spatio-temporal details of T cell search for and interaction with DCs in LNs – such as the mode of T cell search and the duration and frequency of T cell-DC contacts – will help to infer the underlying cellular and molecular mechanisms, which unlocks the potential for developing more effective ways of therapeutic targeting of the components of this system for clinical benefit. Better quantitative understanding could, for example, allow a better estimation of the optimum dose of antigen to trigger the appropriate immune response, aiding in vaccine design.

The internal structure of the LN is highly relevant to the process, as immune cell movement and interacions do not take place in a homogeneous space. The LN contains complex structures composed of different types of stromal cells, forming distinct morphological and functional compartments, which preferentially attract different types of immune cells [10, 12]. A diagram of the simplified structure of LN, based on [10] and adapted from [11], is presented in Fig. 1.2. The lymph node is an organ consisting mainly of a fibrous structure (called reticular network) composed of stromal cells and extracellular product. Lymphocytes move on the surface of this structure and in the gaps between it, and also through a dense network of lymphatic vessels. The organ is enclosed by a capsule composed of dense connective tissue and muscle fibres. Lymph flows from somatic tissue into the node through afferent lymphatic vessels. These feed into a space below the cortex (the subcapsular sinus) and from there into the cortical sinuses, deeper inside the lymph node in an area called cortex. Eventually, lymph is collected in an area called the medulla and flows out of the LN through the efferent lymphatic vessel. The cortex, i.e. the deeper area of the LN between the subcapsular sinus and the medulla, contains a large number of lymphocytes and is where most of the interactions studied in this thesis take place. Different types of reticular network are present in the

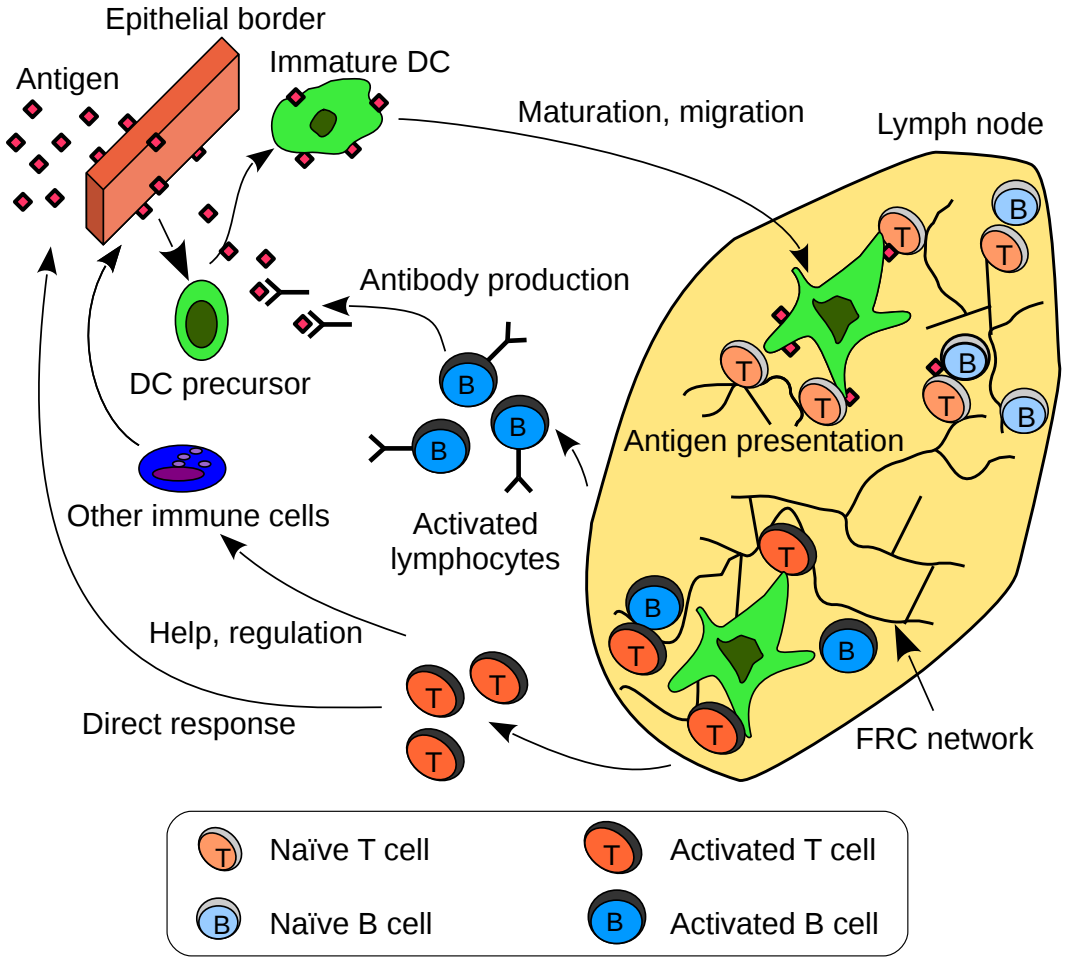

Figure 1.1: A diagram showing the sequence of steps in the initiation of the adaptive immune response in vertebrates; from antigen entry to the activation of T cells, B cells and the following immune response.

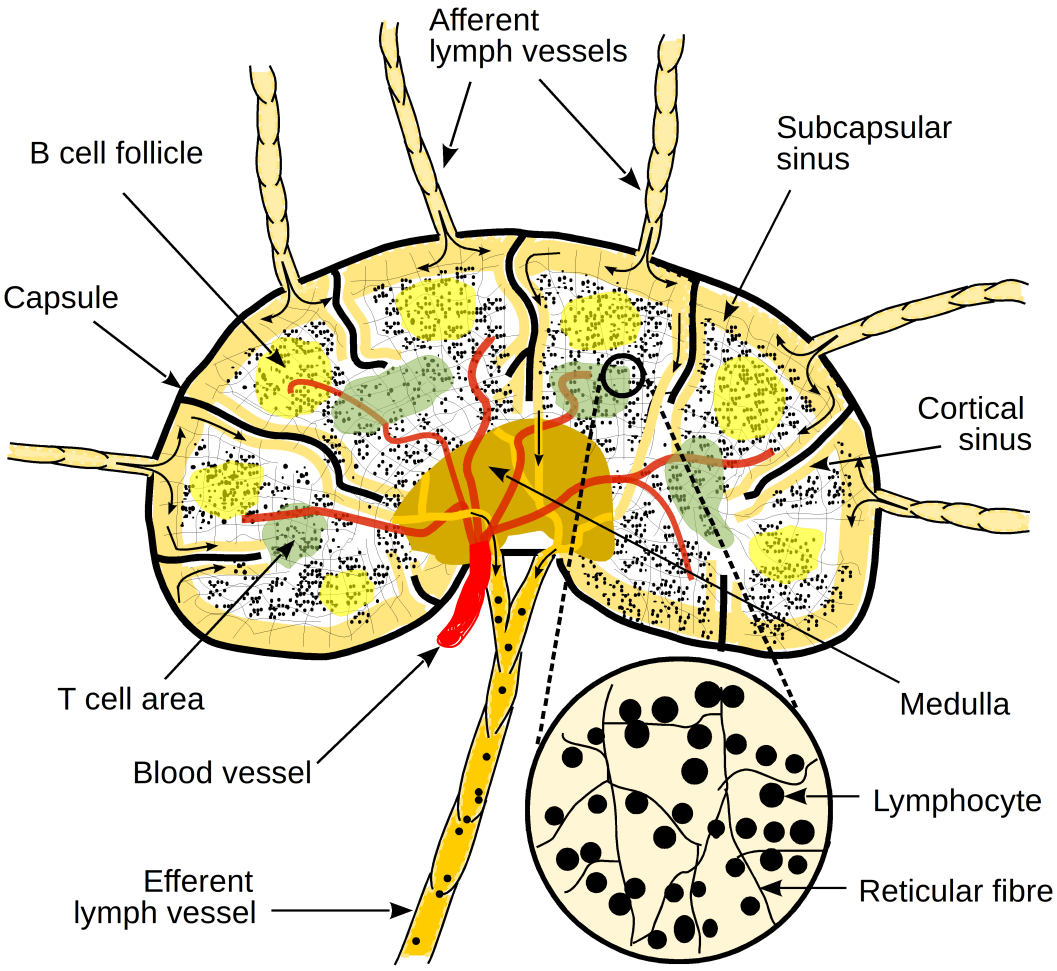

Figure 1.2: A diagram of the simplified structure of LN, showing the flow of the lymph through the organ, and the different morphological and functional zones including B cell follicles and T cell areas. Based on [10], adapted from [11].

cortex, forming areas containing preferentially B cells (follicles) or T cells (T cell areas).

1.2 Multi-photon imaging

The latest and most promising method to obtain insight into immune cell migration and interactions *in vivo* is multi-photon microscopy, which can be used to generate 3D videos with high frequency and in great depth *in vivo* [1, 13]. Previously, data on antigen presentation have mainly come from *in vitro* studies or indirect examinations of the consequences of antigen presentation *in vivo*. Multi-photon microscopy has enabled the direct observation of the spatio-temporal details of the early steps of antigen-presentation in a live tissue *ex vivo* and recently even *in vivo*. Multi-photon microscopy uses two infra-red laser photons to excite a fluorophore molecule, rather than one photon of visible/UV light as in conventional fluorescent or confocal microscopy. This helps to overcome several issues. The higher wavelength (lower energy) excitation radiation used is less absorbed and scattered by the tissue covering and surrounding the volume of interest. As the fluorophore is excited when it simultaneously absorbs two low-energy photons, this allows a selective excitation of fluorescence in a specific focal point where the photons coincide. This results in lower phototoxicity, less photobleaching, and less autofluorescence, so that tissue damage and the intensity of out-of-focus emission are minimised, allowing imaging deeper in the tissue (on average approximately 300 μm as opposed to 80 μm for confocal microscopy) [14, 13]. Although confocal microscopy can be and has been used to track lymphocytes in intact LN [15], the increased depth of imaging is a very useful feature of multi-photon microscopy, because of the size and non-homogeneous morphological structure of the organ [5]. Indeed, the movement behaviour of cells seems to vary with depth within the LN; a 2-photon study revealed rapid migration in regions of depth above 100 μm below the surface of LN in contrast to a markedly slower migration in the superficial areas [16]. The first paper describing the use of 2-photon microscopy to examine lymphocyte movement *in vivo* [17] in explanted lymph nodes, presented a simple analysis of speeds and directionality of naive T and B cell migration and cell

clustering upon antigen exposure, and has demonstrated the extraordinary suitability of the method for immunological studies.

1.3 Project motivation

While a number of experimental studies have been performed in the field in the last 15 years, enabled by the rapid development of imaging techniques, many fundamental questions and controversies remain. The current understanding of the cellular migration and interactions underlying the initiation of immune responses in LN is limited and patchy, and most of the current models focus only on certain arbitrary aspects of the process, generally with the main aim of closely reproducing the data rather than inferring the underlying mechanisms. Due to the relative novelty of this detailed spatio-temporal imaging data, these models also make a number of assumptions and use a variety of methodical approaches, so there is no consistent framework to build upon and little basis for making comparisons. Most of the studies have a pilot character at this stage, the analyses have often not been carried out quantitatively and statistically with large enough datasets, and the methods used are often not well suited to the particular problems, which leads to ambiguous or controversial conclusions – this will be discussed and referenced in relevant detail in each following data chapter. Despite our ability to visualise the cellular behaviour *in vivo*, our understanding of the system is still very limited. More quantitative and rigorous approaches are needed to better analyse larger datasets and generate predictive quantitative models and testable hypotheses to motivate novel experiments. In this thesis, I hope to contribute to some of the first steps in this transition. The main aim of the thesis is to develop and apply quantitative methods, novel in this field, for analysing these data more formally.

I used multi-photon microscopy to take nearly real-time, three-dimensional videos of T cells and DCs in explanted mouse lymph nodes (LN). This technology is relatively new and is only beginning to be made full use of, requiring novel approaches to data processing and analysis. I address these immunological problems by employing quantitative methods novel to the field. Many of these are used primarily in ecology, as there are many parallels between immunology

and ecology at this level and many methods suitable to this type of problem have been developed in ecology. T cells are one of the many times of cell types participating in the immune response; they have a limited life-span and in order to extend this and proliferate, they need to find DCs carrying appropriate antigen in the complex environment of the lymph node. An interesting feature of this environment is a network of fibroblastic reticular cells (FRC), which seems to influence the movement of T cells and positioning of DCs. An ecological analogy would be the movement of different species of animals through a landscape in search for food, their interactions, and the resulting community-level ecology.

The methods developed and findings made here represent an important step in improving our understanding of immune cell migration and interactions, fundamental biological processes underlying antigen presentation. This process is a critical step in eliciting the adaptive immune responses associated with protection against pathogens and pathology in autoimmune diseases. There is a continued interest in studying this system with the potential for developing more effective ways of therapeutically modifying it for clinical benefit. Specifically, the models presented here are intended to constitute a platform on which to build in order to infer the underlying mechanisms, and to make more realistic estimations of parameters such as T cell speed, their turning angles and the resulting antigen search efficiency, which is of importance in both basic and medical immunology. The methods and models developed provide a means for making future studies more rigorous, reproducible and mutually comparable.

Chapter 2

Spatial clustering and overdispersion of T cells and dendritic cells in lymph nodes

The cell imaging data for this chapter has been generated by me, Dr Robert Benson and Dr Agapitos Patakas. The analysis is entirely my own work.

2.1 Abstract

This chapter presents a quantitative study of T cell and DC spatial arrangement in lymph nodes (LN). Changes in the spatial patterns of these cells presumably occur due to cellular interactions, i.e. repulsive (over-dispersion) or attractive (clustering) action mediated possibly by chemokines, DC dendrites, or by changes in the arrangement of the LN physical environment. Clustering of T cells has been reported previously as one of the features of antigen presentation in both tolerogenic and priming conditions. This has been assumed to be caused by the aggregation of T cells around antigen-bearing dendritic cells and the degree of this clustering conjectured to be proportional to the strength of T cell response being elicited, although neither have been shown rigorously. The necessary analyses have not been carried out quantitatively and statistically with large enough datasets, and different methods have been used in different studies, which are often purely descriptive, and with varying results. The spatial patterns of dendritic cells (DCs) were not investigated, although these too might potentially vary with immunological state. Another unknown characteristic is the spatial scale at which these departures from spatial randomness (clustering or over-dispersion) occur. This scale is potentially very important as it should reflect the spatial scale of the underlying cellular interactions or other processes.

Here, I quantitatively analyse the spatial arrangement of T cells and DCs in lymph nodes (LN), based on a large dataset of 2-photon microscopic images of both cell types in naive and primed (immunised) state. Specifically, I analyse the spatial clustering and over-dispersion of these cells in these two states. I employ several different spatial statistical approaches to measure clustering or over-dispersion of cells; to explore the degree of spatial clustering or over-dispersion over a range of spatial scales and to make quantitative and statistical comparisons between naive and immunised states.

Using pair correlation function as an exploratory graphical method to visualise the clustering or over-dispersion of cells over a range of spatial scales, both types of cells in both treatments are found to be clustered in some cases over a certain spatial range. This is variable, but for data where significant clustering occurs, this is generally between 20 and 50 μm. Most importantly,

further statistical analysis does not support the hypothesis that T cells cluster more during priming compared to the naive state. T cells are significantly clustered, while DCs seem to assume random spatial patterns, but no significant difference can be detected between naive and primed cells.

This chapter also highlights that there are two possible 'nuisance' variables which can bias the results; the cell diameter and cell spatial density, and I account for these in the analyses and develop a method which is not sensitive to cell spatial density.

Apart from this particular application, the quantitative methods employed here can be used to analyse cell spatial patterns generally to provide rigorous and reproducible measurements of cell clustering and over-dispersion.

2.2 Introduction

T cell search for and recognition of antigen-presenting dendritic cells (DCs) bearing cognate peptide/MHC molecules in LNs are crucial steps in eliciting the adaptive immune responses associated with protection against pathogens and pathology in autoimmune diseases. Confocal microscopy, and more recently multi-photon laser-scanning microscopy (MPLSM), have been providing valuable insights into immune cell behaviour within intact tissues [18, 15, 17]. A number MPLSM imaging studies have been carried out since, e.g. [19, 20, 21, 16, 5, 22, 7, 23, 24, 25]. A study [24] using two-photon microscopy *in vivo* has shown – by manipulating the T cell-DC interaction – that the duration of contacts between T cells and DCs was linked to the activation of the T cells; at least 6 hours of T cell-DC interaction was required for naive T cells to undergo clonal expansion and efficient activation *in vivo*. This has indicated the importance of understanding these interactions for potential applications in therapeutic interventions at this level. There is a continued theoretical interest in the mechanisms underlying these processes and their optimisation [8, 9]; and continuing experimental efforts in studying these processes in the medical context of both infection and autoimmune diseases, for example in mouse models of malaria infection and arthritis [26, 27].

Here, I specifically focus on the static spatial patterns of DCs and T cells in lymph nodes in naive state and during immunisation. Changes in cell spatial patterns presumably occur due to cellular interactions, i.e. repulsive (over-dispersion) or attractive (clustering) action mediated possibly by chemokines or DC dendrites, or by changes in the arrangement of the LN physical environment. Spatial clustering of T cells has been suggested previously as one of the features of antigen presentation in both tolerogenic and priming conditions, e.g. in [18, 22, 23]. Presumably, this clustering is caused by the aggregation of T cells around antigen-bearing dendritic cells and the degree of this clustering is proportional to the strength of T cell response being elicited, although neither conjecture has been proven quantitatively and statistically. As I discuss below, there is a lack of rigorous quantitative analyses of cell clustering, and different methods were used in different studies, mostly purely qualitatively descriptive,

with varying results.

In [18], fixed LN sections were imaged. This study utilised an adoptive transfer system in which T cells specific for a given antigen and DCs pulsed *in vitro* with this antigen, are transferred to recipient mice, and subsequently observed in explanted LN. The results provided an indication that T cells cluster around DCs in priming, however, no quantitative and statistical analyses were performed. In a similar study [15], no difference in clustering between naive state and priming was reported or visually obvious in the images presented. The first paper describing the use of 2-photon microscopy to examine lymphocyte movement *in vivo* [17] in explanted lymph nodes, presented an analysis of speeds and directionality of naive T and B cell migration and cell clustering upon antigen exposure. The study reports 'swarms' and 'clusters' of T cells during priming, however, this is purely descriptive (a simple verbal description of the imaging data). Similarly, [22] also describe clusters and dynamic swarms in a purely descriptive manner. In contrast, in a study employing *in vivo* immunisation [7] the authors report the following: "We rarely noted formation of discrete T cell–DC clusters, but this was expected, as large numbers of DEC-205^+ DCs in the lymph node present antigen after targeting with α-DEC–OVA and the number of T cells in each cluster is inversely proportional to the number of antigen-presenting DCs." This indicates that the method utilised for immunisation may be critical to whether clustering is observed or not, which I will discuss below. Another study using 2-photon microscopy [23] demonstrated different behaviour of antigen-specific T cells during the induction of priming and tolerance *in vivo*. In both tolerance and priming, T cells changed their motility behaviour upon injection of antigen, and increased cell clustering was reported in both cases compared to naive state. This study represents the first quantitative assessment of clustering, measuring the proportion of T cells in clusters and the mean number of cells per cluster, although there are some quantitative concerns with using these metrics. For example, these metrics are dependent on both the T cell and DC density, and the chosen definition of what constitutes a cluster makes reproducibility difficult. The authors also performed simple simulations of cell patterns under the null hypothesis (random cell locations) to verify that the clustering in their data is greater than in the

simulation. Importantly, this simulation goes some way to address the problem of T cell density-dependence of the apparent magnitude of clustering, although it does not entirely eliminate this, as I discuss later, nor does it compensate for the density of DCs, which could vary considerably between treatments.

The spatial patterns of dendritic cells (DCs) were not investigated previously, although these too might potentially vary with immunological state. For example, DCs could be over-dispersed upon activation by means of protruding dendrites, to increase the chance of a T cell migrating through a LN to encounter an antigen-bearing DC, thus shortening the time required for the initiation of an adaptive immune response. Another characteristic that has not been analysed is the spatial range at which these departures from spatial randomness (clustering or over-dispersion) occur. This range is potentially important as it should reflect the spatial scale of the underlying cellular interactions or other process, and so can be a useful clue to identifying the underlying mechanisms of T cell and DC behaviour.

In summary, despite our ability to visualise the cellular behaviour *in vivo*, our understanding of the system is still very limited. A number of metrics of cell behaviour have been measured using MPLSM, but these have not resulted in a consistent overarching predictive model of lymphocyte behaviour in LN in different immunological scenarios. In order to improve our understanding of and confidence in the results of these imaging studies, more rigorous quantitative analyses are required to objectively and quantitatively measure clustering or over-dispersion of these cells; to explore the degree of spatial clustering or over-dispersion at different spatial ranges and to make quantitative and statistical comparisons between different immunological states.

I performed statistical analyses of spatial clustering and over-dispersion of cells using pair-correlation function (PCF), counts of cells in contiguous spatial quadrats (using the variance and mean of the counts to assess departure from spatial randomness) and pairwise point distances and a scale- and density-independent statistic calculated from the pairwise distances. I also investigated whether the data are consistent with Taylor's law [28], an empirical law originating in ecology linking the spatial variance and mean of the number of individuals, which defines an index of aggregation characterising this relation-

ship and the given spatial pattern. It was proposed [29] that this relationship results from a density-dependent balance of attraction and repulsion between individuals trying to maximise resource exploitation. Such mechanism could possibly also drive the behaviour of immune cells in LN, serving to optimise the search for antigen.

Using these methods, static images of T cells and DCs in naive and primed (immunised) state in the LN were analysed to quantify the degree, spatial range and statistical significance of clustering or over-dispersion of cells. Beyond this particular application, the quantitative methods employed here can be used to analyse cell spatial patterns in various systems and contexts to provide rigorous and reproducible measurements.

2.3 Methods

2.3.1 General discussion of methods used

Although the term clustering is intuitive, there is no simple definition and a number of different processes that can lead to spatial clustering (or over-dispersion). The meaning in the most general sense is some spatial departure from complete spatial randomness (CSR). CSR is a scenario where points are located randomly (with uniform probability distribution of coordinates) and independently of each other. The departure of any chosen spatial statistic CSR should ideally be in the opposite directions for clustering and over-dispersion.

Statistics derived from the spatial variance of density are an often employed metric to measure this – a general review of the subject can be found in [30]. This review describes the history of the search for a suitable statistic to quantify departure from CSR and the associated problems.

The effect of cell density on cell spatial patterns

One of these problems is the explicit density dependence of these statistics; these statistics depend on density even when other parameters of the underlying process which generates clustering or over-dispersion do not change. It is unsurprising that the sensitivity of detecting clustering/over-dispersion based on spatial variance is density-dependent; if there is a certain interaction distance between points, then at very low densities the effect on the summary statistic will be very small as points will relatively frequently be outside this interaction range. At very high cell densities the effect will be much higher. This is especially true and obvious for over-dispersion, when the underlying process prevents points from being located closer than a certain 'inhibition' distance, and at a very high density they will therefore be forced to form a very regularly spaced pattern.

Cell density varies considerably between the individual datasets, which, apart from the effect of treatment, could partially be due to the spatial heterogeneity of LN. Therefore, I paid close attention to the potential effect of density when using the statistics used below, and also attempted to develop a density-independent

statistic.

The effect of cell diameter on cell spatial patterns

If we were to make statistical tests for individual data sets (images) based on comparison to theoretical expectations or simulation results under null hypothesis, we would need to account for the mean cell diameter in the null hypothesis. As DCs are larger than T cells, they would be expected to create apparently more over-dispersed patterns even under the null hypothesis because there is spatial inhibition over a larger range than for the smaller T cells. To make it impossible for simulated cells to overlap, i.e. for the point-to-point distance to be less than the mean cell diameter, Simple Sequential Inhibition (SSI) process, where points are added consecutively and discarded if they are closer than a certain range to already existing points, would be a more appropriate null hypothesis than CSR. In my analyses, I measured the cell diameters to be able to include this variable as a covariate and thus investigate and account for its effect. There is very little variability in T cell diameter in this kind of imaging data, and based on the data it was assumed to be 8.2 μm. The DC diameter is more variable and known to vary with the degree of cell activation, therefore I measured and recorded it for all the datasets individually (the mean value for all DCs is 18.45 μm).

2.3.2 Animals, tissue and cells

Naive fluorescent T cells were isolated from DsRed mice, and T cell receptor-transgenic cells specific to Ovalbumin $OVA_{323-339}$ were isolated from OT-II DsRed mice on the c57BL/6 background. The mice were 8-16 weeks old. LN and spleens were homogenised using Nitex mesh (Cadish Precision Meshes, London, UK) and resulting suspensions washed and resuspended in RPMI 1640 (Life Technologies, Paisley, UK). $CD4^+$ T cells were purified by magnetic bead-based cell separation, allowing for negative selection by depleting a wide range of non-$CD4^+$ cells. This was accomplished using anti-CD8 (specific for CD8+ cytotoxic T Cells), anti-CD19 (specific for B cells and follicular dendritic cells), anti-CD11b (specific for monocytes, granulocytes, macrophages,

and natural killer cells), and anti-CD16/32 (specific for natural killer cells, neutrophils, granulocytes, dendritic cells, monocytes, macrophages and B cells) selection over MACS columns (Miltenyi Biotec, Gladbach, Germany), following manufacturer instructions for concentrations, reaction times and centrifugation for the 'MACS $CD4^+$ T Cell Isolation Kit II, mouse'. The purity of $CD4^+$ cells was above 98%, verified using flow cytometic analysis, staining in 1 $\mu g/ml$ PE-labelled anti-CD4, clone RM4–5 (BD Biosciences, Oxford, UK). $5{\times}10^6$ $CD4^+$ T cells were adoptively transferred to CD11c-YFP mice intravenously in 200 μl of complete RPMI. The efficiency of transfer was verified by flow cytometric analysis using the background strain C57BL/6. For immunisation (priming), recipient mice were challenged (20 h after T cell transfer in case of the imaging of T cell motility) with 100 μg of OVA (fraction V; Sigma-Aldrich, St. Louis, Missouri, USA) in 50 μl of 50% CFA (25 μl CFA (Sigma-Aldrich) and 25 μl PBS (Life Technologies)) subcutaneously in the footpad. 20 h later, the mice were sacrificed and popliteal LN draining the injection site were excised. When referring to data from naive and immunised (primed) mice, I use the term 'treatment' to refer to these two categories. All mice were maintained at the Central Research Facility and Joint Research Facility of the University of Glasgow under specific pathogen-free conditions. All procedures were in accordance with UK Home Office and local University of Glasgow regulations.

2.3.3 Multi-photon imaging

Imaging was performed essentially as described in [23, 25], using a Zeiss LSM7 MP system (Zeiss, Oberkochen, Germany). Excised LN were bound with veterinary-grade glue Vetbond (3M, St. Paul, Minnesota, USA) onto a plastic coverslip that was adhered with grease to the bottom of the imaging chamber continuously supplied with oxygenated CO_2-independent medium at 36.5 °C. The excitation source was a tunable Ti:sapphire laser system (Chameleon Ultra II; Coherent, Santa Clara, California, USA) combined with an Optical Parametric Oscillator (Coherent). The emission spectrum was separated with a 555 nm dichroic mirror (Chroma Technology, Bellows Falls, Vermont, USA). A 20×/1.0NA water-dipping objective lens (Zeiss) was used.

2.3.4 Data processing

Primary image processing and analysis was preformed using the program Imaris (Bitplane, Zurich, Switzerland). The location (centroid) of cells within each three-dimensional image stack was determined using an object detection algorithm that automatically locates all discrete blocks of contiguous voxels exceeding a given intensity and size. The Cartesian 3D coordinates of T cells and DCs were exported to a csv file. Thus, a 3D point pattern plus a list of object diameters were obtained. Further analysis was performed using the statistical language R (R Development Core Team, http://www.r-project.org).

There is a problem with general non-homogeneity of cell density within the LNs, probably caused by the inhomogeneous environment of the LN which affects T cell and DC localisation. This results in spatial gradients of cell density - especially higher DC and T cell density in the outer layers of paracortex and lower in the deeper areas (medulla) and in B cell follicles. This can give rise to over-dispersion or clustering which are not caused by cellular interactions. To compensate for this and to select relatively homogeneous areas, the images could be cropped manually so that any visually obviously non-homogeneous areas with low or high cell density would be excluded. However, apart from drastically reducing the number of cells included in analysis in potentially important anatomical locations, this approach does not solve the problem as this is a subjective method and so there still might remain finer-scale gradients or non-homogeneities and inversely some interaction-driven patterns might be falsely identified and discarded as non-homogeneities. Also as a subjective method it would have poor reproducibility. Therefore, I consider it better not to censor the data in such a way. More sophisticated and objective quantitative methods for identifying cell density gradients might be employed, but again the distinction between interaction-driven patterns and non-homogeneities caused by other mechanisms could not be made confidently as it is generally impossible to completely distinguish these using only the spatial patterns without any further data on underlying processes and their spatial scales. The only processing I performed was in order to reduce some bias resulting from the existence of completely cell-devoid areas; by defining the x, y and z coordinate boundaries

of the spatial patterns by the coordinates of the most extremely located cells in terms of x, y and z coordinates.

Despite this difficulty, the spatial ranges at which clustering or over-dispersion occur will point to the different causing processes, which have different characteristic spatial scales. For example, if T cells cluster around the antigen-bearing DCs, the distance between cells within a cluster can be expected to be fairly small, not much more than one cell diameter, the size of clusters will be slightly over the DC diameter plus two T cell diameters and the distances between individual clusters will be roughly equal to the distance between neighbouring DCs. On the other hand effects like the cortex-to-medulla cell density gradient or the effect of T cell poor B cell areas will be associated with a larger spatial scale. Therefore, some inferences can be made without the need to treat the data to normalise for the effects which are not of primary interest. Also importantly, as all the data sets are treated equally, differences between naive and primed states will not be biased by this treatment or by those processes which affect cells in both scenarios equally.

2.3.5 Ripley's K

My goal is to quantitatively measure point clustering or over-dispersion and also to examine how this varies with spatial range. Ripley's K [Ripley, 1976] is a spatial statistic for point patterns reflecting the dependency of the spatial density of points on distance from an average point of the pattern. It is therefore proportional to the amount of clustering or over-dispersion between the points. When λ is the average spatial density and $n(r)$ the average number of points within certain radius r from a point of the pattern, Ripley's function $K(r)$ is a function of r defined as:

$$n(r) = \lambda K(r) \tag{2.1}$$

For a pattern of N points occupying area or volume A, λ equals N/A, and $n(r)$ can be calculated by counting the number of points within radius r of each of the points of the pattern and averaging. Thus an estimate of K can be made as:

$$\hat{K} = A/N^2 \sum_{i=1}^{n} \sum_{j=1, i \neq j}^{n} w_i I_r(i,j) \tag{2.2}$$

$I_r(i,j) = 1$ is a function representing the counting of neighbouring points with index j around points with index i which are within distance d_{ij}, therefore $I_r(i,j) = 1$ for $d_{ij} \leq r$ and $I_r(i,j) = 0$ for $d_{ij} > r$. w_i is an edge effect correction factor for point i. Edge effect is caused by the lack of data on points outside the observed area and results in an apparent lower number of neighbouring points within range r for those points lying within distance less than r of the edges of the observed area. To correct for this, I used Ripley's isotropic correction (Ohser, 1983; Ripley, 1988) built into the R package *spatstat*.

$\hat{K}$ can then be compared to complete spatial randomness (CSR), where the points are located randomly and independently of each other - therefore the CSR forms a baseline scenario for point patterns with no interactions between points. For CSR, the number of points $n(r)$ within a certain radius r of any point is proportional only to the average spatial density λ and the area of the circle with radius r (πr^2):

$$K_{CSR} = \pi r^2 \tag{2.3}$$

Values higher than this correspond to clustering and values lower to over-dispersion. The range of r values chosen to evaluate K should reflect the spatial scale of the problem. The statistic is obviously meaningless at ranges below object diameter. Also, no effects can be observed at scales corresponding to the entire size of the area under study, where all points are included in the estimation of $\hat{K}$ and therefore it equals the theoretical K for CSR. This is reflected in the spatial range of the plots presented in the results section.

2.3.6 Pair correlation function

K is a cumulative function as at a given range r it reflects the behaviour of the point pattern within the whole radius r, so it is not suitable for quantifying local behaviour at only one given value of r. To evaluate spatial patterns only at specific values of r, a type of distribution function called the pair correlation

function (PCF) can be calculated from K. The pair correlation function $g(r)$ is the derivative of K with respect to r (the rate of change of K with r), divided by the derivative of K_{CSR} for a completely spatially random pattern with respect to r (which is $d(\pi r^2)/dr = 2\pi r$):

$$g(r) = \frac{dK(r)}{dr}\frac{1}{2\pi r} \tag{2.4}$$

The division by $2\pi r$ serves to normalise the function to CSR so that when the pattern follows CSR, its PCF equals one and is lower or higher than one for over-dispersion or clustering, respectively.

2.3.7 Statistical evaluation of K and PCF: significance envelopes by simulation

Spatstat package for R was used to estimate Ripley's K and PCF as defined above. Because of mathematical complications with the tractability of the statistical distributions of K and PCF, Monte Carlo (MC) randomisation significance tests were carried out to test for departure from an appropriate null hypothesis. To achieve this, I simulated point patterns with random and independent point locations (CSR), using a spatial window equal to the imaged volume and the number of simulated points equal to the total cell number observed. Note that CSR is not an entirely correct null hypothesis as that should also account for the mean cell diameter. Cells are not points and have a non-zero volume, and as they can not physically overlap, there will be some degree of over-dispersion even under the null hypothesis. Therefore, if the significance envelopes were actually used for inference and not just as a visual guide for exploratory analysis, they would underestimate clustering and overestimate over-dispersion of the observed cell spatial patterns.

These MC tests consisted of simulating point patterns under the null hypothesis repeatedly M times and calculating values of K and PCF for different values of r across the range at which these functions were calculated for data. Then, the k-th lowest and k-th largest value at each of the values of r was taken as the critical value for the test, defining the points on the significance

envelope. When the K of PCF function lies outside these envelopes, we can conclude that for the given range, the patterns is clustered or overdispersed with a certain p-value. Thus generated simulation envelopes do not represent confidence intervals of the calculated function, but rather significance bands under the null hypothesis. The significance level α (equal to p-value for rejecting the null hypothesis under which the envelope was generated) for this statistical test at any fixed r is:

$$\alpha = 2k/(M+1) \tag{2.5}$$

It is important to note that for the significance test to be used correctly and provide unbiased values, any evaluation of departure from null hypothesis would require that r is chosen in advance and the significance is only evaluated at this value. When evaluating K or PCF along a range of r and then utilising for analysis points where the function departs from the MC envelope, the above formula for significance does not hold and the true significance for thus derived conclusions would be lower, as this would effectively constitute performing multiple comparisons (at multiple values of r).

While it is possible to assess whether a pattern is significantly clustered or over-dispersed at a given value of r by generating MC significance envelopes, statistical comparison of the functions as a whole is difficult as we would need to find a summary statistic to compare the entire spatial patterns but avoid multiple comparisons (at multiple values of r). Completely describing the whole pattern by such one summary statistic is not possible, as the spatial patterns are fully described by the whole K function or PCF and as I will show in the next section, at least two spatial scales are needed for defining even the simplest clustered patterns.

2.3.8 Interpretation of K and PCF

Here I will examine in more detail how these functions can serve to quantitatively explore the cell patterns over a range of distances. As mentioned above, there is not a single statistic for comparing the whole spatial patterns as at least 2 spatial scales are needed to characterise simple clustered spatial patterns.

These are the size of clusters and the distance between clusters, with more parameters needed to describe more complex patterns with several spatial levels of clustering or over-dispersion. Therefore I will discuss how K and PCF plots reflect these characteristic scales, by examining simulated random, clustered and over-dispersed patterns.

Let us first consider a simple pattern with one level of clustering and its 2 characteristic scales: cluster size and cluster-to-cluster distance (Fig.2.1 left). K function for this pattern (Fig.2.1 centre) will start above baseline ($2\pi r$), start levelling-off (decreasing rate of increase) at just before cluster size and flatten-off around cluster size at which point no more neighbouring points are being counted. It will then cross the $2\pi r$ baseline at 1/2 cluster-to-cluster distance (at which point the point density is the same as if the pattern followed null hypothesis). Eventually, it will converge to the baseline around cluster-to-cluster distance, when the mean increase in cell density with r corresponds to that for a CSR pattern.

The PCF for this pattern (Fig.2.1 right) will start at high values, which is an artefact due to estimating point density near zero r. Just before cluster size, it will drop to 1 (baseline) where the gradient of K is the same as that for a random pattern. Then it will drop to a minimum where K is most flat around 1/2 cluster-to-cluster distance (this will be zero for well-defined and separated clusters, as then no more neighbouring points are being counted). It will then converge to 1 around cluster-to-cluster distance. It may oscillate around 1 with decreasing amplitude (converging to 1) as more clusters are included with growing r.

An over-dispersed pattern (Fig.2.2 left) has only 1 characteristic scale, plus its variation. The lower the variation, the more regular the pattern is. K (Fig.2.2 centre) will be zero until nearest neighbours start to be counted (at the smallest inter-cluster distance) and reach maximum rate of increase around point-to-point distance and converge to the baseline. The PCF (Fig.2.2 right) will start at zero, and start slowly growing where K starts lifting off zero as well. It will cross 1 at where growth of K is the same as for a random pattern, reach maximum around point-to-point distance and then oscillate around and converge to 1.

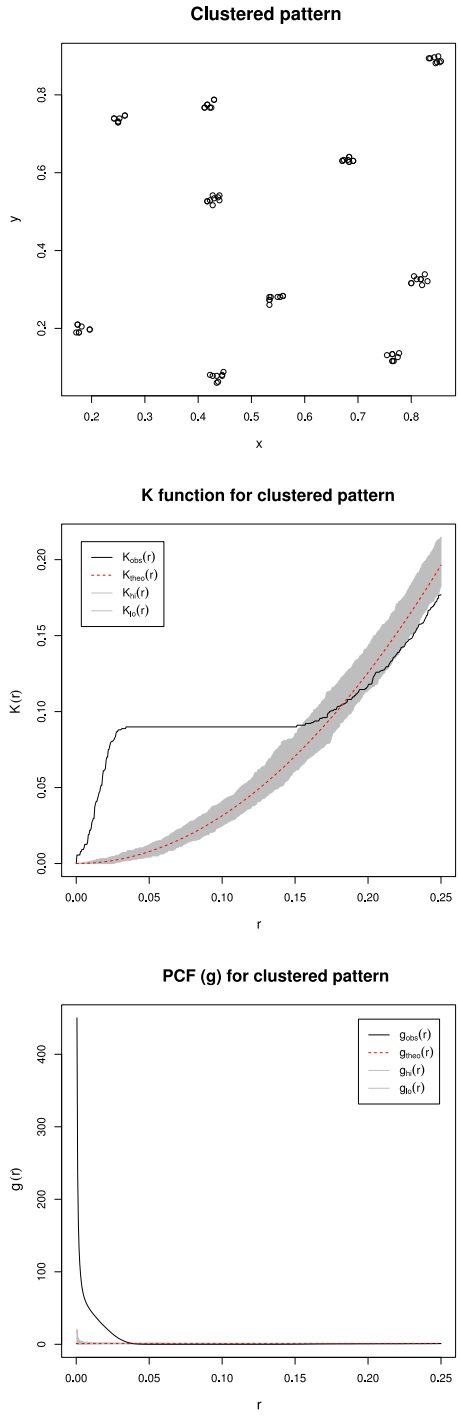

Figure 2.1: A simple clustered pattern with only one spatial level of clustering and its K and PCF functions. The red dotted lines indicate K and PCF under null hypothesis (CSR) and the grey envelopes are 95% confidence intervals around CSR.

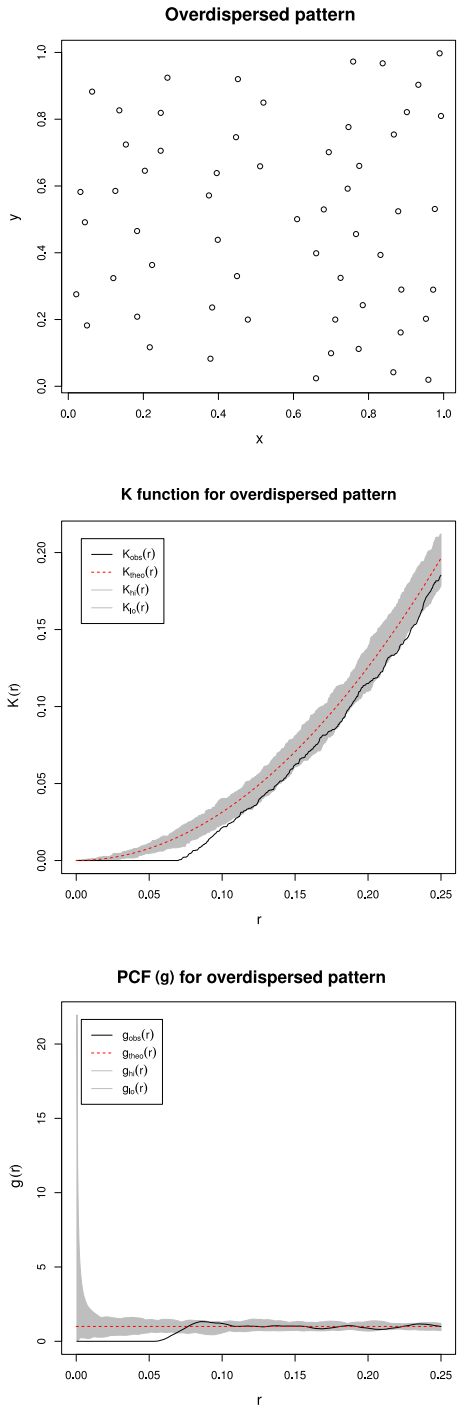

Figure 2.2: An overdispersed pattern and its K and PCF functions. The red dotted lines indicate K and PCF under null hypothesis (CSR) and the grey envelopes are 95% confidence intervals around CSR.

Therefore by performing a graphical exploration of K or PCF it is possible to compare cluster sizes and cluster-to-cluster distances. In the absence of any prior hypothesis on the scales at which clustering or over-dispersion might occur, the functions could simply first be evaluated to identify where large departures from null hypothesis (CSR). Alternatively, Kolmogorov-Smirnov test (test for the significance of the largest difference between two cumulative functions) could be used to test for the largest departure of the data K function from the K function for CSR (K is a cumulative function). Below, I describe the use of other methods to test for the significance of departure from CSR at a certain scale.

2.3.9 Variance and mean of spatial quadrat counts

K and PCF, evaluated at any given range, do not explicitly account for variance in cell density, as they are calculated from the mean counts of neighbours around cells at the given ranges. However, the variance in cell density can also be implicitly used to test for randomness of spatial patterns; with high and low variance characterising clustered and over-dispersed patterns, respectively.

To quantify how cell density varies, I divided the imaged volume into equally-sized contiguous quadrats (cubes or nearly cubical boxes to allow the division of the whole pattern into contiguous spatial subsets) and counted numbers of cells in these. Then, I calculated the variance and mean number of cells in the quadrats. Mean to variance ratio of counts in different quadrats should be equal to one for a CSR (mean equals variance for a Poisson process) independent of quadrat size. This ration will depend on quadrat size for non-Poisson patterns; at any given quadrat size, this ratio will be smaller than one for overdispersed patterns (zero for completely regular patterns) and larger than one for clustered patterns. The spatial resolution of the method is proportional to the size of the quadrats; this method is most sensitive to departure from spatial randomness at the scale corresponding to size of quadrats and its sensitivity decreases the more cluster size differs from the size of quadrats.

2.3.10 Cell distance Q-Q plot off-diagonal summary statistic

I calculated all the pairwise distances between cells, and for each dataset (image), generated a reference point pattern by simulation under the null hypothesis (CSR). The imaging volume was taken as the volume for the simulated reference pattern, so that the range of point pairwise distances would be equal to the range of distances in the given dataset. The number of simulated points was set to be very high (2000) to minimise variation. For these pairs of patterns (observed and generated by simulation under the null hypothesis), Q-Q functions (as in Q-Q plot) for distances were generated as described below.

Quantiles were generated for the distribution of simulated distances at regular probability intervals (let us call these the null probabilities and null quantiles). Then, probabilities were generated for the observed pattern (observed probabilities) corresponding to the same quantiles – i.e. probabilities from the observed distance cumulative distribution function for distances equal to the null quantiles. The Q-Q function then is the relationship between the null probabilities and the observed probabilities, visualising the differences between the two distance distributions. Fig. 2.3 shows pairwise point distance distributions and corresponding Q-Q plots for simulated patterns.

The area between the $x = y$ line (where observed probabilities would equal the simulated probabilities) and the plotted Q-Q function can then be used as a statistic to measure the degree of departure of the observed pattern from CSR. I calculated a simplified statistic linearly proportional to this area: the mean of the absolute value of the difference between the $x = y$ line and the Q-Q function at regular intervals. For simplicity, I will refer to this as the Q-Q distance summary statistic.

The advantage of this statistic is that it is scale- and density-independent. However, there are some disadvantages too, as by testing this method on simulated patterns, I found it to be a poor (low sensitivity) measure, especially for overdispersion, relative to other methods. Also, this method will only indicate if different groups (e.g. primed/naive or T cells/DCs) differ significantly, not if they are significantly different from CSR in a particular direction.

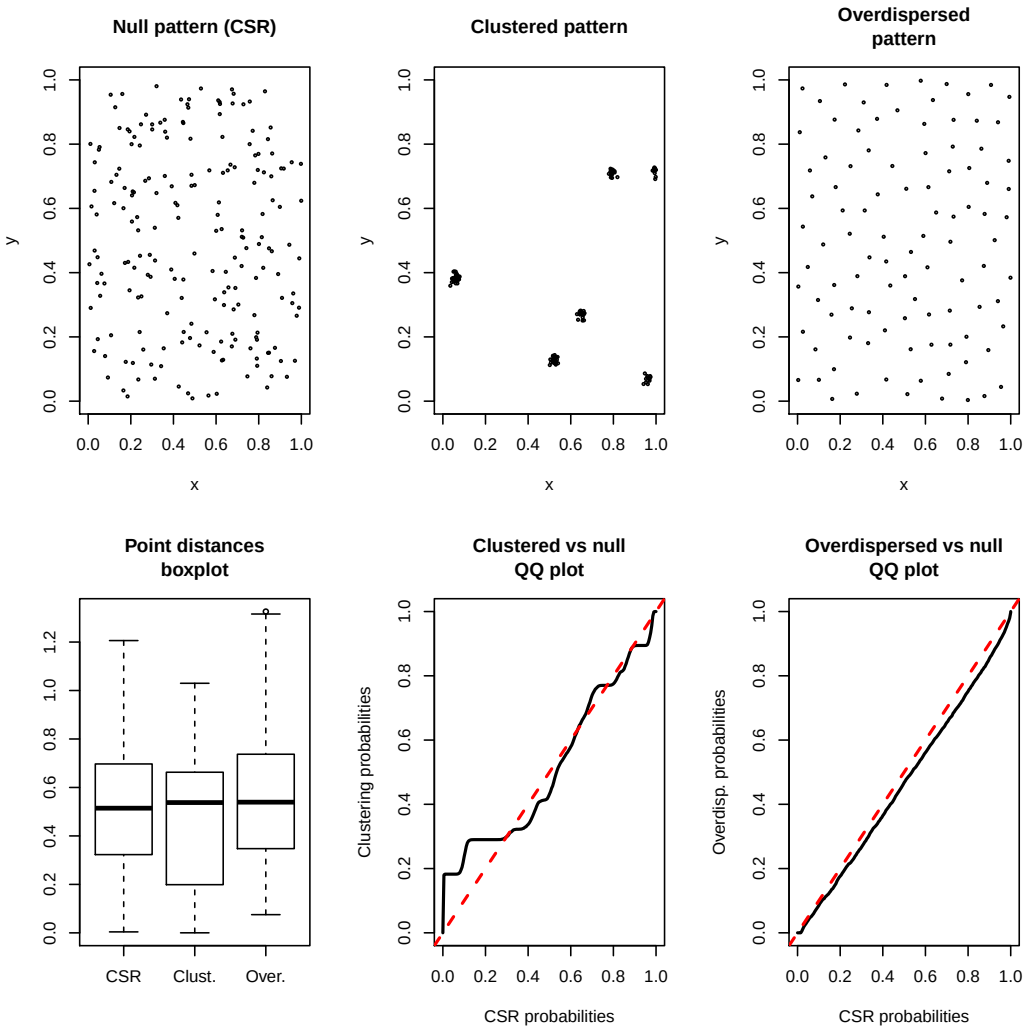

Figure 2.3: Simulated patterns and their pairwise point distances and Q-Q plots.

2.3.11 Statistical models

Linear models were performed using the *glm* package in *R*. The Gaussian family was assumed and the residuals were plotted to visually check that this assumption is valid. Akaike's Information Criterion (AIC) was used to assess model quality for model selection.

2.3.12 Simulations of point patterns

To simulate clustered, random and overdispersed patterns, I utilised the Thomas process, Poisson process and Simple Sequential Inhibition (SSI), respectively.

The Thomas process is composed of two spatial processes. First, cluster centres are determined by a Poisson process. Then, points are added to each cluster, where their displacement from cluster centre along each axis is normally distributed with a pre-determined standard deviation (which determines the degree of clustering).

In the Simple Sequential Inhibition (SSI) process, points are added one by one with coordinates drawn from uniform distribution within the defined volume independently of preceding points. If a new point lies closer than the mean cell diameter from an existing point, it is rejected.

2.4 Results

2.4.1 Description of data

The table presented in Fig. 2.4 summarises all datasets along with accompanying meta-data; the number of cells, cell type, treatment and the x, y and z dimensions of the analysed imaged volumes. Each row corresponds to one MPLSM image, each taken for a lymph node from a different mouse.

2.4.2 Pair correlation function

(Fig. 2.5 – 2.8) presents plots of PCF for the whole dataset. From investigating these functions, there does not seem to be a significant difference between naive and primed state in terms of spatial patterns of T cells or DCs.

Both types of cells in both treatments are clustered over certain spatial scales, which is possibly due to non-homogeneities in the LN environment. This might reflect the confinement of T cells and DCs to the FRC network; if immune cells attach to this network; this might be the cause for the detected cell spatial clustering and the structure of the network would be reflected in the cell spatial patterns. Further investigation of the spatial structure of FRC networks along these lines in both treatments could provide insight into this possibility. Note that the apparent over-dispersion at very small spatial scales is due to the fact that cells have a finite diameter (the PCF is obviously meaningless at ranges below cell diameter).

It is difficult to derive general trends from this analysis, as there is obviously a high degree of variation between datasets. I used these exploratory functions as a starting point for further investigation – as the most marked departures from randomness appear roughly around the spatial scale of 35 μm, I chose this scale for analysis of the cell spatial patterns using other methods. This value might also be a sensible choice for another reason; as this seems to roughly correspond to the geometry of the problem. This range is roughly the average distance of DCs to their immediate neighbours, and as T cells are presumably clustering around DCs, this might correspond to the size of T cell clusters (or at least the distance between them).

Name	No. of cells	Cell type	Treatment	x dimension [µm]	y dimension [µm]	z dimension [µm]
Primed DCs 1	47	DC	P	282	282	40
Primed DCs 2	58	DC	P	282	282	40
Primed DCs 3	72	DC	P	210	413	34
Primed DCs 4	69	DC	P	415	288	34
Primed DCs 5	37	DC	P	173	402	31
Primed DCs 6	38	DC	P	241	271	40
Primed DCs 7	31	DC	P	282	267	40
Primed DCs 8	25	DC	P	282	152	32
Primed DCs 9	34	DC	P	202	219	40
Primed DCs 10	91	DC	P	423	407	40
Primed DCs 11	37	DC	P	139	312	42
Primed DCs 12	47	DC	P	416	306	42
Primed DCs 13	151	DC	P	282	282	42
Primed DCs 14	51	DC	P	282	279	40
Primed DCs 15	82	DC	P	277	259	42
Naive DCs 1	31	DC	N	279	195	40
Naive DCs 2	28	DC	N	271	235	40
Naive DCs 3	72	DC	N	282	282	40
Naive DCs 4	36	DC	N	282	185	40
Naive DCs 5	50	DC	N	282	224	40
Naive DCs 6	33	DC	N	253	278	42
Naive DCs 7	35	DC	N	186	282	40
Naive DCs 8	49	DC	N	282	275	42
Naive DCs 9	68	DC	N	282	282	42
Naive DCs 10	28	DC	N	272	277	30
Naive DCs 11	49	DC	N	282	282	50
Naive DCs 12	68	DC	N	275	262	98
Primed T cells 1	12	T	P	151	201	40
Primed T cells 2	15	T	P	198	220	35
Primed T cells 3	68	T	P	172	419	37
Primed T cells 4	48	T	P	418	269	38
Primed T cells 5	42	T	P	163	403	38
Primed T cells 6	4	T	P	166	80	26
Primed T cells 7	26	T	P	232	202	40
Primed T cells 8	9	T	P	251	147	40
Primed T cells 9	21	T	P	122	194	28
Primed T cells 10	53	T	P	400	384	40
Primed T cells 11	33	T	P	180	295	42
Primed T cells 12	22	T	P	408	356	42
Primed T cells 13	28	T	P	250	282	37
Primed T cells 14	16	T	P	245	179	40
Primed T cells 15	24	T	P	235	238	32
Naive T cells 1	27	T	N	263	202	36
Naive T cells 2	27	T	N	241	204	40
Naive T cells 3	27	T	N	239	235	40
Naive T cells 4	45	T	N	256	253	40
Naive T cells 5	42	T	N	283	235	40
Naive T cells 6	26	T	N	281	275	37
Naive T cells 7	29	T	N	283	265	42
Naive T cells 8	29	T	N	264	248	30
Naive T cells 9	17	T	N	205	180	30
Naive T cells 10	141	T	N	275	274	30
Naive T cells 11	14	T	N	273	247	50
Naive T cells 12	38	T	N	262	227	76

Figure 2.4: A summary of all the datasets used.

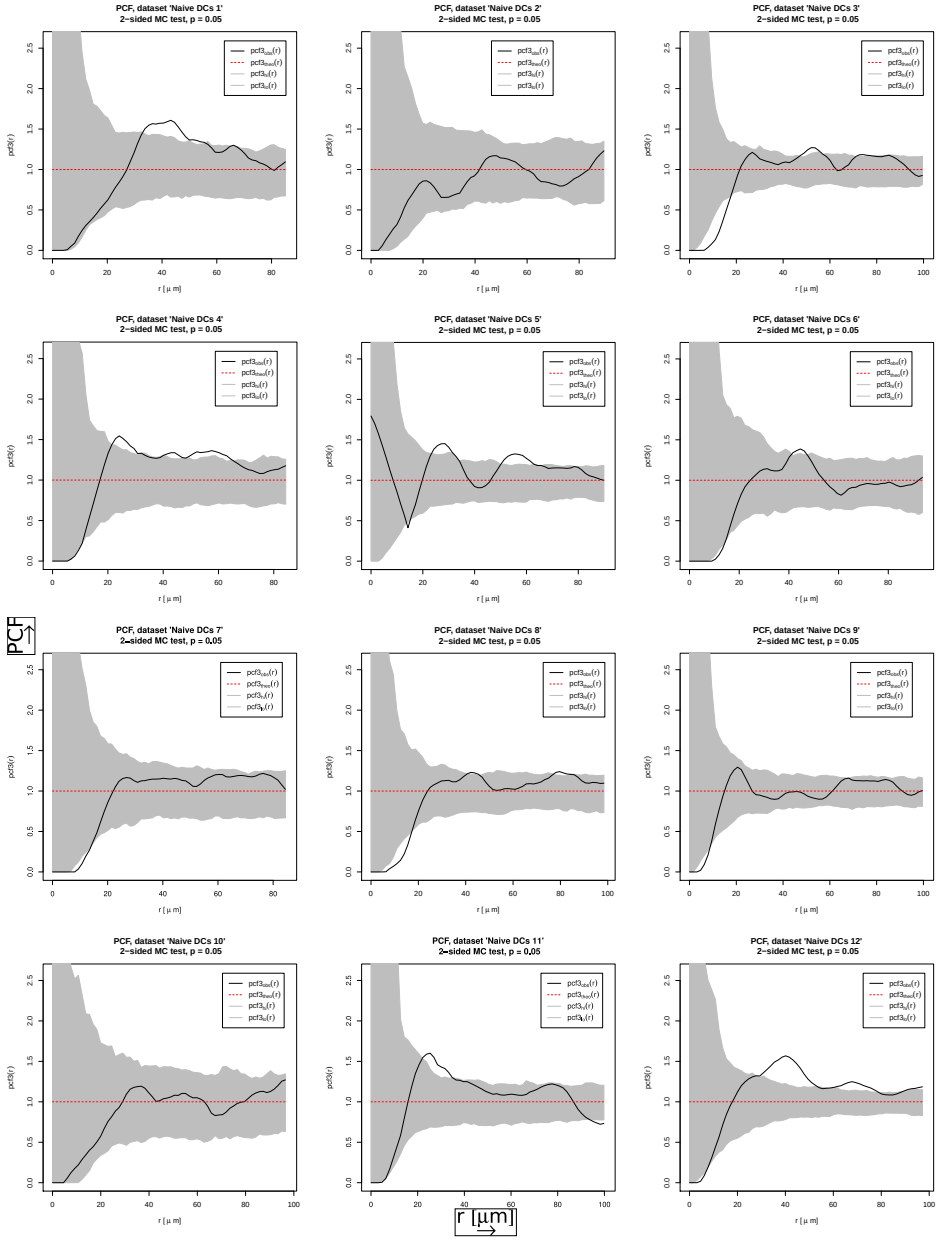

Figure 2.5: PCF functions for naive DCs with 5% significance envelopes (grey) around null hypothesis scenario (red dotted line).

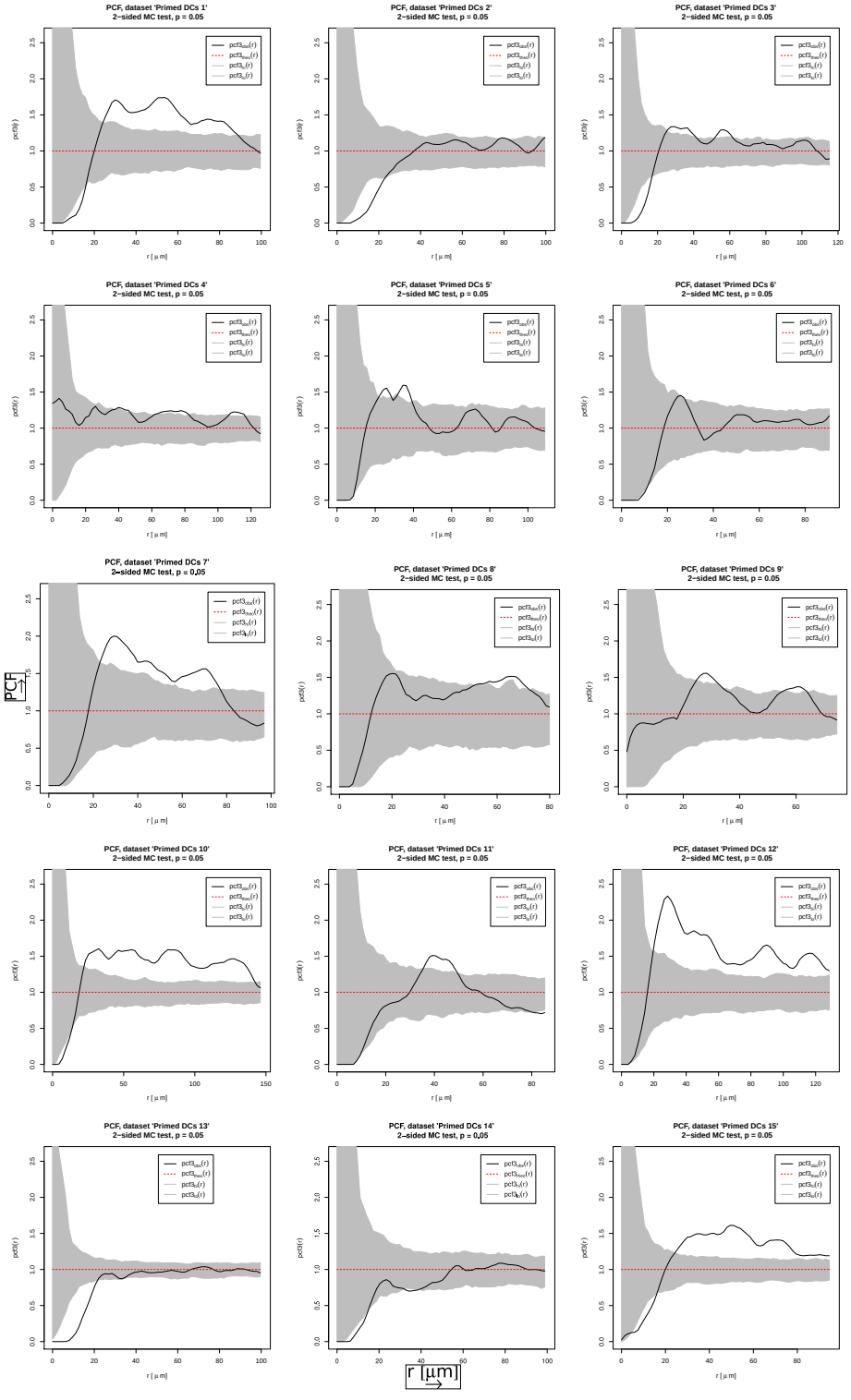

Figure 2.6: PCF functions for primed DCs with 5% significance envelopes around null hypothesis.

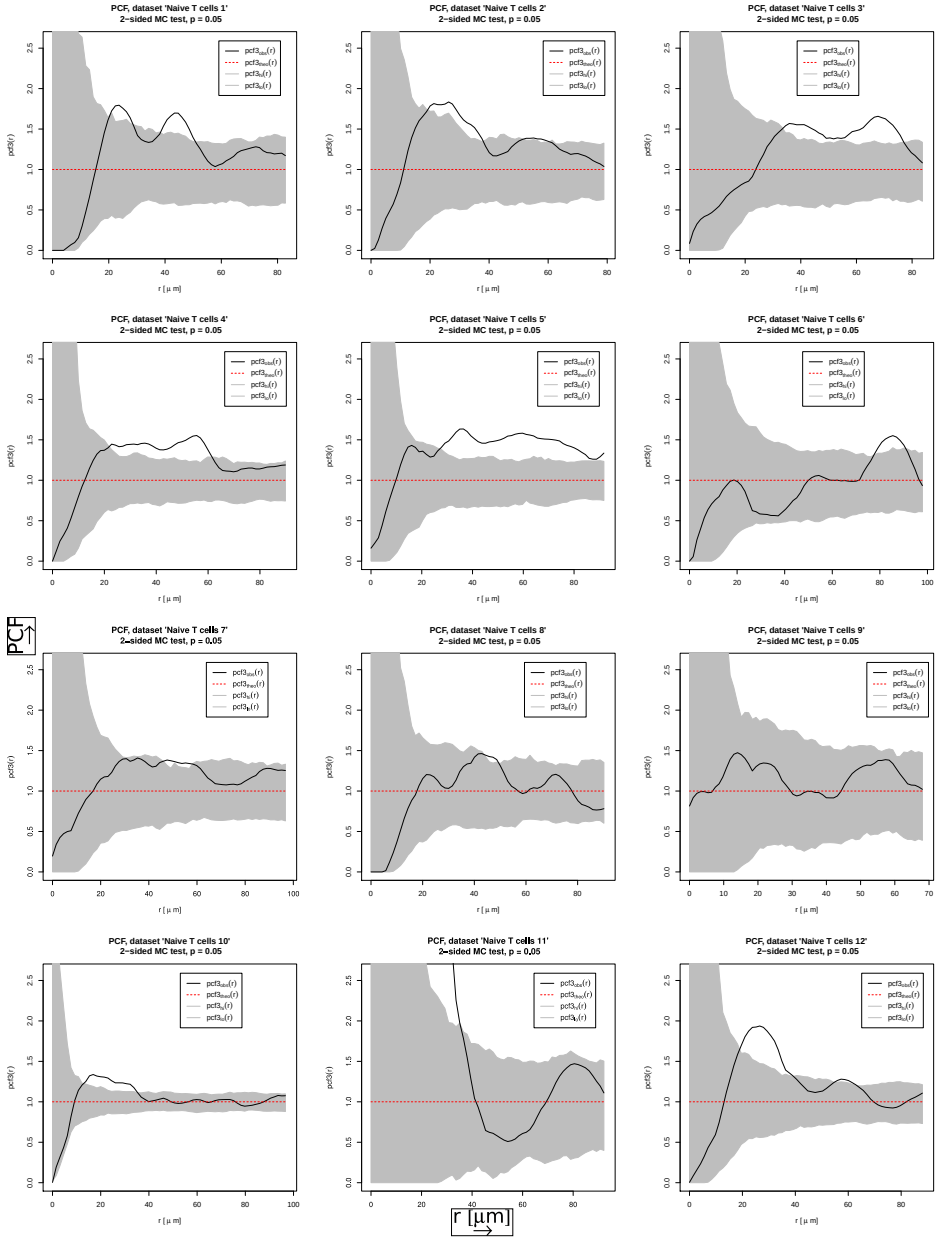

Figure 2.7: PCF functions for naive T cells with 5% significance envelopes (grey) around null hypothesis scenario (red dotted line).

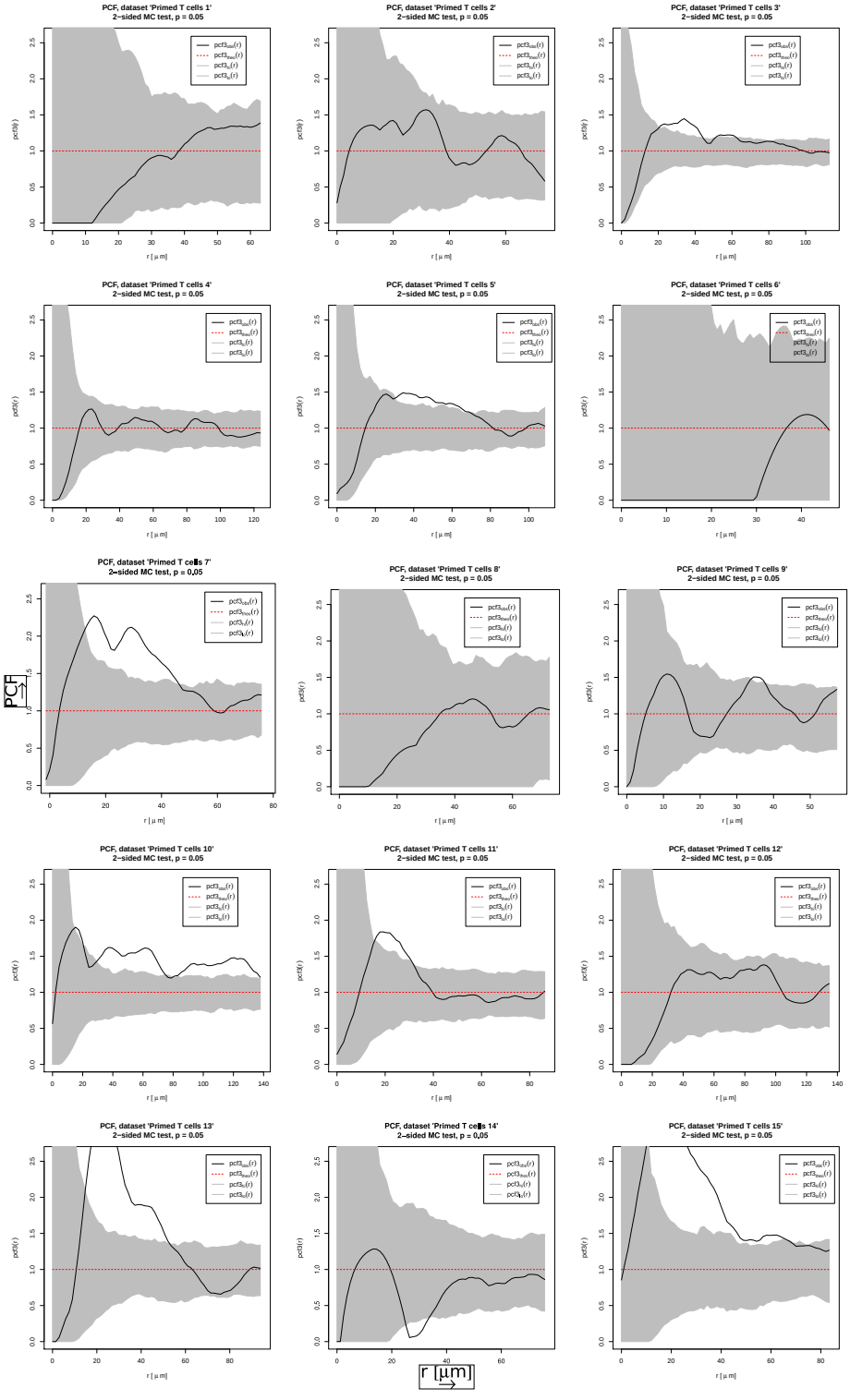

Figure 2.8: PCF functions for primed T cells with 5% significance envelopes around null hypothesis.

2.4.3 Variance and mean of quadrat counts

I chose to measure the ratio of variance to mean (var/mean) as a statistic for analysing the cell spatial patterns. The advantages of this statistic are that it is simple to calculate and interpret, being very intuitive - the variance should be higher for clustered patterns and lower for overdispersed patterns relative to CSR; and dividing the variance by the mean normalises for differences in cell density (at least partially, as this is generally only true for CSR, as I will discuss further). It is more sensitive than the alternative coefficient of variation (standard deviation/mean) as standard deviation is a square-root of variance – which stabilises variance and thus decreases sensitivity. Another advantage is that var/mean is expected to be equal to one for CSR (mean equal to variance for Poisson patterns). It should therefore be lower than 1 for overdispersed patterns (low variance) and higher than 1 for clustered patterns (higher variance).

To evaluate how this statistic depends on spatial scale, I plotted the var/mean as a function of spatial scale, by calculating it for varying quadrat size. This might reveal any scales at which the pattern deviates from CSR. For example a clustered distribution is expected to result in a peak in var/mean when the quadrat size equals the size of clusters. The spatial scale of marked deviations from CSR will also correspond to spatial scales of processes underlying the patterns.

However, no striking pattern is obvious directly from these plots (Fig 2.9 – 2.12).

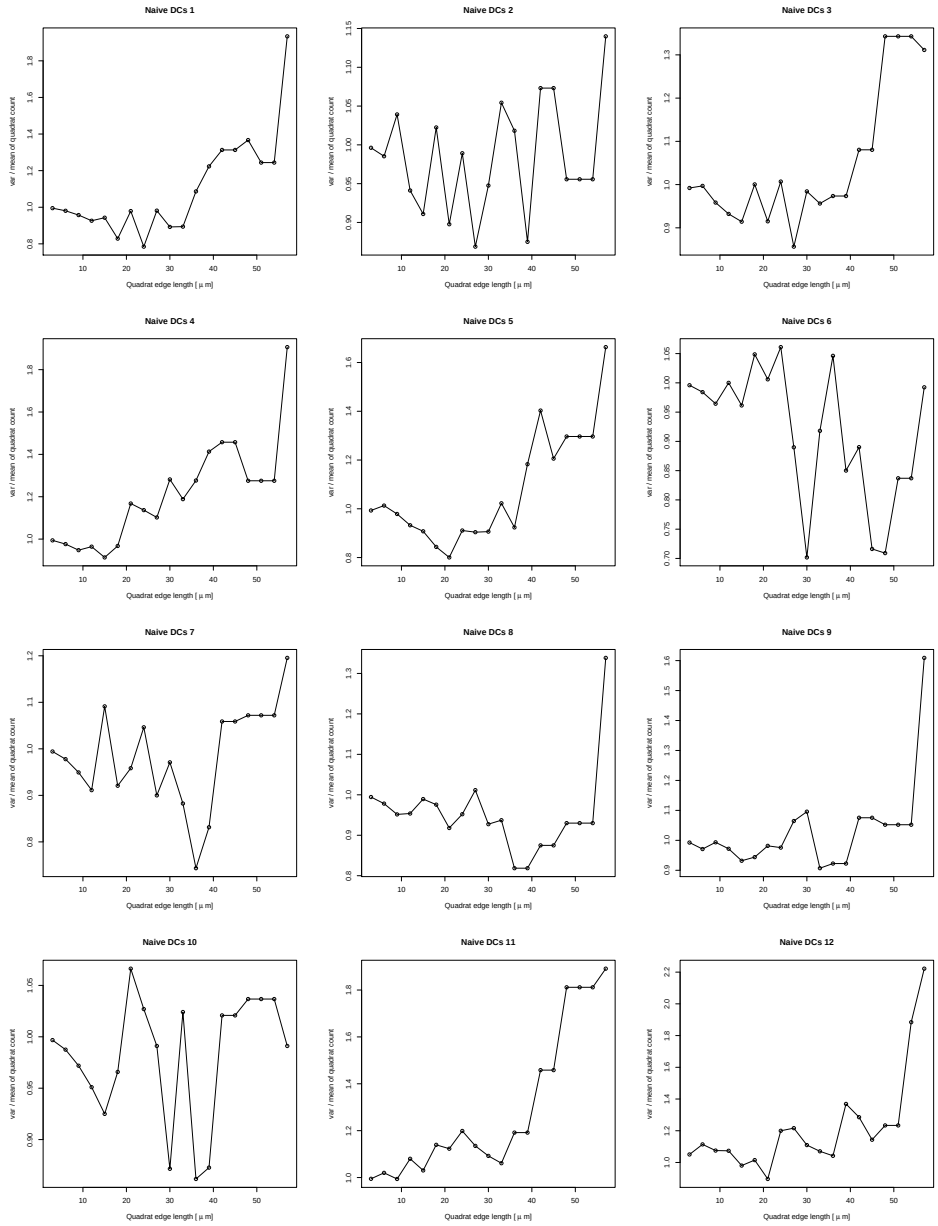

Figure 2.9: Variance to mean ratios for naive DCs

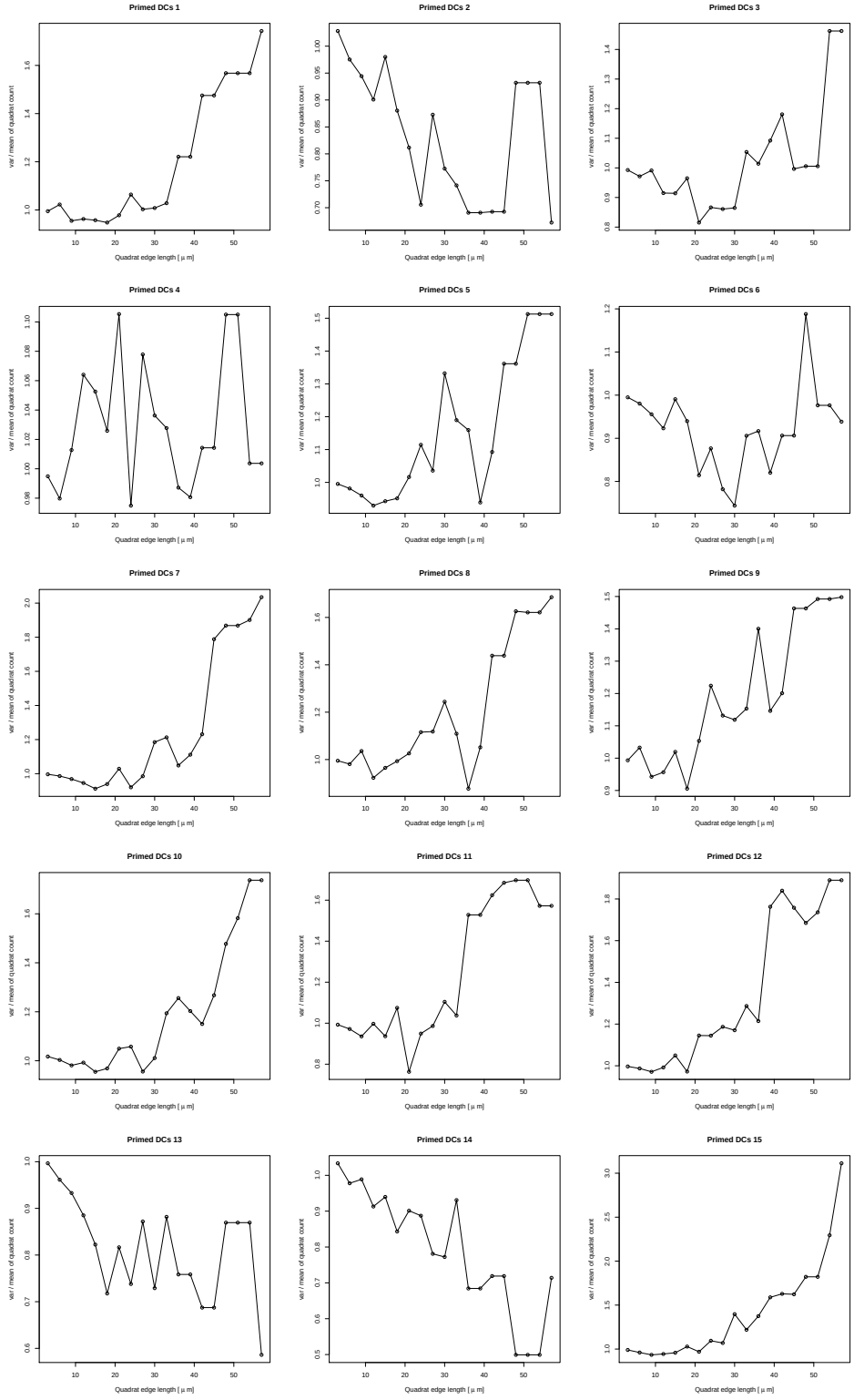

Figure 2.10: Variance to mean ratios for primed DCs.

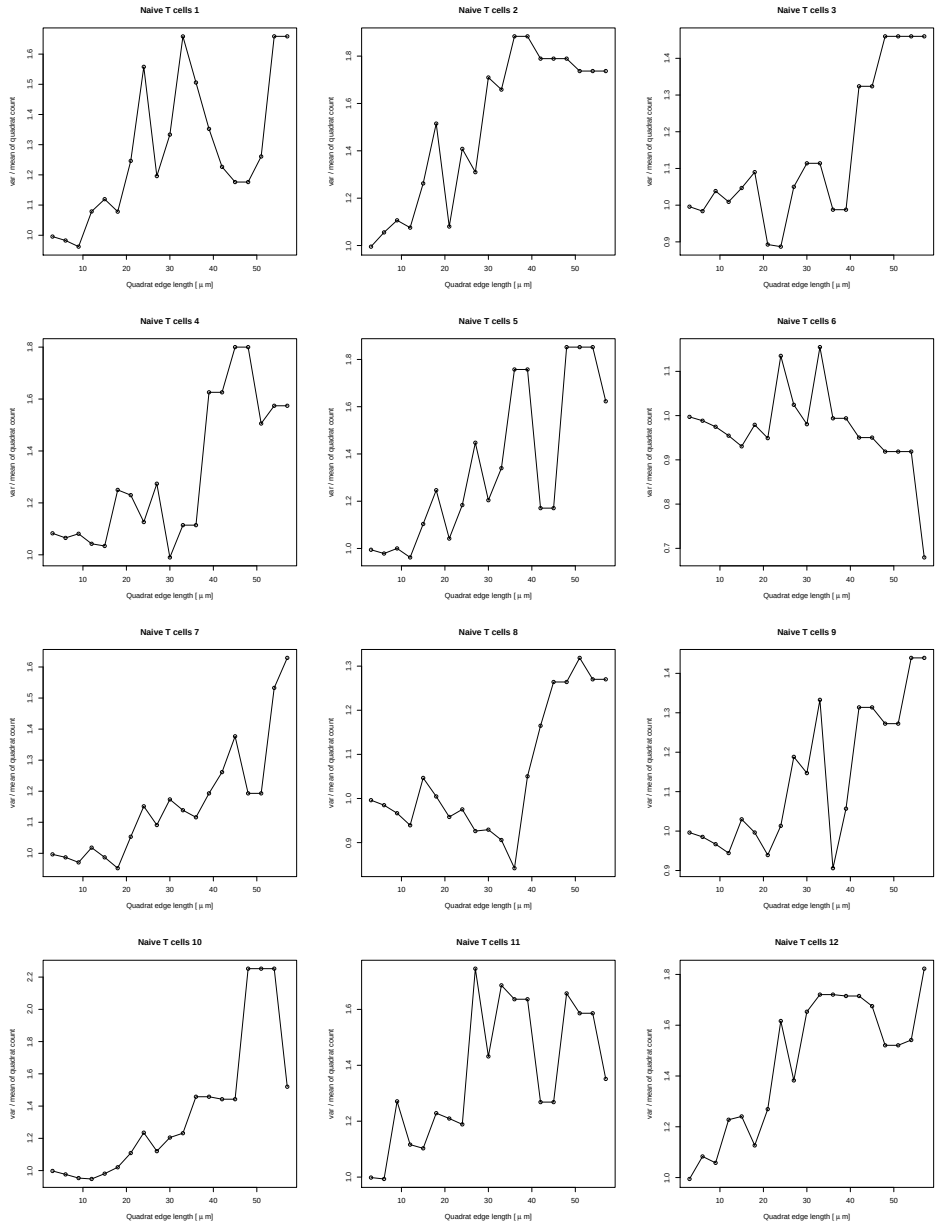

Figure 2.11: Variance to mean ratios for naive T cells.

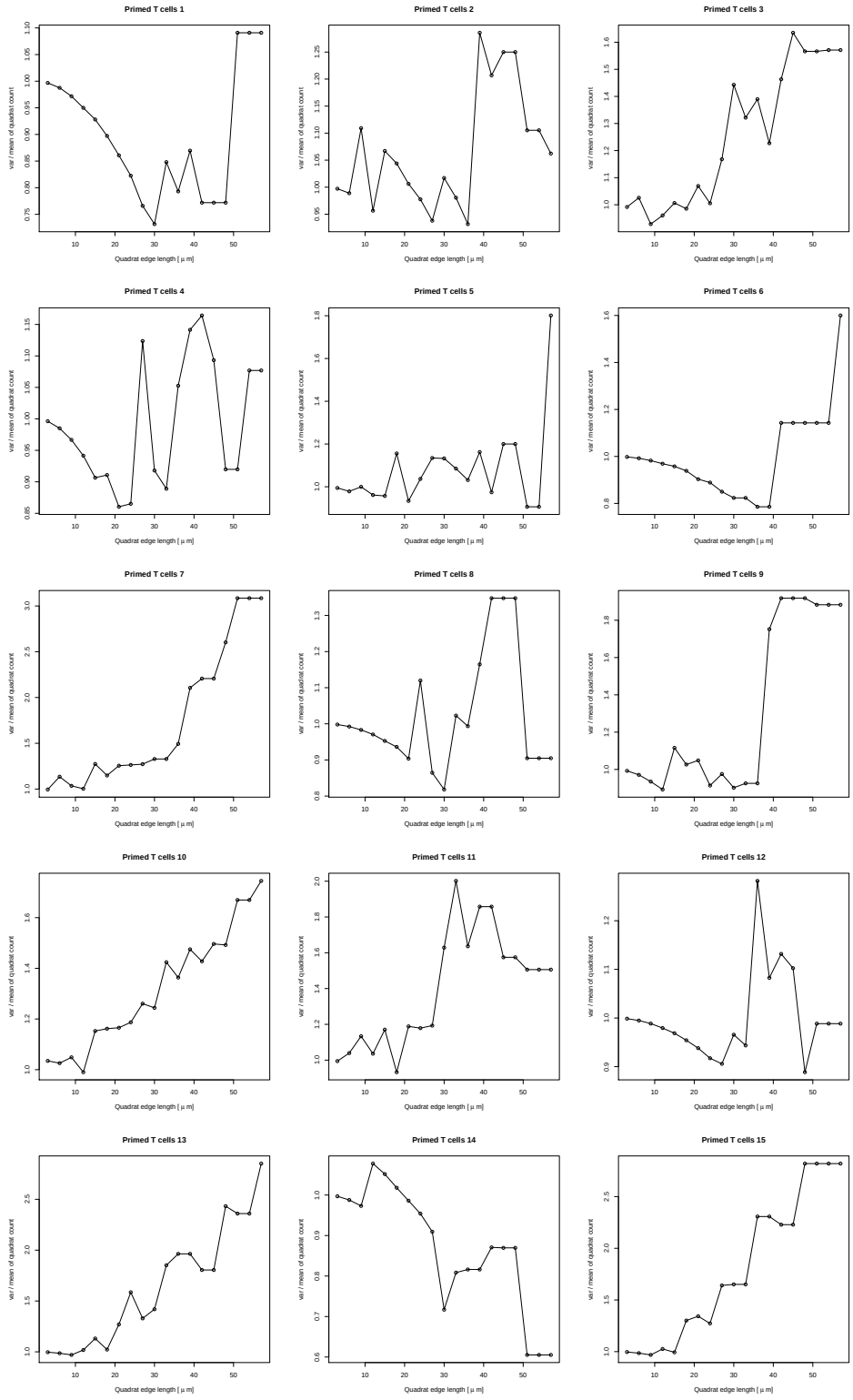

Figure 2.12: Variance to mean ratios for primed T cells.

Variance to mean ratio at a fixed spatial scale

Following from results using PCF, I aimed to test clustering at one spatial range (35 μm, which is roughly where K/PCF seem to be most deviating from CSR generally), with the goal to obtain a single statistic for each dataset, allowing the use of linear models to statistically examine the dependence of spatial patterns on cell type, treatment and other variables.

To perform this analysis, I counted the numbers of cells in quadrats of size as close as possible to 35 μm (as we need to adjust this slightly to divide the entire patterns by contiguous quadrats) and calculated the var/mean ratio of the counts of cells in these quadrats. This ratio will reflect the degree of clustering or overdispersion at that spatial range - so it is possible that if this occurs at very different range, it will be undetected by this method. The values of var/mean will also be influenced both by cell diameter and by cell density. Therefore, these were included as covariates in my models.

I utilised general liner models with var/mean as a response variable and treatment (naive/primed, labelled as N/P), cell type (T cell/DC, labelled as T/DC), cell density and cell diameter all included as explanatory variables to investigate how var/mean, and therefore the degree of clustering or overdispersion at a range of 35 μm, depends on these. Cell type and treatment are the explanatory variables of interest and cell density and diameter were included as covariates to analyse their effect and to be able to control for this, if needed.

Model comparison and selection was performed based on the Akaike's Information Criterion (AIC). The lower the AIC, the higher quality the model is. Only models with the lowest AIC are considered. Generally for two models to be considered justifiably different a difference in AIC (δAIC) of at least 2 is required. I therefore only report the detailed results for the best model (with the lowest AIC) and models with $\delta AIC < 2$ relative to the best model. A table in Fig. 2.13 at the end of this section summarises the comparison of all the models.

Alternatively, PCF could be somehow summarised for the entire patterns into a single statistic, e.g. by taking the area under the PCF curve, and linear models performed for this kind of statistic. However, using var/mean is preferred

due to its simplicity and ease of interpretation. A problem associated with calculating the area under PCF curve would be that the meaning of this number is not immediately clear, making the interpretation difficult. The approach would also be computationally less feasible.

A model including all variables

$$var/mean \sim cell.type + treatment + density + diameter$$

The AIC of this model is 37.97 and it is a poor quality model compared to some of the other models below ($\delta AIC = 5.53$ compared to the best model). I therefore proceeded with simplified models, modelling the explanatory variables individually, and also including some of their combinations of interest.

A model including all variables and pairwise interactions

$$\begin{aligned} var/mean \sim\ & cell.type + treatment + density + diameter \\ & + cell.type * treatment + celltype * density + cell.type * diameter \\ & + treatment * density + treatment * diameter + desnity * diameter \end{aligned}$$

Again, this model is of a relatively very poor quality ($AIC = 45.30$, $\delta AIC = 12.86$ compared to the best model). The coefficient for cell type interaction with diameter could not be defined by the *glm* package - this indicates that these two variables are collinear (not linearly independent). This is to be expected as diameters vary significantly between T cells and DCs; for T cells they are fixed at 8.2 μm and for DCs they range between 13.2 and 22.4 μm with a mean of 17.9 μm (mean values for individual datasets, not individual cells); the p-value for the difference is less than $2 \cdot 10^{-16}$. This means that these two variables are probably indistinguishable as explanatory variables, which I discuss further below.

A model including only treatment

$$var/mean \sim treatment$$

Again, the AIC of this model (39.16) does not justify its selection as a good

quality model ($\delta AIC = 6.72$ compared to the best model).

A model including cell type and treatment

$$var/mean \sim treatment + cell.type$$

This is probably a model of the most interest, as several previous studies attempted to measure differences in clustering between naive and primed T cells, with ambiguous results. The AIC value of 34.49 means the model is just beyond the borderline for selection ($\delta AIC = 2.05$ compared to the best one). There was no significant effect of treatment, which would indicate that there is no significant difference in terms of clustering between treatments for either T cells or DCs. The only significant difference was between T cells and DCs; T cells having higher var/mean, therefore being more clustered relative to DCs. However, due to the model not being selected over some better models, the final conclusions will be based on the higher quality models.

A model including treatment and cell type and their interaction

$$var/mean \sim treatment + cell.type + treatment * cell.type$$

In addition to the previous model, this model also analyses the interaction between cell type and treatment, i.e. whether cell type affects what the difference between treatments is. The AIC of this model is 35.83, not justifying its selection ($\delta AIC = 3.39$ compared to the best model). Even if this model was selected, the only significant difference was between T cells and DCs on the whole.

A model including only cell type

$$var/mean \sim cell.type$$

This is one of the best models with $AIC = 32.59$ and passed selection (and is very close to the best one, with $\delta AIC = 0.15$). The model confirms that cell

type is a significant explanatory variable for var/mean ($p = 0.012$), i.e. there is a significant difference in var/mean between T cells and DCs. DCs have a var/mean ratio of 1.05 and T cells have a significantly higher var/mean of 1.28. Therefore T cells are more clustered than DCs (or less overdispersed as this does not imply that they are clustered relative to a CSR). To evaluate whether T cells and DCs are clustered or overdispersed, their var/mean values have to be assessed for departure from 1 (a value for CSR). By performing a t-test with a null hypothesis that these values are equal to 1, we obtain p-values for the departure from CSR for T cells and DCs:

$$p_T = 0.0017$$

$$p_{DC} = 0.15$$

Therefore, T cells are most likely not following CSR, but we can not conclude this for DCs. An appropriate null hypothesis for T cells would be that the var/mean is not greater than 1, therefore that they are not clustered, for which the p-value = 0.00084. T cells are therefore statistically very significantly clustered.

A model including only cell diameter

$$var/mean \sim diameter$$

This is the highest quality model with $AIC = 32.44$. The proportion of total variance explained by the model is only 11.9 %. This is not surprising, given that we are not aiming to find the best possible functional fit and that a large unaccounted for variation in cell spatial patterns is to be expected. As these models are performed purely for comparison of datasets rather than parameter/functional inference, this is not of concern. The model is indistinguishable in terms of AIC from the model with cell type only ($\delta AIC = -0.15$). The similarity is to be expected as these two variables are collinear as discussed above. Var/mean is significantly correlated with cell type, but as diameter is also significantly correlated with var/mean ($p = 0.011$) (as expected; the coeffi-

cient for diameter in the $var/mean \sim diameter$ model is negative (-0.0224), i.e. the higher the diameter, the more overdispersed the cells are), the variation in the diameter values for DCs may explain some additional variation in var/mean compared to just modelling DCs as a single level of the cell type factor, thus slightly improving the model fit compared to the model with cell type. Therefore this model does not convey much new information compared to a model with cell type only. Using this data and this type of analysis, we are unable to determine whether the cause for difference in spatial patterns between T cells and DCs is driven by differences in cell diameters or other differences between these cell types. To test whether cell diameter improves the model compared to model with just cell type (i.e. whether cell diameter explains a considerable additional amount of variation in var/mean), I performed the following model.

A model including cell type and diameter

$$var/mean \sim cell.type + diameter$$

The AIC summary of this model is 34.36, so it closely passes selection ($\delta AIC = 1.92$ compared to the best model). Cell diameter does not improve the model compared to just cell type; it is a relatively worse model in comparison, with $\delta AIC = 1.77$. This means that cell diameter does not explain a considerable amount of variation in var/mean in addition to just cell type, i.e. we can not conclude that diameter has any additional effect beyond that of cell type. Neither of these variables are significant in this model – again, this is expected due to their collinearity.

A model including only cell density

$$var/mean \sim density$$

The AIC of 39.17 is relatively too high to select this model ($\delta AIC = 6.73$ compared to the best model). Even if the model was of a higher relative quality, there was no significant effect of cell density.

Model	AIC	δAIC	signif. variables (best models only)
diameter	**32.44**	**0.00**	**diameter (-)**
cell.type	**32.59**	**0.15**	**cell.type (T)**
cell.type + diameter	**34.36**	**1.92**	**none**
cell.type + treatment	34.49	2.05	-
cell.type + treatment + cell.type* treatment	35.83	3.39	-
all variables	37.97	5.53	-
treatment	39.16	6.72	-
density	39.17	6.73	-
all variables + pairwise int.	45.30	12.86	-

Figure 2.13: A summary of all models performed for var/mean. δAIC is relative to the best model. Significant variables are shown for models that passed selection, followed in parentheses by the higher level of the variable (for discrete variables) or the direction of the relationship (for continuous variables). Symbol '*' represents interaction.

In summary, the analysis utilising the ratio of variance to mean of spatial cell counts suggests that the only significant explanatory variables are cell type and cell diameter and that T cells are more clustered than DCs. No distinction can be made between treatments. We can not distinguish between the effect of cell type and diameter, i.e. it is impossible to say based on this analysis whether the cause for difference in spatial patterns between T cells and DCs is driven by differences in cell diameters or other differences between these cell types. I was not seeking this information here, but in a case where this became of interest, a simulation could be performed to quantify the influence of cell diameter on var/mean to identify if there are likely to be other variables linked to cell type determining this.

Density dependence of var/mean

As discussed in 2.3.1, many spatial statistics explicitly depend on cell density (i.e. even when parameters other than density of the underlying process which generates clustering or overdispersion do not change). There is of course no density dependence for random patterns as variance always equals mean, but var/mean for both clustered and overdispersed patterns does depend on density. This dependence is in the opposite directions for these two cases.

For clustered patterns, var/mean grows with density and for overdispersed patterns it drops with density (Fig. 2.14). This is expected as for clustered patterns, the cell density (and corresponding quadrat counts) increases mainly around the clusters/patches but much less elsewhere, thus increasing variance disproportionately more than the mean; and for overdispersed patterns, variance increases much less than the mean (or even decreases) as by adding points to a dispersed pattern, these will be preferentially added in areas with lower density (as there is inhibition between points, which is why the pattern is over-dispersed). I also tried calculating the variance/mean ratio statistic for simulated patterns with varying density and with quadrat size adapted to density so that the mean number of cells per box would constant. However, even this did not remove the described density dependence entirely.

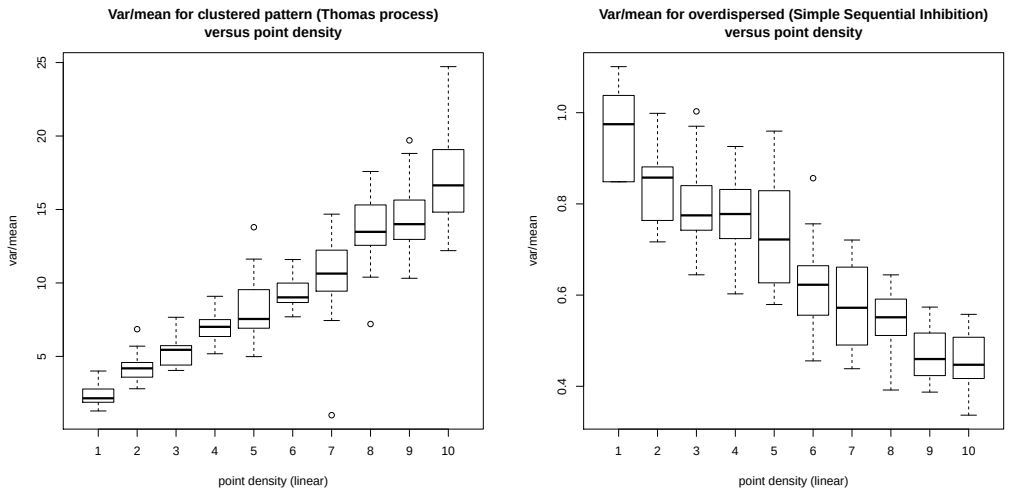

Figure 2.14: Var/mean ratio explicitly depends on density for non-Poisson point patterns. Simulated clustered and overdispersed patterns.

In other words, this means that it is easier to detect clustering or overdispersion (as the summary statistics like var/mean deviate more from the mean) as density increases, rather than that the underlying processes driving clustering or overdispersion actually change with density. However, this dependence of var/mean on density is another way in which we can evaluate spatial patterns - the direction of the dependence can be used to distinguish whether patterns are clustered or overdispersed, and its strength can be utilised to quantify the

degree of this departure from CSR in either direction.

Dependence of spatial variance on mean and Taylor's law

Attempts have been made previously to characterise spatial patterns using the dependence of spatial variance on mean. Taylor's law [28] is an empirical ecological law linking the spatial variance and mean number of individuals per certain area; and defines an index of aggregation characterising this relationship:

$$var = a \cdot mean^b \tag{2.6}$$

Where b is an index of aggregation. The coefficient b is expected to be equal to 1 for CSR, lower than 1 for overdispersed patterns and higher than one for clustered patterns.

I verified the fit of this law and the behaviour of b dependent on cell type and treatment by fitting the Taylor's law formula to variance and mean values obtained at a fixed quadrat size chosen previously (35 μm) for all datasets. To enable the use of general linear models, I linearised the relationship by logarithmic transformation, i.e. by applying the natural logarithm (ln) function on the Taylor's law equation:

$$ln(var) = ln(a) + b \cdot ln(mean) \tag{2.7}$$

And performed a general linear model:

$$ln(var) \sim ln(mean) \tag{2.8}$$

First I tested the fit of the Taylor's law to simulated data. Fig. 2.15 shows the expected behaviour: the fit is linear for random patterns ($b_r = 1.00$), convex for clustered patterns ($b_c = 1.82$) and concave for overdispersed patterns ($b_o = 0.64$).

Then I performed models with all the combinations of variables which I used previously for the var/mean ratio (treatment, cell type, cell density and cell diameter). The only significant variables were cell type and diameter (which I have shown to be collinear). Similarly to the previous section for var/mean ratio,

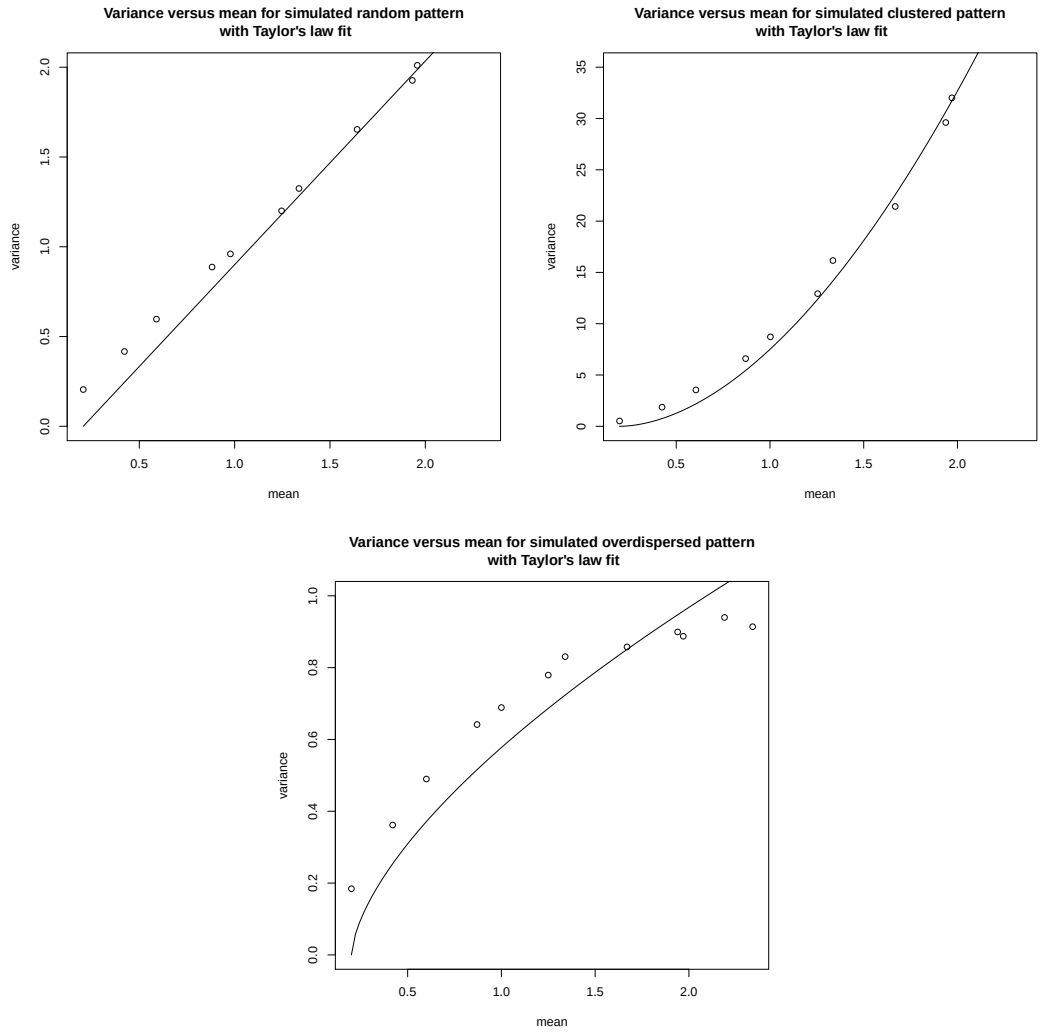

Figure 2.15: Variance versus mean for simulated patterns with Taylor's law fit, showing the expected behaviour.

diameter did not improve the model compared to cell type. The models with cell type and its interaction with mean and the same models for cell diameter had decisively the lowest AIC values.

Taylor's law model including cell type and its interaction with mean

$$ln(var) \sim ln(mean) + cell.type + ln(mean) * cell.type$$

This model will directly determine the coefficients b (as linear coefficients for $ln(mean)$) for both cell types and whether they differ significantly. The summary of this model is:

```
Deviance Residuals:
     Min        1Q    Median        3Q       Max
-0.39892  -0.15075  -0.01751   0.13184   0.63922

Coefficients:
                        Estimate Std. Error t value Pr(>|t|)
(Intercept)              0.04932    0.06853   0.720   0.4750
ln(mean)                 1.03424    0.14168   7.300 2.04e-09 ***
cell.type    T           0.25232    0.10425   2.420   0.0192 *
ln(mean):cell.type    T  0.11257    0.16774   0.671   0.5052
---
Signif. codes:  0 ‘***’ 0.001 ‘**’ 0.01 ‘*’ 0.05 ‘.’ 0.1 ‘ ’ 1

(Dispersion parameter for gaussian family taken to be 0.05799026)

    Null deviance: 15.9335  on 53  degrees of freedom
Residual deviance:  2.8995  on 50  degrees of freedom
AIC: 5.3255
```

The interaction term is not significant, indicating that there is no significant difference detectable in b (the index of aggregation) between T cells and DCs. Only cell type itself is a significant variable, therefore the only significant difference is in the intercept ($ln(a)$) between cell types. I also tested if coefficients b for T cells (b_T) and DCs (b_{DC}) are significantly different from 1, i.e. whether

using the available data we can detect a departure from a linear relationship between variance and mean (i.e. departure from CSR, where $b = 1$). I ran 2 models for $ln(var) \sim ln(mean)$ for T cell and DC data separately, and the estimated coefficients and their standard errors are $b_T = 1.15 \pm 0.11$ for T cells and $b_{DC} = 1.03 \pm 0.10$ for DCs. This corresponds to p-values of 0.52 for T cells and 0.84 for DCs for the null hypothesis that these values are equal to 1. This indicates that the Taylor's power law fit is not distinguishable from a linear fit for this data, therefore the data can not be shown to conform to Taylor's law (or can not be distinguished from CSR in terms of Taylor's law). The difference in $ln(a)$ shows that there is a significant difference for coefficient a between T cells and DCs, i.e. for the slope of a linear fit for variance and mean for these two cell types. Fig. 2.16 shows the data (untransformed) with linear models fitted for T cells and DCs.

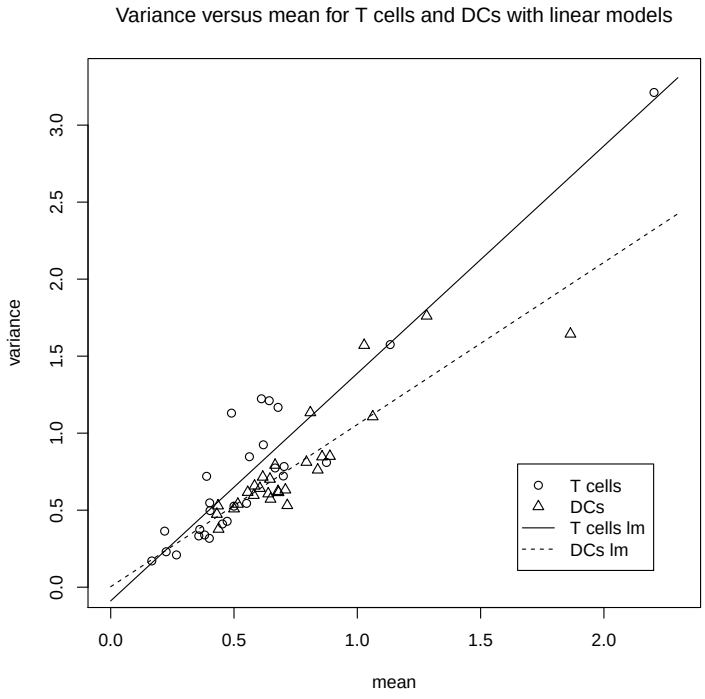

Figure 2.16: Variance versus mean for T cells and DCs, with linear function fit.

2.4.4 Cell distance Q-Q plot off-diagonal summary statistic

A drawback of methods using variance and mean and their relationship is that they only convey information for one given selected spatial scale. Also, as I have shown, these methods are generally density-dependent, i.e. will explicitly depend on the cell pattern density and not just the strength of the underlying clustering or overdispersion processes.

Therefore, I developed a scale- and density-independent statistic based on cell pairwise distances. This statistic was derived from Q-Q plots of these distances comparing observed cell patterns and point patterns generated by simulation under the null hypothesis (CSR). Fig. 2.3 in the Methods section shows pairwise point distance distributions and corresponding Q-Q plots for simulated patterns. To measure the degree of departure of the observed pattern from CSR, I calculated a summary statistic which I will refer to as the Q-Q distance summary statistic (variable $QQ.summary$), as described in the Methods. The statistic indicates if different groups (e.g. primed/naive or T cells/DCs) differ significantly, but not if they are significantly different from CSR in either direction. Statistical models and their selection were performed same as in the previous section for var/mean. A table in Fig. 2.17 at the end of this section summarises the comparison of all the models.

A model including all variables

$$QQ.summary \sim cell.type + treatment + density + diameter$$

This model passed selection, with $AIC = -179.75$ and $\delta AIC = 1.44$ compared to the best model. Surprisingly, in this model only treatment is significant ($p = 0.031$), with primed cells deviating more from CSR than naive cells. As cell diameter is collinear with cell type, a better model will be obtained by excluding diameter. Indeed, diameter should be excluded as only then can the effect of cell type be correctly tested for significance.

A model including all variables except cell diameter

$$QQ.summary \sim cell.type + treatment + density$$

With $AIC = -180.90$, this is a slightly better model (but not considerably) in terms of quality compared to the previous one ($\delta AIC = -1.15$). This model passes selection at $\delta AIC = 0.29$ compared to the best one. In addition to treatment ($p = 0.044$), cell type is also a significant variable ($p = 0.0080$), with T cells deviating more from CSR than DCs.

A model including all variables and pairwise interactions

$$\begin{aligned} QQ.summary \sim\ & cell.type + treatment + density + diameter \\ & + cell.type * treatment + celltype * density \\ & + cell.type * diameter + treatment * density \\ & + treatment * diameter + density * diameter \end{aligned}$$

The AIC of this model is -170.59, therefore this model is decisively inferior relative to the best one ($\delta AIC = 10.60$). The coefficient for cell type interaction with diameter could not be defined (same as for the var/mean models) indicating that these two variables are collinear. An improvement can be made by excluding cell diameter, same as was done for the two models above.

A model including all variables excluding diameter, and all pairwise interactions

$$\begin{aligned} QQ.summary \sim\ & cell.type + treatment + density + cell.type * treatment \\ & + cell.type * density + treatment * density \end{aligned}$$

The AIC of this model is -176.06. As expected, the model is improved by excluding diameter, however, still decisively inferior compared to the best model ($\delta AIC = 5.13$).

A model including only density

$$QQ.summary \sim density$$

One reason I calculated the Q-Q distance summary statistic is that it should be density-independent. This model verified the assumption; density is not significant ($p = 0.32$). The model is of poor quality with $AIC = -173.21$ and $\delta AIC = 7.98$ compared to the best model.

A model including only cell type

$$QQ.summary \sim cell.type$$

This model passed selection ($AIC = -179.69$, $\delta AIC = 1.50$ compared to the best model). Cell type is significant ($p = 0.0074$), with T cells departing from CSR more than DCs.

A model including cell type and treatment

$$QQ.summary \sim cell.type + treatment$$

This model tests the effect the two variables of most biological interest. The model is of the highest quality ($AIC = -181.19$) of all the models considered. Treatment is not significant ($p = 0.071$). Cell type is significant ($p = 0.0063$), with T cells having a higher Q-Q distance summary statistic than DCs, same as in all the previous models that passed selection. The proportion of total variance explained by the model is 18.4 %. Again, this is not surprising, given that we are not aiming to find the best possible functional fit and that we can expect a large unaccounted for variation in cell spatial patterns. As these models are performed purely for comparison of datasets rather than parameter/functional inference, this is not of concern.

A model including cell type and treatment and their interaction

$$QQ.summary \sim cell.type + treatment + cell.type * treatment$$

Again, the model quality ($AIC = -179.76$) is indistinguishable from many of the other selected models including the best one, from which it differs by

$\delta AIC = 1.43$). None of the terms are significant. This means that when the interaction between treatment and cell type is taken into account, cell type stops being significant.

A model including only treatment

$$QQ.summary \sim treatment$$

With $AIC = -175.21$, this is a decisively worse model than some of the previous ($\delta AIC = 5.98$ compared to the best model). Even if this model passed selection, treatment is not significant ($p = 0.089$).

Model	AIC	δAIC	signif. variables (best models only)
cell type + treatment	**-181.19**	**0.00**	**cell type (T)**
cell.type + treatment + density	**-180.90**	**0.29**	**cell type (T), treatment (P)**
cell.type + treatment + cell.type* treatment	**-179.76**	**1.43**	**none**
all variables	**-179.75**	**1.44**	**treatment (P)**
cell.type	**-179.69**	**1.50**	**cell type (T)**
all variables except diameter + pairwise int.	-176.06	5.13	-
treatment	-175.21	5.98	-
density	-173.21	7.98	-
all variables + pairwise int.	-170.59	10.60	-

Figure 2.17: A table summarising all the models performed for Q-Q summary statistic. δAIC is relative to the best model. Significant variables are shown for models that passed selection, followed in parentheses by the higher level of the variable (for discrete variables) or the direction of the relationship (for continuous variables). Symbol '*' represents interaction.

In summary, treatment is significant in two of the selected the models (a model including cell type, treatment and cell density and a model including all variables), with primed cells departing more from CSR than naive cells, although this is slightly below the boundary for being considered significant in the best model in terms of AIC (model including cell type and treatment, $p = 0.071$) and also not significant in the model including only treatment ($p = 0.089$). There are several models for which AIC values are too close to distinguish between. Cell type is significant in several of them including the one with the lowest AIC (with treatment and cell type) and the one which includes cell type only.

Cell type stops being significant when the interaction between treatment and cell type is taken into account. The results would indicate that there might be an effect of treatment (primed cells might be departing from CSR more than naive cells), however, it is impossible to detect this with confidence in the available data using this method. The results also agree with my previous conclusions based on the other methods that cell type is significant (T cells departing from CSR more than DCs), although this is undetectable when the interaction between treatment and cell type is taken into account (i.e. when we try to differentiate this effect between treatments).

2.5 Discussion

In this chapter I presented a quantitative study of T cell and DC spatial clustering and over-dispersion in lymph nodes (LN) in the naive state and during priming, employing several quantitative and statistical methods to analyse a large multi-photon imaging dataset. In addition to quantifying the degree of spatial clustering or over-dispersion and assessing differences between cell types and treatments (naive versus primed), I explore what the spatial scales of clustering or over-dispersion are. This scale is of interest as it should correspond to the spatial scale of the processes underpinning the mechanism of T cell and DC behaviour in LN. I also account for two possible 'nuisance' variables which can bias the results; the cell diameter and cell spatial density.

Initially, I performed statistical analyses of spatial clustering and over-dispersion of cells using pair-correlation function (PCF). The PCF functions provide a convenient method to assess clustering and overdispersion of individual images. The statistical significance of the departure from CSR in either direction can be assessed at a range of spatial scales. Generally, both types of cells in both treatments are clustered over certain spatial ranges (Fig. 2.5 – 2.8). This is variable between datasets, but significant clustering ($p < 0.05$) occurs roughly between 20 and 50 μm. This is possibly due to non-homogeneities in the LN environment and might reflect its physical structure. In the LN T cell areas, there is a dense network of fibroblastic reticular cells (FRC) and extracellular products serving as a scaffold for the lymphocytes to attach to and move along; and these reticular cells can participate in the process of antigen presentation and other lymphocyte stimulatory processes [31, 32, 33, 34, 35]. If the underlying FRC network reacts to activation by changing geometry or the spatial pattern of expression of lymphocyte adhesion molecules, this could be an important factor driving the changes in T cell and DC spatial arrangement, apart from direct responses of these two cell types. A further investigation of the spatial structure of FRC networks using the methods employed here in different treatments could provide insight into this possibility. For example if the FRC network nodes (points where FRC fibres intersect) were found to cluster at similar spatial ranges to those at which T cells and DCs have been found to

cluster here, this would further support the increasingly likely hypothesis that these cells are attached to the FRC network. As the most marked departures from CSR appear roughly around the spatial scale of 35 μm, I chose this scale for analysis of the cell spatial patterns using other methods.

I proceeded with an analysis utilising variance and mean of the counts of cells in contiguous spatial quadrats to statistically assess departure from spatial randomness at this scale. Importantly, I explicitly consider both cell diameter and cell density as variables in my models, as these variables generally influence the apparent level of departure from spatial randomness and might bias the results. The effect of cell diameter is due to the fact that cells can not physically overlap, so there will be some degree of over-dispersion even under the null hypothesis. Without addressing this, analyses would underestimate the level of clustering and overestimate the level of overdispersion of the cell spatial patterns. Also, for many statistics quantifying the departure from spatial randomness, the results will be explicitly density-dependent (all other things being equal) as I show in the Results section (see Fig. 2.14). Upon this formal quantitative analysis, I concluded that the only significant difference is between T cells and DCs, with T cells being significantly clustered, while DC spatial patterns are indistinguishable from random (i.e. Poisson point process). There was no significant effect of treatment. Cell type and cell diameter are collinear variables (linearly dependent) and are equivalently good explanatory variables for our data - therefore it is not possible from this analysis to determine whether the cause for the difference between T cells and DCs is driven by differences in cell diameters or other differences between these cell types.

I also investigated whether the data are consistent with Taylor's law [28], an empirical law originating in ecology linking the spatial variance and mean of the number of individuals, which defines an index of aggregation characterising this relationship and the given spatial pattern. It was proposed [29] that this relationship results from a density-dependent balance of attraction and repulsion between individuals trying to maximise resource exploitation. Such mechanism could possibly also drive the behaviour of immune cells in LN, serving to optimise the search for antigen. I utilised the values of variance and mean calculated above to test whether data conforms to Taylor's law, however,

there was no sufficient support for this.

The spatial resolution of methods based on variance and mean of cell counts is proportional to the size of the selected quadrats; therefore, the results are specifically relate to a certain range, but might be different at other scales. I developed a density- and scale-independent method to assess departure from CSR (the Q-Q distance summary statistic), thus allowing the comparison of patterns with different cell densities without bias, and without the limitation of the result to a specific spatial scale. In agreement with the previous analyses, this does not support the hypothesis that T cells cluster more during priming compared to the naive state. The conclusion based on the best models is that T cells are significantly more departing from CSR compared to DCs, although this is undetectable when the interaction between treatment and cell type is taken into account (i.e. when we try to differentiate this effect between treatments) (Fig. 2.17).

There is some indication from using the Q-Q distance summary statistic method that both cell types (when treated as one group) might be more clustered in priming compared to naive state, but the corresponding p-value was 0.071 in the best model and even higher when distinction was made between T cells and DCs; therefore, it is not possible to reliably make such a conclusion even with the relatively large dataset used.

In summary, these findings are in contrast to conclusions of some of the previous studies, where T cells were generally considered to be clustered in the primed state more than in the naive state. This was attributed to the aggregation of T cells around antigen-bearing DCs. Here I show that in a system using *in vivo* immunisation, this is not necessarily true, i.e. such an effect is undetectable even for the relatively large dataset used.

As mentioned when discussing the previous studies in the Introduction, the method of immunisation might be critical in determining the magnitude of T cell clustering and whether this can be detected. Indeed, many of the studies that were cited in the introduction and reported clustering utilised the *in vitro* route of immunisation. When DCs are labelled and pulsed with antigen *in vitro* prior to transfer *in vivo*, it is likely that clusters are detected due to the very high concentration of antigen on these relatively scarce DCs, which

thus form spatially disperse centres of intense clustering. In studies utilising immunisation *in vivo* of animals with transgenic fluorescent DCs, the situation is very different. Presumably, all or most of the DCs present in the lymph node carry some antigen in a much lower concentration compared to *in vitro*-pulsed DCs. Therefore, clustering of T cells around these DCs should be both weaker, and potential clusters should be much smaller and closer together due to the higher density of DCs, thus making the overall magnitude of clustering much smaller.

I hypothesise that the cellular interactions accompanying immunisation are too subtle to detect significant changes in T cell spatial patterns compared to naive state when immunisation is performed *in vivo*. At physiological and natural pathological concentrations of antigen or antigen-bearing DCs, the effect is likely even smaller. The ability to detect clustering will be determined, apart from cell density, by the balance between T cell search time for a cognate antigen-bearing DC and the interaction time between these; if search times are long relative to interaction duration, then only very few small clusters will be present. It is likely that T cell-DC interactions are too infrequent due to low density of antigen-specific T cells and DCs carrying a cognate antigen to create a detectable increase in T cell spatial clustering. I suggest that rather than quantifying spatial clustering, effort should be made to quantify the temporal duration of individual T cell-DC interactions (as was done e.g. in [16, 24, 25]), where more notable differences should be detected between different immunological states.

Using both the method based on variance and mean of cell counts in quadrats and the density- and scale-independent Q-Q distance summary statistic, I did not detect any departure of DC spatial patterns from CSR. Although an overdispersed spatial pattern of DCs could theoretically serve to increase the efficiency of T cell search for cognate antigen, it appears that in both naive and primed state, the DCs occupy the imaged areas of LN in a random spatial pattern (i.e. indistinguishable from a Poisson point process).

The quantitative methods used and developed can be used to further investigate these processes beyond this particular application to rigorously analyse cell spatial patterns in various systems and contexts. Generally, it is important

to account for cell diameter and cell density, and the Q-Q distance summary statistic which I developed allows the comparison of patterns with different cell densities without bias, and without the limitation of the results being limited to a specific spatial scale.

Chapter 3

Analysis of T cell movement in relation to DC locations in lymph nodes using Bayesian state-space models

The cell imaging data for this chapter has been generated by me, Dr Robert Benson and Dr Agapitos Patakas. The analysis is entirely my own work.

The results are currently in preparation for publication.

3.1 Abstract

T cell search for antigen-presenting cells in lymph nodes is a critical process for the outcome of the adaptive immune response, and understanding the underlying processes has important implications for both basic immunology and for potential applications in therapeutic interventions. Much data have been collected recently, enabled by the rapid development of imaging techniques, however, analytical and theoretical work remains to be done to fully exploit these data in order to address fundamental questions about the mechanisms of T cell movement and their interactions with DCs.

There has been considerable interest in inferring the mode of T cell movement, particularly whether this is a random walk or exhibits some form of taxis. Here, I address the question within a rigorous formal statistical framework, directly, at a single-cell-level, using T cell and DC multi-photon imaging data.

I developed Bayesian state-space models of the movement of T cells in both naive and primed lymph nodes, to represent different mechanistic processes of T cell movement and assess how well these are supported by the data. This is the first time that this modern and highly flexible framework has been applied in this field, enabling analysis of the cell behaviour in a statistically tractable way, accommodating the formal testing of movement models based on observed cell speed and turning angles combined, rather than in isolation.

I formulated and tested several alternative mechanistic models of taxis-type behaviour. This allows us to make an important differentiation between a behaviour where T cells 'become aware' of a DC only at a certain threshold distance, e.g. through physical interaction with DC dendrites, and a behaviour where there is a 'gradient of migration behaviour', possibly following a gradient of chemokines.

From this analysis, it appears that there is no detectable chemotaxis or other attractive action at distance between T cells and DCs, at least in the sense of a continuous functional dependence of T cell speed or turning angles on the distance to the nearest DC, and that T cells only change their movement parameters once they interact with a DC. T cells seem to switch between different movement states only once they physically encounter a DC. I also

inferred how much of the observed decrease in average T cell speed during priming compared to naive scenario is due to a proportion of T cells interacting with DCs and how much actual slowing down occurs when cells are 'freely migrating'.

The analysis highlights the complexity of the system and the need to for using large datasets and rigorous statistical analyses.

3.2 Introduction

T cell search for and recognition of antigen-presenting cells bearing cognate peptide/MHC molecules in LNs are crucial steps in eliciting the adaptive immune responses associated with protection against pathogens and pathology in autoimmune diseases. For more than 15 years now, confocal microscopy, and more recently multi-photon laser-scanning microscopy (MPLSM), have been providing fine-scale data on immune cell behaviour within intact lymphoid tissues [18, 15, 17]. A number of MPLSM imaging studies have been carried out since, e.g. [19, 20, 21, 16, 5, 22, 7, 23, 24, 25] and a large amount of data have been collected. There were various attempts at analysing T cell movement data, however, there is a lack of underlying theoretical framework and rigorous quantitative studies. Therefore the impressive advance in ability to generate data has not been matched by similar progress in analysing these data and generating quantitative models to address the underlying mechanisms and make predictions to stimulate novel experiments.

The first paper describing the use of 2-photon microscopy to examine lymphocyte movement in explanted lymph nodes [17] presented observations of the speed and motility coefficient (a metric related to the assumption that movement is diffusion-like) of naive T and B cell migration. In another early study [22], a similar descriptive analysis was performed *in vivo* and also for T cells undergoing priming (after the delivery of antigen and immunoadjuvant). The study found that the mean speed of T cells decreases during priming. This is unsurprising given that T cells during priming presumably spend a proportion of time interacting with relatively slow-moving antigen-bearing DCs and therefore presumably decrease their speed during this time, but it remains unclear how much of this decrease is caused by interaction and how much by actual decreased migration speed of cells not interacting with DCs. A study of the migration of CD-8 T cells in lymph nodes [21] defines and reports a 'confinement ratio' of cells as the ratio of displacement (straight line distance between two time points defining a certain time interval) to observed path length during that time interval; and an 'arrest coefficient' defined as the percentage of time for which a T cell has an apparent instantaneous speed of less than

2 μm/min. These early studies were purely exploratory, as presenting these rather arbitrary parameters in a descriptive manner sheds little light on the process as it is unclear what these metrics mean mechanistically, e.g. what values would be expected under different hypotheses of interest or how they should depend on other important variables. The study [21] confirmed previous findings that the mean T cell speed decreases in priming. A more quantitative study [23] similarly examined T cell speed (again lower in priming compared to the naive scenario), quantified a 'meandering index' (the same parameter as the 'confinement ratio' in the previous study) and the motility coefficient. Interestingly, the speed estimate was carried out after excluding cells classified as 'in clusters', which are presumably interacting with DCs, and the speed was still decreased, which would indicate that cells that are not interacting also slow down. Here, I further investigate this in more detail.

Importantly, a study [24] using two-photon microscopy *in vivo* has shown that the duration of contacts between T cells and DCs which is critical to the activation of the T cells; at least 6 hours of T cell-DC interaction was required for naive T cells to undergo clonal expansion and efficient activation *in vivo*. This has indicated the importance of understanding cell migration and interactions in LN for potential applications in therapeutic interventions at this level. As such, there is a continued theoretical interest in the mechanisms underlying these processes and their optimisation [8, 9]; and continued experimental efforts to study these processes in the medical context of both infection and autoimmune diseases, for example in mouse models of malaria infection and arthritis [26, 27].

Some of the early studies started the trend of examining plots of mean displacement (or mean squared displacement) versus square root of time, and the related motility coefficient, as a basis for deciding whether movement is following a random walk (meaning diffusion-type movement or Brownian movement) or not [17, 22]. In these two studies, mean displacement was plotted against square root of time and linear regression performed, which was taken as a support for a hypothesis that T cells follow a random walk. While the movement matches random walk in this one characteristic over a certain temporal range, this only provides a description of the movement from a narrow perspective and can lead to conclusions that are not necessarily robust – it does not permit the

inference of the mechanism underpinning the generation of movement patterns and does not prove that movement is following a random walk [36, 37]. Another difficulty is that these examinations were only performed over a short time interval (of about 7-13 minutes in the mentioned studies). Thus, many of the early studies characterising lymphocyte motility in LNs concluded that T cells performed random walks, with phases of linear 'persistent' motion over time-scales of 2-3 minutes [17, 20], and many modelling studies assumed T cells perform movement based on variants of a random walk [9, 38, 39], often one in which T cells follow straight paths for a given 'persistence time' between turns.

There have been few attempts to study the mechanisms underlying the observed cell behaviour. In particular, there has been a special interest in inferring whether T cell movement exhibits some form of chemotaxis. A recent study [40] presened some indication of chemotaxis of CD-8 T cells towards CD4-DC interaction sites – the accumulation of CD-8 T cells was observed in LN in areas of CD4-DC specific interaction. It is possible that CD-4 T cells exhibit similar attraction towards activated antigen-bearing DCs. [41] studied the behaviour of CD-8 cells in brains of mice during infection with *Toxomplasma gondii* and show that chemokine CXCL10 is a potentially important agent for a type of CD-8 T cell chemotaxis. According to this study, CXCL10 "speeds up the average migration speed without changing the nature of the walk statistics." Although it is unknown whether the speed of all CD-8 T cells is elevated uniformly in the tissue where CXCL10 is expressed, or whether there are gradients which lead to chemotactic behaviour of CD-8 T cells, the findings presents an interesting possibility for a mode of taxis where the speed but not the directionality of the movement is influenced by proximity to target, and this serves to increase the probability of target encounter (shortening the search time). The authors claim that a Lévy walk is a better model than a random walk (Brownian movement) and present this as a likely mode of CD-8 T cell movement. Lévy walk models have been popular to model the movement of organisms, as they often provide a more parsimonious fit than a random walk. However, this apparently better match provides little support for the Lévy walk hypothesis, as many other models will often provide a better fit than a simple random walk in some respects. The Lévy walk hypothesis has

recently come under a well substantiated criticism as unrealistic; and when revisited, the claimed evidence that organisms perform Lévy walks has been shown to be spurious or non-existent [42, 43]. While a Lévy walk is likely not an appropriate model for cell movement, I addressed some of the interesting questions that follow from this research – especially whether we can detect a type of cell speed-mediated taxis in our data for CD-4 cells.

In [44], the authors match several different simulations to data on the movement of CD-8 cells in naive LN and find relatively good support for a combination of random (Brownian) and persistent walk (where cells have a tendency to persist in the current direction for a certain time) , based on the fact that the cell displacement distribution could be well fit by a sum of two Gaussian distribution. This led to a construction of a movement simulation where 30% of the cells are set to migrate via a Brownian walk and the rest via a random walk with persistence. The simulation then reproduced certain statistical measures of the observed cell movement reasonably well, but no penalisation was implemented for the additional complexity of this model over the simpler ones, which would be required to achieve a fair comparison of different alternative models. It is, however, quite possible that there are multiple behavioural states underlying T cell movement (e.g. random walk, directed antigen search, interaction with a DC and the following movement state of activated cells that will eventually proliferate and leave the LN) and below I put these ideas to the test using a well established statistical method, which should enable the detection of distinct movement modes directly based on the measured step lengths (proportional to cell speed) and turning angles.

T cells move within a densely packed cellular environment rather than a homogeneous space, and there is some indication that a dense network of fibroblast reticular cells (FRC) guides the T cell movement, at least to some extent [35]. While it remains unclear whether the FRC network dictates the entire trajectory or, for example, is responsible only for some of the T cells turns and associates with T cells only transiently, it seems very likely that at least some of the T cell turning behaviour is driven by this structure. The effect this might have on the potential taxis of T cells towards DCs and on its detection will be addressed in the Discussion.

To sum up, the availability of large amounts of detailed imaging data on cell behaviour calls for appropriate rigorous analytical methods and theoretical development. Our understanding of immune cell migration and interactions is still fairly limited and it is becoming increasingly clear that more powerful and formal statistical methods are required to better address the underlying mechanisms.

Here, for the first time in this field, I develop a set of statistically robust Bayesian state-space models (SSMs) fitted using Markov-chain Monte Carlo (MCMC) to analyse multi-photon microscopic data on the movement of T cells in both naive and primed lymph nodes. This highly flexible methodology enables the analysis of cell behaviour making the minimum of assumptions in a data-driven and mathematically and statistically tractable manner. It is especially suitable as it accommodates the formulation of a wide range of mechanistic movement models within one framework, and allows a formal, straightforward assessment of how well these are supported by the available data.

The models are based on Bayesian data analysis, where prior distributions of parameters of interest are updated using data likelihood to generate posterior distributions of the parameters. First, prior distributions are specified, either based on available data, expert judgement, or – when these are not available – minimally-informative (vague) priors can be used. Next, a model is defined as a set of stochastic and deterministic variables and the relationships between them – in this aspect, the approach is identical to frequentist statistical models. Based on the model and data, likelihood is defined and samples are generated from the posterior distribution. The MCMC is a stochastic algorithm, progressing from the specified initial values towards the solution – convergence diagnostics are used to check when the sampling algorithm has reached equilibrium, making sure that samples are drawn from the equilibrium posterior distribution.

A comprehensive review of SSM approaches is presented in [45]. The particular strength of SSMs for our purpose is their flexibility – a large array of statistical distributions can be used to describe the observed metrics; and specific deterministic and stochastic relationships between these can be implemented, with a large degree of hierarchical complexity possible. It is for example possible

to decompose the movement into different behavioural states described by different distributions of movement metrics – relevant for example for detecting different behavioural states of cells. Beyond a simple categorisation of behaviour, the probability of being in a particular state can be estimated, thus explicitly accounting for the uncertainty of categorizing the behavioural states. Models can be constructed so that the behavioural states of cells depend on other variables such as anatomical location within tissue or the proximity to other cell types. The SSM can be used to generate a set of competing models, and the relative support of these models by the data can be assessed objectively, enabling direct comparison of hypotheses based on data.

Our approach is inspired by [46], where the data similarly comprise of a time series of step lengths and turning angles, in this case representing the telemetric data of the movement of elk *Cervus elaphus*. By using SSMs for mixtures of random walks with different parameters, the authors found that the elk performed two distinct movement modes; 'encamped' (slow with tortuous paths) and 'exploratory' (faster and more directed).

I also employed some of the methodological details discussed by [47], who present a suite of mechanistic models for various types of movement, of which most important for this application are models accounting for centres of attraction and the allocation of movement to different movement states.

I formulated specific quantitative models to analyse T cell movement parameters and link these to the distance of T cells to their nearest DC in naive and immunised contexts. I quantified the differences between these two scenarios and aim to infer whether T cells follow a taxis or other form of directed movement towards DCs, and to infer the range of such attraction.

There are two mechanistically distinct categories of models I compare here. In the 'gradient taxis' models, T cells continuously change their movement parameters in response to the distance to the nearest DC, corresponding to a response to a concentration gradient of a chemokine. In contrast, in the interaction models, cells can switch between two different behavioural models based on their distance to the nearest dendritic cell (DC), and the switch happens at a certain critical 'interaction threshold' distance. It was possible to statistically infer this 'interaction threshold' distance from the data. This also

allowed me to detect which cells are in interaction mode and which are 'freely migrating' and to address how much of the observed decrease in average T cell speed during priming compared to naive scenario is due to a proportion of T cells interacting with DCs and how much actual slowing down occurs when cells are 'freely migrating'. An alternative type of taxis-type behaviour which I considered is where the probability of being in a certain movement state is a smooth function of the distance to the nearest DC ('state probability model'). I also analysed T cell step lengths and turning angles simultaneously to detect different movement types, which is a conceptual improvement to analysing these two measured properties of the cell movement in isolation.

3.3 Methods

3.3.1 Data collection

This is described in chapter 2 in sections 2.3.2 and 2.3.3. T cell movement was imaged with a scanning period of 45 s, the imaging duration was 26.25 min and each imaged volume consisted of planes 2 μm apart. T cell tracking data was corrected for whole-tissue drift – this was inferred by determining the mean velocity vector of the DCs (which are used as a reference stationary background).

3.3.2 Cell trajectory measurement

The measured trajectories consisted of a time-series of 3D locations l_i, $i = 1...N$ of the detected cell centroids, captured with a fixed time period T given by the microscope set-up, in this case $T = 45s$, i.e. at fixed time intervals of $45s$. These data were imported to R, where all further analysis was preformed.

Fig. 3.1 illustrates how the movement metrics were measured. Step lengths s were measured as distances between consecutive locations, i.e. for step j, the step length s_j is the length of the step vector between location j+1 and location j:

$$\vec{s_j} = l_{j+1} - l_j$$

The turning angle τ_j between two consecutive step vectors, $\vec{s_j}$ and $\vec{s_{j+1}}$, is measured as:

$$\tau_j = \arccos(\vec{s_j} \cdot \vec{s_{j+1}} / |\vec{s_j}||\vec{s_{j+1}}|)$$

which gives values between 0 and π (0° and 180°) for no turn and for double-backing, respectively. Therefore, while the movement is measured in 3D and not as a 2D projection, I do not distinguish between left-hand turns and right-hand turns (where angles would range between 0 and 2π). This is different to some 2-dimensional trajectory analyses, e.g. [46], as in 3D space it is ambiguous which turn is left-handed and right-handed and there is no

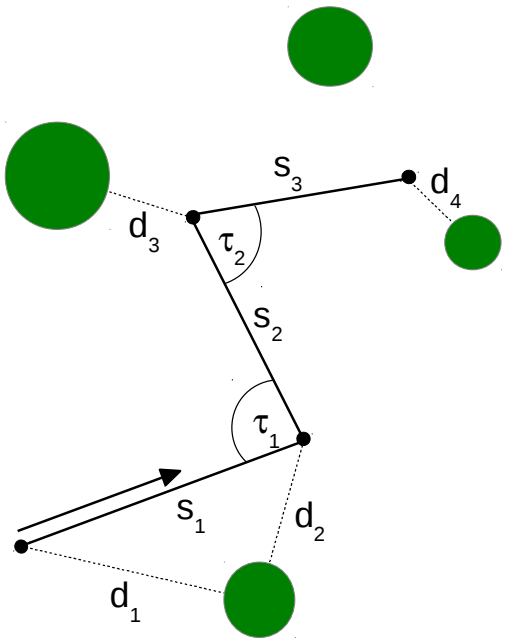

Figure 3.1: The definition of T cell trajectory parameters. The green discs represent DCs, the black dots represent detected T cell locations, and the arrow indicates the direction of T cell movement. Steps: s; turns: τ, distances of the T cell to the nearest DC: d.

biological or mathematical reason to make such a distinction. This also provided convenience in further analysis, where the angle values were linearly rescaled to values between 0 for 0° and 1 for 180°. Note that both these metrics depend on the scanning interval, which I will discuss in detail further, and is one of the main focus points of chapter 4.

To explore various models of directed migration of T cells towards DCs, the distance (d in Fig.3.1) to the surface of the nearest DC was calculated at the beginning of each step. Surface distance, rather than centroid distance, was chosen as the DCs vary substantially in size. The surface was estimated as the surface of a sphere centred on the centroid of the detected DC with a diameter estimated automatically by the Imaris software.

3.3.3 'Null' models

First, I formulated baseline models with no covariates, defining minimally informative priors and likelihoods that reflect the theoretically possible parameter values and that match the data well. These will be referred to as null models and can be used to analyse the distributions of turning angles and step lengths and compare these between treatments.

Perhaps more importantly, they serve as a baseline to judge the appropriateness of more specific models that include covariates, to assess whether these more specific models are justified over the baseline ones, i.e. whether they better explain cell behaviour. These null models correspond to model numbers 1-3, 7, 14-16, 24, 33-35 and 37 in Fig. 3.2 in the Results section.

I considered step lengths to be drawn from a Weibull distribution:

$$s \sim Weibull(a, b)$$

This notation means that the density function of step lengths is a Weibull distribution with parameters a and b. Parameter a is also known as the shape parameter and b as the scale parameter – although various alternative parameterisations are also used. Apart from an obviously good fit of this distribution to our data, there also are theoretical and technical justifications

and advantages of choosing this distribution, which are discussed in [46].

Definitions of the Weibull probability density functions slightly vary in different literature, and in JAGS, the density function $dweib(v, \lambda)$ is defined in the form:

$$W = v\lambda x^{(v-1)} \exp(-\lambda x^v)$$

To prevent confusion, note that this is different to the definition of Weibull distribution in R and some other literature. In this alternative formulation, the probability density function W_2 is:

$$W_2 = a/b(x/b)^{(a-1)} \exp(-(x/b)^a)$$

The shape parameters a and v are equivalent, but the scale parameter b differs from scale parameter λ.

The beta distribution was used for turning angles as these values are bounded to 0,1 and the beta distribution is a very flexible one:

$$\tau \sim Beta(\alpha, \beta)$$

The probability density function is:

$$B = \frac{x^{(\alpha-1)}(1-x)^{(\beta-1)}}{\mathbf{B}(\alpha, \beta)}$$

Where $\mathbf{B}$ is the beta function.

3.3.4 The effect of priming

I ran the null models for turns, steps and also for both of these parameters in combination. First, data from both naive and primed animals were pooled. Then, models were fitted with data separated by 'treatment', where movement parameters would come from different distributions for these two scenarios, to make a distinction between primed and naive T cells. This serves to test statistically whether movement of primed and naive T cells differs, i.e. whether

the latter ('treatment-separated') model proves to be better. All the models from this point on were fitted for naive and primed data separately, unless stated otherwise.

3.3.5 Speed-mediated 'gradient' taxis

This 'gradient taxis' model explores the possibility that taxis is mediated through the action of DCs on the speed of T cells. This could be mediated by a gradient of chemokines, for example chemokine CXCL10, as discussed in the introduction following from the findings in [41]. The T cell step length s would then be a smooth function of the distance to the nearest DC:

$$s = f(DCdist)$$

Similar to [46], I modelled this as a linear dependence of the scale parameter of the Weibull distribution of step lengths on DCdist:

$$b = m_1 + m_2\, DCdist$$

The intercept (m_1) and coefficient (m_2) of the linear function are then estimated by the model. These linear models for speed-mediated taxis are models numbered 4 and 8 in Fig. 3.2.

As the strength of spatial effects mediating interactions rarely scales linearly and is likely to exhibit an asymptotic behaviour (for example the chemokine concentration as a function of distance from the source – the DC), I also tested another functional dependence of speed on $DCdist$, in the following form:

$$b = m_1 + m_2\, \tanh(m_3\, DCdist)$$

This is proposed in [47], as a model for the preferential movement towards or away from a centre of attraction. As this function is more flexible, and has an asymptote, it is likely to provide a better fit than a linear model. This corresponds to models 5 and 9 in Fig. 3.2.

3.3.6 Turn-mediated 'gradient' taxis

Alternatively, chemokines may be affecting the turning behaviour of T cells in a similar fashion to the previous model, so that the turning angle τ is:

$$\tau = f(DCdist)$$

Unlike in the case of the Weibull distribution, neither of the parameters α and β for the beta distribution have a clearly dominant effect on the location (mean turning angle) of the distribution, therefore I ran 2 separate models, one for each of these parameters:

$$\alpha = m_1 + m_2\, DCdist$$

$$\beta = m_1 + m_2\, DCdist$$

This means that in these two options, one of these was modelled as a function of DCdist and the other one was unconstrained so that the optimal value could be found under the constraint imposed on the first one. Theoretically, these two forms should not differ much and in each case the MCMC algorithm should find the optimal solution - but in the eventuality that this would not be the case, I included both these options in the model selection to assess which of them performed better. These are models 17, 18, 25 and 26 in Fig. 3.2.

Same as I did for the step lengths, I also tested models in the form:

$$\alpha = m_1 + m_2\, \tanh(m_3\, DCdist)$$

and

$$\beta = m_1 + m_2\, \tanh(m_3\, DCdist)$$

These are models 19, 27 and 28 in Fig. 3.2.

3.3.7 State probability models

A taxis towards DCs might not necessarily be mediated by a 'smooth function' of distance on speed or turning angles of T cells. An alternative model is that T cells can be in different movement states with different speed and different turning behaviour, i.e. exploratory versus directed towards a nearby DC, and that the probability of being in these states is affected by the proximity to the nearest DC.

In this model, T cells can be in two states characterised by different parameters a, b for the Weibull distribution of steplengths and α, β parameters for the beta distribution of turning angles. The probability of being in these two states is modelled as a function of the distance to the nearest DC. This is achieved by defining the probability of being in state 1 as:

$$p_1 = \exp(m_1 + m_2\, DCdist)/(1 - \exp(m_1 + m_2\, DCdist))$$

This inverse logit function transforms the linear function of $DCdist$, which can theoretically take real number values $(-\infty, \infty)$, to a range $(0, 1)$, i.e. the range for the probability.

The probability of being in state 2 is then complementary to p_1:

$$p_2 = 1 - p_1$$

Thus, T cells can theoretically be in either of these two states at any given time, but they are increasingly likely to be in one of these states as they approach their nearest DC. This is an alternative form of taxis to the 'gradient taxis' models in sections 3.3.5 and 3.3.6, where steps and turns were coded directly as continuous smooth functions of this distance. These are models 12, 13 and 38 in Fig. 3.2, denoted with an affix 'probab'.

3.3.8 Interaction models with interaction threshold distance

In these 'interaction models', T cells are assumed to switch deterministically between states when they traverse a certain 'interaction threshold' distance from DCs (variable *thresh*). This threshold was coded as an unconstrained parameter to be estimated by the model. This corresponds to a situation where there is no action of DCs on T cells at distance (e.g. chemotaxis), but once T cells once they approach to a certain distance to a DC, an interaction is initiated, which results in a switch to a different movement state. Therefore, in contrast to the state probability models, this corresponds to a simpler 'deterministic switch' behaviour with a 'sharp' threshold between the two movement states.

For $DCdist \geq thresh$:

$$s \sim Weibull(a_1, b_1)$$

$$t \sim Beta(\alpha_1, \beta_1)$$

For $DCdist < thresh$:

$$s \sim Weibull(a_2, b_2)$$

$$t \sim Beta(\alpha_2, \beta_2)$$

Similar to the state probability model, this model was run for steplength and turn both in isolation and together. These are models 6, 10, 11, 20-23, 29-32, 35 and 36 in Fig. 3.2, denoted with an affix 'interact'.

3.3.9 SSM implementation and prior distribution choice

In these Bayesian models, prior distributions are updated using data likelihood to generate posterior distributions. Therefore I will rationalise here the prior distribution and likelihood choice, and describe the details of model implementation. Convergence assessment and model selection are discussed below in sections 3.3.10 and 3.3.11. The details provided here are sufficient to reproduce the approach taken, but more discussion and detail can be found in [46] – an animal movement study which inspired this approach. Some of the technical details described below were also inspired by the methodology presented in [47].

The models were implemented in JAGS version 3.4.0 (Martyn Plummer, http:// mcmc-jags.sourceforge.net/) within R through the runjags package (Matt Denwood, https://cran.r-project.org/web/packages/runjags/index.html).

The prior distributions selected for the parameters of the distributions describing the measured values were minimally informative, to allow the exploration of a wide range of values. For parameters that can take real-number values, a Normal distribution with mean 0 and variance of 100 was used as a prior. For parameters that can only take positive real-number values, a gamma distribution with both parameters (shape and scale) equal to 0.001 was used. Both of these define extremely broad density functions, thus being minimally informative and resulting in data-dominated posterior distributions.

3.3.10 Model comparison and selection

By comparing these alternative models, we are comparing the hypotheses of undirected movement to chemotaxis (or other form of action at distance, for example mediated by DC dendrites) and to an undirected movement with cell interaction.

The model quality in terms of explaining the data was compared based on the deviance information criterion (DIC). Similar to AIC widely used in more conventional statistics, this quantifies the goodness-of-fit and penalises for complexity, so that the simplest models that fit well are selected as the best models (with the lowest DIC). For two models to be considered to be different, a difference in DIC (δDIC) of at least 5 is required. A safer criterion, where a

model is almost certainly better than another one, is for a $\delta DIC > 10$. The DIC values are data-dependent and therefore can only be compared within a group of models based on the same data.

3.3.11 Model convergence

MCMC is a stochastic algorithm – the time it takes to reach convergence, the errors associated with the estimated parameters, and even the final solution (parameter values) can generally vary even if the model is run repeatedly with the same parameters. The achieved solution can also be sensitive to the starting values. The model can converge to a 'local' solution which is inferior to the best global solution, especially if the priors or starting values are too restrictive. This can be minimised by choosing minimally-informative priors and running several chains with over-dispersed starting values.

All models were run in 3 parallel chains with over-dispersed starting values, and the convergence was assessed based on the Gelman-Rubin statistic, which compares variance between and within the chains and asymptotically approaches one as chains converge. Sufficient convergence was considered to have been reached for values below 1.05. The trace plots of individual parameters (values plotted throughout the model iterations) were always visually checked for convergence, and the initial samples before reaching convergence ('burn-in') were discarded.

Where possible, I tried to run a sufficient number of iterations to minimise MCMC sampling error so that it would be less than 5% of the total standard deviation (SD) for each parameter, although this is not crucial as this had little effect on the overall measure of model quality used for model comparison and selection (DIC – section 3.3.10) and in most of the models, the actual values of most of the parameters were of little interest. In a few cases, the final MCMC sampling errors obtained were larger than 5% of the total SD, as the chains progressed with a large variation so that obtaining smaller MCMC errors was computationally prohibitive due to the very large number of iterations required.

A common problem with mixture models (with multiple states) is label switching, where parameters for different states are not entirely distinguished –

i.e. they can switch values throughout the iterations or can simply have different values for different chains, so that their labels (state assignments) differ between chains. This is due to the fact that high likelihood can in principle be achieved for any permutation of labels other than the one corresponding to a unique solution under full convergence. A common method to prevent this is by prior ordering, where finite differences between states for selected parameter values are explicitly encoded – thus imposing a certain numerical value ordering of the parameters. I utilised prior ordering in the following form. For step lengths, the scale parameter b was forced to be higher in one state than the other. As we do not know what the direction of this difference is between states in terms of distance of T cell from the nearest DC (and therefore should not impose this *a priori*), this difference was coded in both directions consecutively (i.e. b for state 1 both higher and lower than b in state 2), to compare which model would be superior (through DIC model selection) – this would not generally be necessary, but as the two states are coded as 'near' and 'far' from nearest DC, this needs to be performed. For turning angles, the same was performed for parameters α and β.

Despite this, some of the models did not converge within reasonable time, which is not uncommon for these types of models. Non-convergence does not mean that the model is inferior, but simply means than no unique solution was found within the given time for the given model formulation and starting values – not that there is none. It is also likely in my models that there are multiple solutions with similar likelihood , so the chains will be 'unstable'. For example, some of the models that did not converge provided an improvement over corresponding null models (lower DIC), which indicates that there is a better solution than the null model within the scope of the given model, but it could not be identified due to non-convergence.

3.4 Results

A summary of all the models that converged is presented in Fig. 3.2, divided into relevant groups. 'Taxis' denotes models with smooth function 'gradient taxis' effect of distance to the nearest DC on T cell speed or turning angles, 'interact' denotes the interaction models with interaction threshold distance to DC, and 'probab' denotes models with probabilities of being in two different states as a function of the distance to nearest DC. Models denoted 'step+turn' use both step length and turning angle to define behavioural states of T cells. Affix 'opp' indicates that prior ordering was performed in the opposite direction than in the relevant model without the affix (as discussed in section 3.3.11). In this case, state one was first coded as having a lower value of a given parameter (e.g. b for step lengths, i.e. **higher** step length mean), and then, in the 'opposite' model, denoted 'opp', the value was set to be higher for state 1. I then selected the model which was superior (in terms of DIC). Affix alpha and beta for the models for turning angles indicate which of these two parameters were modelled as a function of $DCdist$, and affix pooled means that naive and primed data were pooled together for the given model (i.e. no distinction between treatment was made).

Models were selected based on the difference in DIC compared to a relevant null model (δDIC_0). A column labelled 'quality' denotes how well the models perform: 0 - null model, * - similar to null ($\delta DIC_0 \leq 10$), ** - improvement to null ($\delta DIC_0 > 10$), *** - best models within a group (with a difference of DIC less than 5 from each other).

3.4.1 'Null' models

The posterior distributions obtained were in good agreement with data (Fig. 3.3), indicating that Weibull distribution for step lengths and beta distribution for turning angles are reasonable choices.

#	model	DIC	δDIC_0	QUALITY
1	step_pooled	99178.9	0	0
2	step_treatment	72640.6	-26538.3	***
3	step_naive	43367.6	0	0
4	step_naive_taxis_lin	43368.5	1	*
5	step_naive_taxis_tanh	43268.9	-98.7	**
6	step_naive_interact	43245.7	-121.8	***
7	step_primed	54317.3	0	0
8	step_primed_taxis_lin	54312	-5.3	*
9	step_primed_taxis_tanh	53846.1	-471.3	***
10	step_primed_interact	53846.3	-471	***
11	step_primed_interact_opp	54138.8	-178.5	**
12	step_primed_probab	85610.2	31292.9	
13	step_primed_probab_opp	55686.8	1369.5	
14	turn_pooled	-612.6	0	0
15	turn_treatment	-878.8	-266.2	***
16	turn_naive	-756.6	0	0
17	turn_naive_taxis_lin_alpha	-755.8	0.8	*
18	turn_naive_taxis_lin_beta	-757.4	-0.8	*
19	turn_naive_taxis_tanh_beta	-824.3	-67.7	***
20	turn_naive_interact_alpha	-824.6	-68	***
21	turn_naive_interact_alpha_opp	-824.4	-67.8	***
22	turn_naive_interact_beta	-770.7	-14.1	**
23	turn_naive_interact_beta_opp	-827.2	-70.6	***
24	turn_primed	-114.4	0	0
25	turn_primed_taxis_lin_alpha	-119.4	-5	**
26	turn_primed_taxis_lin_beta	-119.9	-5.5	**
27	turn_primed_taxis_tanh_alpha	-224.3	-109.8	**
28	turn_primed_taxis_tanh_beta	-212.8	-98.4	**
29	turn_primed_interact_alpha	-238.6	-124.2	***
30	turn_primed_interact_alpha_opp	-212.9	-98.5	**
31	turn_primed_interact_beta	-224.5	-110.1	**
32	turn_primed_interact_beta_opp	-237.9	-123.4	***
33	step+turn_pooled	90167.9	0	0
34	step+turn_treatment	88520.1	-1647.8	***
35	step+turn_naive	38656.7	0	0
36	step+turn_naive_interact	38463.8	-192.9	***
37	step+turn_primed	49863.6	0	0
38	step+turn_primed_probab	52363.9	2500.3	
39	step+turn_primed_interact	49295.1	-568.5	***

Figure 3.2: A summary of all the models that converged.

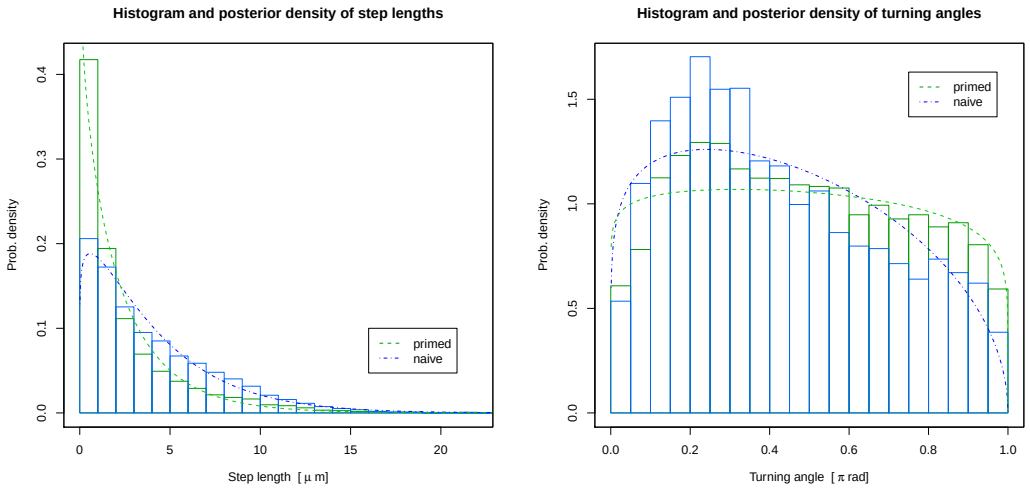

Figure 3.3: Histograms and posterior density distributions for T cell step lengths and turning angles in the naive and primed conditions.

3.4.2 The effect of 'treatment' – naive vs primed

As can be seen in Fig. 3.3, naive cells perform longer steps compared to primed cells, and their distribution of turning angles is more flat, with more turns close to zero (straight movement) and some more double-backing (turns close to one), compared to naive cells. All of the models run to test for difference between naive and primed cells confirmed a significant difference (Fig. 3.2, models 1, 2, 14, 15, 33, 34.).

3.4.3 Models of directed T cell movement

If there are correlations between T cell migratory behaviour and their distance to the nearest DCs, this might indicate either a chemotaxis, where T cells follow a gradient of chemokines by changing their speed or turning behaviour, or alternatively a mechanism of guidance towards DC where T cells far from DC may be in an 'exploratory' mode and in close proximity to DC they may switch to an 'interacting' or alternatively a 'thorough search' mode. Including the distance to nearest DC as a covariate for step lengths and turning angles in my models, and using DIC for model selection, I identified models best fitting the data.

3.4.4 Smooth function taxis ('gradient taxis')

The 'gradient taxis' models suggest that there is a change in turns and steps as the T cells approach their nearest DC.

For naive cell step lengths, the best quality 'gradient taxis' model is model 5, where step length is linked to $DCdist$ via a hyperbolic tangent function. However, the coefficients estimated by the model are such that any considerable change is limited only to a distance very close to the nearest DC (below 0.1 μm). For naive cell turning angles, model 19 is the best from the relevant group of 'gradient taxis models'. Similar to step lengths, this change occurs around 0.1 μm from the nearest DC. The following plot (Fig. 3.4) shows how the scale parameter (b) of the step length distribution, and the β parameter of the turning angle distribution, change with distance to the nearest DC. This clearly indicates that cells are interacting with DCs and not following a long-range chemokine gradient, as the range of such action would be expected to be microns or most likely tens of microns (the mean distance of a naive T cell from the nearest DC in our data is 18.9 microns). The increase in the scale parameter b (for the definition of the Weibull distribution which we follow here) corresponds to a decrease of the mean step length. This indicates T cell-DC interaction where T cells move relatively slow compared to when they are not interacting. These results also indicate that the interaction model, where T cells change behaviour once they cross a (very low) threshold distance to the nearest DC, will probably be an equally good or better model in terms of DIC.

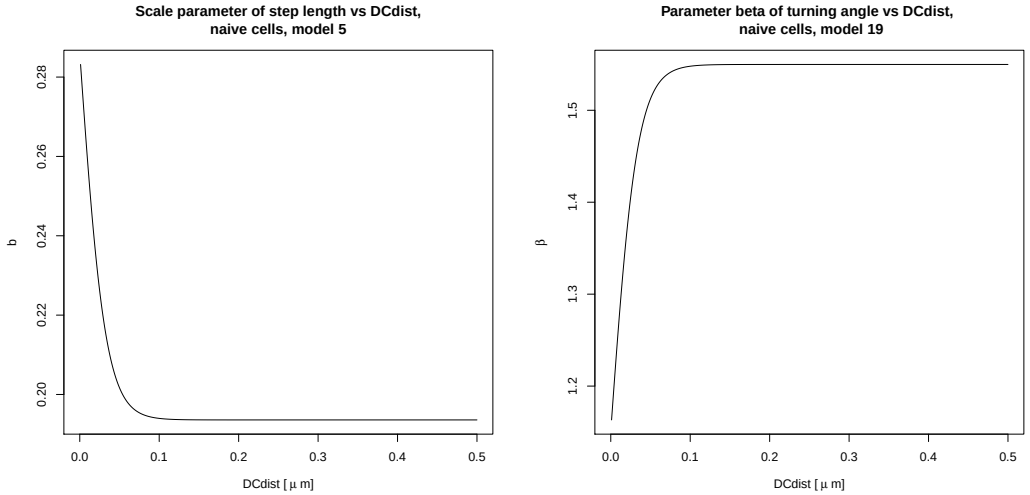

Figure 3.4: The dependence of the scale parameter of the Weibull distribution of step lengths, and of the β parameter of the beta distribution of turning angles, on the distance to the nearest DC, for naive cells. Models 5 and 19.

For primed cell step lengths, the situation is similar. Model 9 is the best gradient taxis model for step lengths. For turning angles, model 27 is the best one. Fig. 3.5 shows how these parameters scale with distance to the nearest DC. Again, this behaviour indicates interaction rather than taxis – the range at which any considerable change happens is again around 0.1 μm. The mean distance of a T cell in the priming scenario from the nearest DC in our data is 15.0 microns. Note that in this case, the model for the α parameter of the turning angle (rather than β as in the case of naive cells) was the best model that converged. The value of the function is therefore declining with DCdist rather than rising – however, β parameter actually also declines with DCdist for primed T cells (confirmed in model 28).

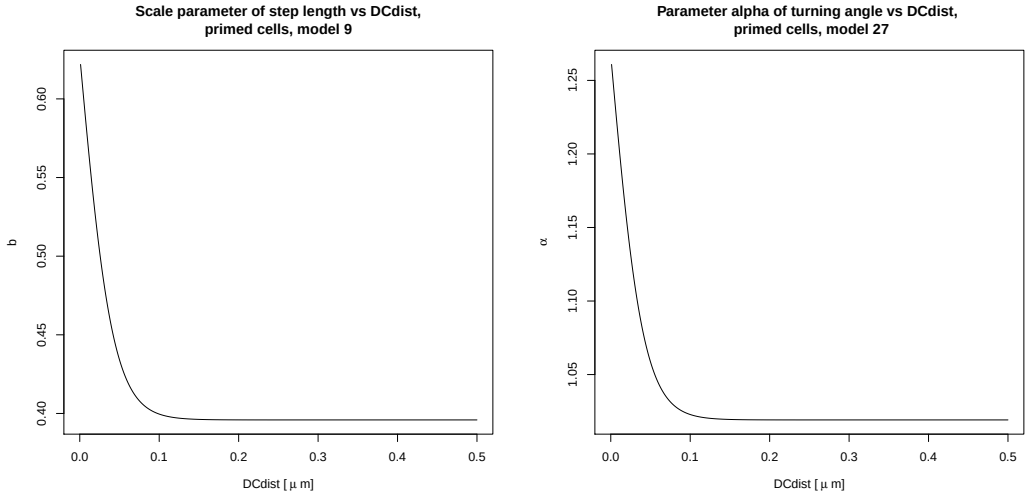

Figure 3.5: The dependence of the scale parameter of the Weibull distribution of step lengths, and of the α parameter of the beta distribution of turning angles, on the distance to the nearest DC, for primed cells. Models 9 and 27.

3.4.5 State probability models

The 'state probability' models did not converge for naive cell step lengths and turning angles. Note that non-convergence does not mean that the model is inferior – it conveys no information about model quality. For primed cells, these models converged only for step lengths, but were very inferior compared to the null model (models 12 and 13). As mentioned in the Methods in section 3.3.11, a common problem with mixture models is label switching, preventing convergence. These models have a larger number of parameters than the other models and are generally less constrained, which is likely to make achieving convergence more difficult.

The models taking into account both step lengths and turning angles in the definition of movement states are novel in considering both these parameters together. Although theoretically they have the potential for better describing the T cell behaviour, resulting in a higher sensitivity of detecting different movement modes, this model converged only for primed cells, but had a poor fit to the data (model 38) and was outperformed by the interaction model (model 40).

It appears that these discrete-state probability models are more prone to converge problems. This is perhaps due to the fact that the change in movement parameters of T cells only happens at an extremely small distance to a DC (which was inferred in the 'smooth gradient' models to be under 0.1 μm)), which separates the two movement states in a fairly clear, discrete way (Fig. 3.4-3.5). Therefore, the interaction models, where a 'state switch' happens at a fixed threshold distance from a DC, will probably be better candidate models, and will represent the data well.

3.4.6 Interaction (threshold) models

In these models, state 1 is a state for cells 'far' from DC ($DCdist \geq thresh$), and state 2 is a state for cells closer to their nearest DC than the threshold. Therefore, state 1 can be thought of as 'exploring' and state 2 as 'interacting to DC'.

In all categories of models of directed movement, the interaction models are the highest quality models, or among the highest quality ones – in case of primed step lengths, the interaction model (model 10) is equivalent in quality to the hyperbolic tangent taxis model (model 9). It is also very similar to the tangent models for naive turning angles (compare model 23 to models 19, 20 and 21). This is presumably because the hyperbolic tangent function is very flexible and allows almost the same (nearly discrete) behaviour as the interaction model, as can be seen in Fig. 3.4 and 3.5.

The best model for naive step lengths is model 6. The inferred parameters are:

State 1:

$$a_1 = 1.14$$

$$b_1 = 0.19$$

State 2:

$$a_2 = 1.00$$

$$b_2 = 0.35$$

The threshold is 0.020 μm (all values are rounded to two significant digits after decimal point). This is indistinguishable from zero, as such a low value is well below the experimental error in the estimated DC diameter and locations of cell centroids (and cells are not perfectly spherical). This supports an interaction model over a gradient taxis one. The fact that $b_1 < b_2$ indicates that T cell speed is lower during interactions with DCs.

The best model for naive turning angles is model 23, with the following parameters:

State 1:

$$\alpha_1 = 1.18$$

$$\beta_1 = 1.56$$

State 2:

$$\alpha_2 = 1.07$$

$$\beta_2 = 1.09$$

Again, the threshold is very low, 0.0092 μm.

Almost the same DIC was obtained for models 20 and 21, as the parameter values were very similar to the best model (model 23). The fact that both these models, with a difference in α between states in opposite directions, perform better than the null model might initially seem counter-intuitive. However, due to the flexibility of the model, the values of α for these models were almost exactly the same (the difference between states was minimal in both cases), and the differences in values of parameter β then account for the good fit to data compared to the null model.

The threshold is similar in the model for step lengths and the model for turning angles, meaning that both T cell speed and turning angles change

abruptly at the same distance from DC. This indicates that there does not seem to be a different mechanism acting on the turning behaviour of T cells and on their speed. This also indicates that the model where both steps and turns are included in the definition of states (let us call this a 'complete model') should provide similar results both in terms of parameter values and the estimated threshold (and indeed does). A graphical comparison of the distributions for the two movement states will therefore be provided below for the complete model.

For primed cell step lengths, model 10 is the best one, together with the hyperbolic tangent taxis one (model 9). The inferred parameters are:

State 1:

$$a_1 = 0.93$$

$$b_1 = 0.40$$

State 2:

$$a_2 = 0.94$$

$$b_2 = 0.62$$

The threshold is 0.0080 μm.

The fact that $b_1 < b_2$ indicates that same as for naive cells, primed T cell speed is lower during interactions with DCs.

For primed cell turning angles, the best models are models 29 and 32. The parameters for model 29 are:

State 1:

$$\alpha_1 = 1.04$$

$$\beta_1 = 1.17$$

State 2:

$$\alpha_2 = 1.19$$

$$\beta_2 = 1.05$$

The threshold is 0.082 μm.

Model 32 is indistinguishable in terms of DIC, as the parameters are almost exactly the same as for model 29 (the difference in α is in the opposite direction to the difference in β in both models, which allows them to converge to the same solution). The parameters for model 32 are:

State 1:

$$\alpha_1 = 1.04$$

$$\beta_1 = 1.17$$

State 2:

$$\alpha_2 = 1.21$$

$$\beta_2 = 1.06$$

The threshold is 0.082 μm.

The 'opposite' models (30 and 31) also provided a better fit than the null model, as each of them has freedom in one of the parameters. Again, the threshold in the turning angle model is similar to the one in the model for step lengths, indicating that the complete model where both steps and turns are included in the definition of states should provide similar results. The graphical summary will therefore be provided for the complete model.

The parameters for the complete interaction model for naive cells (36) are:

State 1:

$$a_1 = 1.14$$

$$b_1 = 0.19$$

$$\alpha_1 = 1.18$$

$$\beta_1 = 1.56$$

State 2:

$$a_2 = 1.01$$

$$b_2 = 0.36$$

$$\alpha_2 = 1.07$$

$$\beta_2 = 1.08$$

The threshold is 0.0049 μm.

Figure 3.6 summarises this graphically.

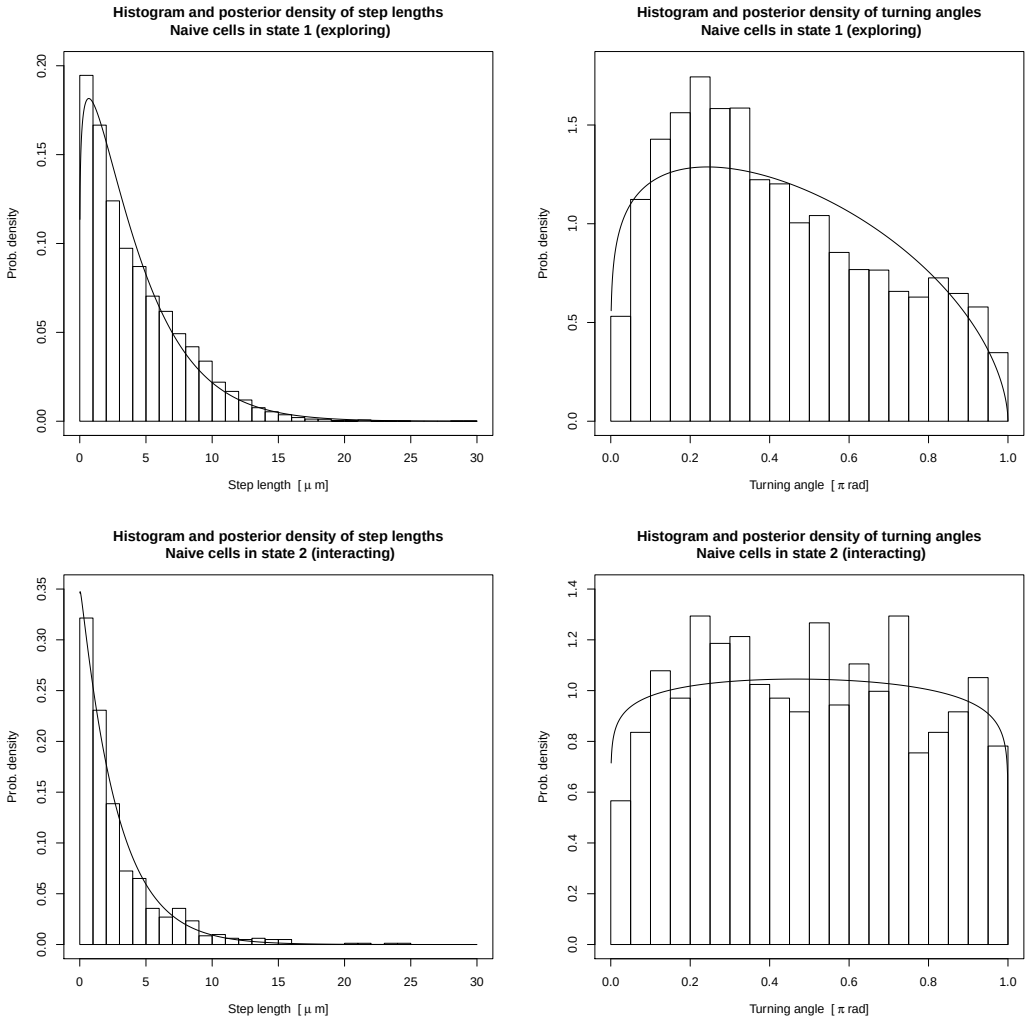

Figure 3.6: A comparison of naive T cell turning angle and step length distributions in state 1 (exploratory) and state 2 (interacting).

Step lengths are larger for the exploratory state, corresponding – expectedly – to higher speed. Turning angles seem to be skewed towards 0 (low turns, corresponding to persistence in the current direction) in the exploratory state.

The parameters for the complete interaction model for primed cells (39) are:

State 1:

$$a_1 = 0.93$$

$$b_1 = 0.41$$

$$\alpha_1 = 1.04$$

$$\beta_1 = 1.17$$

State 2:

$$a_2 = 0.95$$

$$b_2 = 0.63$$

$$\alpha_2 = 1.19$$

$$\beta_2 = 1.05$$

The threshold is 0.0067 μm.

Figure 3.7 summarises this graphically.

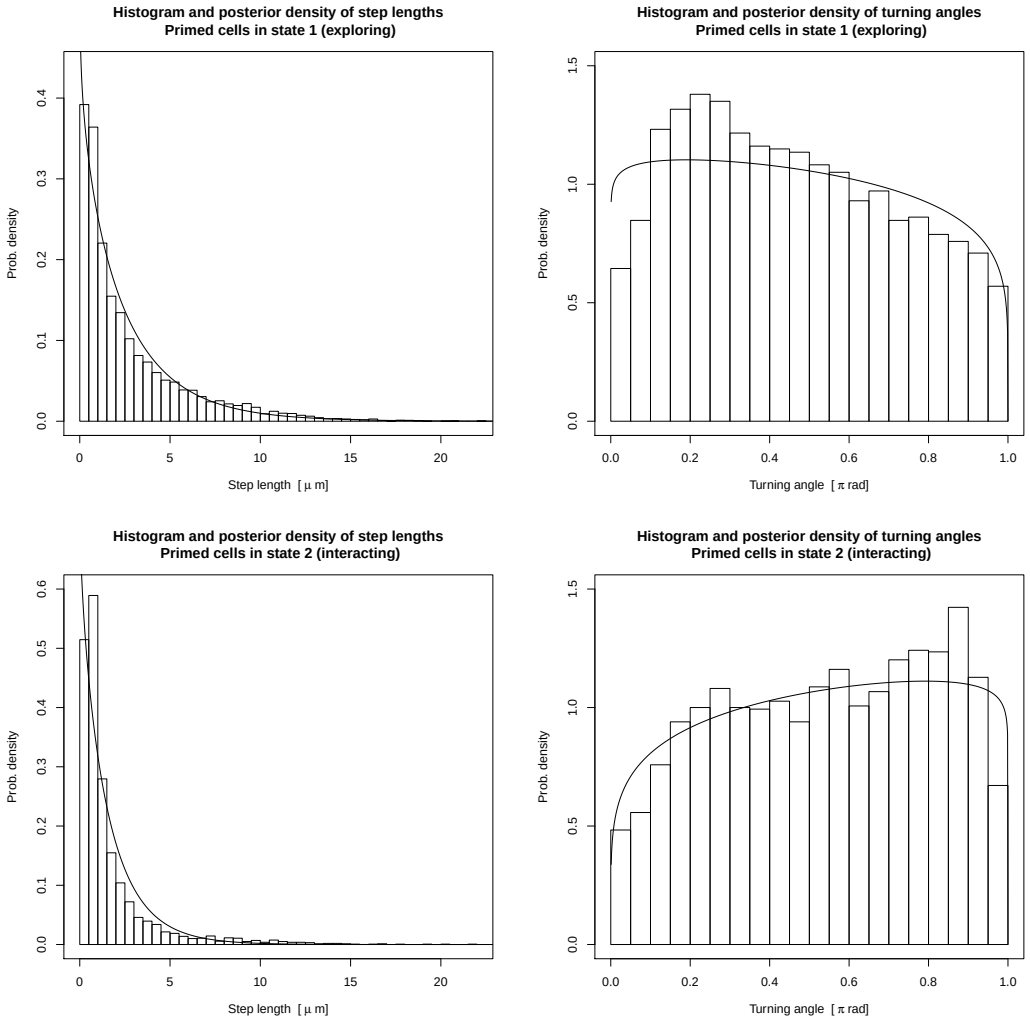

Figure 3.7: A comparison of primed T cell turning angle and step length distributions in state 1 (exploratory) and state 2 (interacting).

Same as in the case of naive cells, step lengths of primed cells are larger for the exploratory state, corresponding to higher speed and turning angles seem to be skewed towards 0 in the exploratory state. In the interacting state, the turning angles are slightly skewed towards higher values – however, this might not reflect the actual movement of the cells, rather the movement of DC membrane plus an error due to the uncertainty of inferring the location of T cell centroids, which for slowly moving cells will be relatively large, as I will discuss later.

3.4.7 The speed of interacting and 'freely migrating' cells

The analysis strongly suggests a model where T cells move unaffected by the proximity of DCs until they physically encounter them (all the threshold values estimated are indistinguishable from zero), and then interact. It is well known that the mean speed of T cell movement decreases during priming, but it was unclear how much of this decrease was caused by interaction and how much by actually decreased migration speed of cells not interacting with DCs. I examine here how many cells are in state 1 and state 2, and what the difference is in their mean speed, using the threshold distance to filter cells into states 1 and 2.

The mean step length of all naive cells pooled is 4.03 microns. In naive data, 9% of cells were classified as interacting ($DCdist < thresh$). The mean step length of naive cells in state 1 (exploring) is 4.14 microns. The mean step length of naive cells in state 2 (interacting) is 2.88 microns. The speed of interacting naive T cells is therefore approximately 70% of the speed in the exploratory state.

The mean step length of all primed cells pooled is 2.55 microns. This confirms the previous findings of the decrease of T cell speed in primed state [22, 21, 23]. In primed data, expectedly, the proportion of interacting cells increased. The proportion of primed cells classified as interacting was approximately 23%. The mean step length of primed cells in state 1 (exploring) is 2.79 microns. The mean step of primed cells in state 2 (interacting) is 1.71 microns. The speed of interacting primed T cells is approximately 61% of the speed in the exploratory state.

The imaging interval was 45 s, so estimates of mean cell instantaneous speeds (in $\mu m s^{-1}$) can be obtained by multiplying by 1.33 s^{-1} – although this is likely to be slightly biased due to the discrete-time nature of the microscopic imaging.

3.5 Discussion

I have shown how state-space models can be applied to T cell movement, and compared several alternative models of movement based on their support by imaging data. The models presented are in no way exhaustive, and it is likely that the framework could be successfully further applied in this field. For example, taxis models where cells are moving along the FRC network could be formulated and tested using imaging structural data on the FRC network geometry. Models can also be formulated in which behavioural states of cells depend on other variables such as location within tissue, concentrations of cytokines, or the proximity to other cell types, and more than two behavioural states can easily be modelled. An inherent advantage of the Bayesian approach is that information about a certain system can easily be updated iteratively - by utilising the results of one study as prior information for a later study - which is certainly advantageous in a field where large amount of data have been collected.

The 'complete models', using both step length and turning angle to define motility state of T cells, have a potential to better describe the data and be more powerful in detecting potential effects than models utilising only one of these variables - particularly where data is scarce. In this case, both the step length and turning angle models were sufficient to distinguish between the two movement states.

Possibly the most interesting finding is that there appears to be no form of chemotaxis or other mechanism guiding CD-4+ T cells towards DCs. Undirected movement through LN seems to be sufficient for T cells to locate antigen-bearing DCs efficiently. It is possible that the continuous program of lymphocyte circulation between LN and other somatic tissue is an optimal mechanism and serves to maintain the balance between immunity and self-tolerance by ensuring continuous surveying of self- and foreign antigens. It is also possible that chemotaxis only occurs at a very short distance. There is a fairly high density of DCs in a LN in the sense that there are usually several DCs at a similar distance to a T cell, so that the concentration of chemokines might be fairly uniform throughout most of the LN, and chemotaxis towards one of the DCs

would then possibly only occur at a very short distance, when this DC becomes the 'dominant' attractor. Therefore it might be impossible to detect chemotaxis without imaging at a much finer temporal resolution (and possibly also spatial). However, for the same reason (relatively high DC density), it is also possible that there is no need for chemotaxis as an undirected movement might be an efficient mechanism for T cells to encounter DCs with sufficient frequency. The mean distance at any given moment from a T cell to the nearest DC in our data is 18.9 μm in the naive case, and 15.0 μm in the primed case. From the results presented earlier in this chapter, the estimated speed of freely-moving T cells is 5.5 μm/s in the naive case and 3.7 μm/s in the primed case. Therefore, due to this high density of dendritic cells and speed of T cells, it indeed seems possible that an unguided migration is sufficient. Interestingly, [9] presented an idea that a chemotaxis of CD4+ T cells towards DCs in the LN might actually be a less effective mechanism than random walk, as T cells tightly clustered around DCs would spatially block the interactions of newly-arriving T cells with these DCs. Therefore, the frequency of unique cell contacts would actually be lower, decreasing the efficiency of antigen-presentation.

By distinguishing between interacting and exploring T cells, we clarify how much of the observed decrease in T cell mean speed during priming is due to interactions and how much is due to the actual decrease of instantaneous speed of the exploring T cells. The mean step length of all naive cells pooled was 4.03 microns. In naive data, 9% of cells were classified as interacting. The mean step length was 4.14 microns for exploring cells and 2.88 microns for interacting cells (approximately 70% of the speed in the exploratory state). The mean step length of all primed cells pooled was 2.55 microns. The proportion of primed cells classified as interacting was approximately 23%. This is, unsurprisingly, higher, as antigen-specific interactions with activated DCs are now taking place. The mean step length was 2.79 microns for exploring cells and 1.71 microns for interacting cells (approximately 61% of the speed in the exploratory state). This could reflect physically more stable interaction for primed cells compared to naive cells. We can see that in both scenarios, the interacting cells slow down significantly. It is obvious that the observed mean speed decrease in primed compared to naive scenario (down to approx. 63%) is caused not only by

the increased proportion of cells interacting, but also largely by the exploring, non-interacting cells also slowing down their migration (down to approx. 67%). The reason for this slowing down is currently unknown. It is possible that these slow cells are the ones that have previously undergone an interaction with DCs and have become activated. Another possibility is that this slowing-down has a function in regulating the T cell transit time through the LN – reducing the probability of premature exit of T cells from an inflamed LN, before these T cells up-regulate CD69 expression, which prevents their exit [48]. It would be of interest to infer whether this observed decrease in speed has a specific function in the adaptive immune response, or is for example simply a consequence of the changes in the LN environment following immunisation - e.g. the increased total density of cells.

It is also unclear what the differences in turning angle distributions for the two distinct states mean mechanistically (Fig. 3.6-3.7). For naive cells, turning angles are almost uniform in the interacting state – the measurements might have no or little biological significance here as the cells are not actively migrating in this state, and their observed movement is slow, so it is likely that their movement patterns are largely driven by random processes (i.e. movements of the DC membrane) - at least at the spatio-temporal scale allowed by the microscopic imaging. Another source of noise is due to the fact that the location of a T cell is inferred as the location of the centroid of the detected fluorescent area corresponding to the cell. As the shape of the T cell changes constantly, and the resolution of the imaging also begins to be a limiting factor at this small scale, there is obviously a relatively large error of this cell location measurement relative to the distance that the T cell actually moves within one imaging period (interacting T cells move slow). In the exploratory state, turning angles are skewed towards 0, corresponding to low turns, i.e. persistence in the current direction for the time-scale of the imaging period ($45s$). This could mean that imaging frequency is higher than the frequency of T cell turns, and thus the cells are often captured 'between turning points', where the deviation from their previous direction is small. Similarly to naive cells, turning angles of primed cells are skewed towards 0 in the exploratory state, although this is less pronounced. In the interacting state, the turning angles are slightly skewed towards higher

values. This indicates higher tendency to perform 'sharp' turns - meaning that primed T cells perform a more erratic movement during interaction with DCs than naive cells. Whether this has any biological significance is unclear, but this is perhaps interesting and warrants further investigation.

The apparent directional persistence in both naive and primed cells (which is lost when cells interact with DCs) could be driven by an intrinsic program ('internal clock driving persistence time'), or possibly by the physical structure of the fibroblast reticular network (FRC), in case that T cell movement is constrained to it - which is investigated in chapter 4. The potential role of the FRC network on the movement of T cells is worth further consideration. While the exact effect of the FRC network on T cell movement is still unclear, it is possible that T cell turns are dictated by this network - they may either turn when they collide or transiently interact with this network, or may be entirely confined to it and turns then occur on junctions in the network. If cells are constrained to an FRC network, and therefore the values of turning angles are imposed by this network and not driven by an intrinsic movement program, there is a possible mode of taxis that would evade this analysis. This would occur if the cells preferentially chose FRC fibres leading towards a nearby DC. Such type of taxis might remain undetected by this analysis, as the values of the turning angles would be unaffected (being fixed - dictated by the network).

Chapter 4

The geometry of the fibroblast reticular network and T cell movement patterns compared

The FRC imaging data for this chapter has been generated entirely by me. The T cell movement imaging data has been generated by me, Dr Robert Benson and Dr Agapitos Patakas. The analysis is entirely my own work.

The results have been submitted for publication.

4.1 Abstract

T cell surveillance of lymph nodes (LN) is critical for both homoeostasis and adaptive immunity. Although the fibroblast reticular cell (FRC) network has been shown to influence the movement of naive T cells in LN to some degree, the exact mechanism remains unclear and the movement is frequently modelled as a random walk. The effect of the FRC network on T cell movement following immunisation has not been experimentally studied, although there has been interest in the potential for FRC network structural changes after immunisation. If T cell movement is constrained by this network, these structural changes might account for some of the observed changes in T cell motility following immunisation. Accordingly, I employed mathematical models to combine measurements of T cell movement and fine-scale FRC network structure in both naive and immunised states in mice. This analysis supports a model of surveillance constrained to the network over an alternative model of random walk with persistence time. Surprisingly, a detailed characterisation of the FRC network structure shows that differences between networks in naive state and following immunisation are minimal, contrary to what would be expected given that the LN expand in volume substantially after immunisation. Strikingly, the mean length of the FRC network connections decreases after immunisation, suggestive of substantial and rapid network growth and remodelling rather than just stretching. Simulating T cell movement on the directly observed FRC networks describes T cell motility data more accurately than a random walk, further supporting the conclusions. The methodology also demonstrates that direct estimates of T cell turning angle and instantaneous speed from scanning microscopy are biased, which can lead to discrepancies between studies. I present a method for obtaining more accurate estimates, which is broadly relevant for all future studies where accurate estimation of motility parameters from scanning microscopy data is essential.

4.2 Introduction

For over a decade, multi-photon microscopy has been used extensively to obtain insight into immune cell migration and interactions on a fine spatio-temporal scale by generating high-frequency 3D videos [13, 5]. As T cell-APC search and subsequent cell interactions mediating antigen presentation in lymph nodes are two of the earliest and most crucial steps in establishing adaptive immune response, there is a continued interest in the mechanisms underlying these processes with the potential to modulate these for clinical benefit [8, 9].

A large amount of data has been collected, yet this impressive advance in ability to generate data has not been matched by similar progress in ability to analyse these data and generate predictive quantitative models. This is important for analysing and interpreting the data and generating hypotheses to motivate novel experiments. Comprehensive reviews of the experimental and quantitative efforts and current problems and limitations can be found in [13, 49, 36].

A frequent feature of imaging studies is the classification of T cell movement as some type of random walk, often with 'mean free path' [17]; another study [20] describes T cell speed as having cyclical fluctuations with a period of around 2 minutes and also reports that at shorter periods (<3 min), T cell displacements increases approximately linearly with time (with a speed of 10.7 μm/min), indicating that cells follow a 'mean free path' of 30 μm along any given trajectory. This is a result of examining plots of displacement versus square-root of time at a certain temporal range. While the movement matches random walk (diffusion) in this one characteristic over a certain range, this only provides a description of the movement from a narrow perspective and can lead to false conclusions - it does not permit the inference of the mechanism underpinning the generation of movement patterns, specifically, it does not prove that the movement is adequately described by a random walk [36, 37].

The LN is by no means a "free liquid" environment – it is supported by a scaffold of dense stromal network formed by several types of cells. These form distinct morphological and functional compartments, preferentially attracting different types of immune cells [31, 12], and performing a number of roles in

both maintenance of homeostasis and activation of lymphocytes in immune responses [50].

The dominant stromal component of the LN T cell zone is a dense network of fibroblastic reticular cells (FR cells or FRC), which are wrapped around extracellular products forming what is called a conduit system [51]. This conduit system has been shown to facilitate the transport of fluid from the efferent lymphatics to high endothelial venules [33]. It is capable of carrying various small molecules such as chemokines and even small antigens [33, 51].

The FRC also produce chemokines, perhaps most notably the CCL-19 and CCL-21. Both are ligands for CCR-7, which is expressed on T cells and activated DCs, and are important for movement and localisation of cells in the LN and the maintenance of T cell homeostasis [32, 34, 52]. The FRC network might hypothetically provide more efficient means of chemokine guidance than soluble chemokine gradients in extracellular liquid. A comprehensive review of stromal functions is presented in [50]. Given all these functions, the FRC and other lymphoid stromal components in general define LN both anatomically and functionally, and its further study is of both interest and potential practical use. The spatial structure of LN tissue is likely to be directly relevant to cell migration and interactions, however, little attention has been paid to this in the analysis and interpretation of T cell movement and antigen presentation.

The most detailed and direct study of the association of T cells with FRC and their movement along this network in naïve LN is [35]. Uniquely, the FRC network and T cells were imaged simultaneously *in vivo*, and the extensive imaging data in this study are a result of a painstaking histological and imaging effort. The presented videos seem to suggest an association between motile T cells and FRC network, however, a rigorous analysis needs to be performed and it remains unclear whether the FRC network dictates the entire trajectory or, for example, it is responsible only for T cells' turning behaviour and T cells associate with FRC network fibres only transiently. The effect of FRC network on T cell movement in the immunised state remains to be experimentally studied.

If T cells utilise the FRC network as a movement substrate, then changes in the network structure should affect the nature of T cell trajectories. This in turn

might affect the efficiency of T cell antigen search. Possible network structural changes could also explain some of the differences between the movement of naive and primed T cells.

The FR cells undergo changes due to inflammation, possibly in direct response to immune cell activation, as was shown for example in [53] – a cytometric and molecular study showing cellular activation and proliferation of blood vascular, lymphatic and FR cells, dependent on $CD11c^+$, T and B cells. It is also well known that LNs swell up during immunization – a visually obvious and generally accepted phenomenon [54, 55], but we know little about how this affects the fine-scale FRC network structure.

LNs increase in volume following immunisation [54, 55], which could be expected to cause structural changes in the FRC network. Yang et al. [55] concluded that activation leads to a network that is expanded but similar to that in the naive state in terms of fibre lengths and percentage of volume locally occupied by FRC. By contrast, a recent study [56] concluded that the FRC network simply stretches following immunisation.

In a detailed study which included lymph node imaging [57], FRC network remodeling in response to priming was described. This constituted a sub-compartmentalisation of LN after priming into 'nodular islands containing discrete B and T zones, enclosed by a single FRC layer'. I made a similar observation, but whether the cell-scale structure of the network changes – which would affect T cell movement on small scale as observed by microscopy – is not clear from this. The above-mentioned study also showed that FRC stimulate T cell and DC adhesion and migration, further supporting the network movement hypothesis.

A recent study [55] has confirmed a rapid response of FR cells to immunization *in vivo*: increase of cell size within 20 h and proliferation within 40 h of immunization. Most importantly for our purpose, this study included a partial analysis of the fine-scale structure of the FRC network to compare naive and activated LN. The total network length and volume occupancy in a given imaged area, and the average length of the FRC network segments were measured. The authors found no statistically significant difference between naive and activated LN and concluded that activation leads to an 'expanded

but similarly organised network'. It is possible, however, that other parameters of the network change which might affect T cell search for antigen.

Given all the available data, it seems very likely that the FRC network is crucial for the movement of T cells and its analysis. If that is so and T cells do not actually perform an unconstrained walk completely driven by an intrinsic motility program, this would have implications for the analysis and interpretation T cell movement, and potential applications where therapies could be targeted to manipulate this process. It is therefore important to further investigate the FRC network movement hypothesis, measure the fine-scale structural parameters of the network and determine possible differences between naive and primed LN networks.

There are many models of T cell movement in LN, e.g. [9, 38, 58], with relatively few taking into account the role of the FRC network [37, 59, 60]. While providing the first steps in quantitative approach to this problem, these models have limited value beyond reproducing some of the known characteristics of T cell movement. Of the studies that consider the FRC network in some way, none so far have utilised the real structure of the network to parameterise the models, instead using hypothetical networks. Also, little attention has been paid to the role of priming in this context.

A popular model is that of T cell random walk with persistence (free) time [39], motivated by imaging studies that used displacement-time plots to try to interpret T cell movement as a random walk. It is also a tempting model due to a possible underlying mechanism, as described for example in [9]: "This short term persistence... is an intrinsic property arising from establishment of T cell polarity by preferential formation of membrane protrusions on the leading edge of a moving cell...", a proposition based on an *in vitro* study of fibroblast migration [61].

In the random walk with persistence (free) time model, T cells follow straight paths for a given time (persistence time), after which they stop, change direction randomly, and so on. This is a simple and efficient descriptive model that reproduces some of the characteristics of the T cell imaging data, rather than a mechanistic one taking in account the role of the physical LN environment and predicting novel results that would motivate further experiments.

In my opinion the most useful model of T cell network movement is presented in [60]. The authors construct an *in silico* FRC network representation by joining points in three-dimensional space by edges, and model T cell movement on this structure. Although this network is hypothetical, some of its parameters can be adjusted to be loosely based on preliminary data. The network density for example was tuned so that average fibre length corresponded to previous experimental data [35], and a connectivity of three edges per point was based on the assumption that FRC network forms by fibres growing and branching in two. However, it is a difficult problem to formulate a tractable model and to tune all parameters according to data.

[60] explores three different modes of movement on a network; Brownian network motion, constant speed network motion and constant speed network motion with double-backing. By comparison to data from previous studies [17, 20, 22], the authors conclude that out of the three models, constant speed network motion is the most likely. The paper also mentions the important problem of the biasing effect of imaging frequency on the apparent T cell speed and turning angle estimates.

In this study I expand on previous work by generating and using imaging data on the structure of the FRC networks.

My detailed characterisation of the FRC network structure shows that differences between networks in naive state and following immunisation are minimal, contrary to what would be expected given that the LN expand in volume substantially after immunisation. Strikingly, this suggests a very substantial and rapid network growth and remodelling, compensating for the increase in LN volume, rather than just stretching.

I hypothesise that T cell step lengths are proportional to FRC fibre lengths and not to cell speed, as would be the case if cells followed a 'random walk with persistence (free) time'. I imaged and measured the fine-scale characteristics of FRC networks and – in separate experiments – T cell movement in both naive and immunised mice. I found that this matches a model of FRC network-bound movement better than an alternative 'intrinsically-driven' movement with a persistence time. While this adds to the accumulating indirect evidence of T cell movement on the FRC network, there still is insufficient evidence from the

analysis of T cell movement data to make an unequivocal conclusion, even when using a relatively large dataset. Unexpected discrepancies occur between both my models and the real T cell movement data, and I discuss possible causes for this interesting finding. I then built a simulation of T cell movement on real, directly observed FRC network structures and compared this to the alternative random walk with persistence time (RWPT) model.

I also investigated the imaging frequency bias of apparent cell speed and turning angle quantitatively to show that direct estimates are biased, and suggest a method to correct this. I made a direct use of this effect to infer the ratio of straight step (persistence) lengths between primed and naive T cells from imaging data on cell movement.

The methodology applied in the previous chapter, i.e. the state-space models, is not suitable for use in this chapter, as it is not possible to explicitly include the measured FRC network structure into the state-space models. Instead, I developed a completely new methodology to make comparisons of the imaging data to the structure of the FRC network.

4.3 Methods

4.3.1 Animals, tissue and cells

The basics are described in chapter 2 in section 2.3.2. For imaging the FRC networks, we used 6-8 weeks old C57BL/6 mice (Harlan, Blackthorn, UK) to obtain lymph nodes (LN).

4.3.2 FRC network tissue preparation

The FRC network can be visualised using antibody to ER-TR7, an unknown FRC-specific antigen located both inside FRC and in their extracellular products [62]. The LN were fixed in a 30% w/v solution of sucrose and 2% w/v paraformaldehyde (PFA) in PBS at 4°C overnight, washed in 30% sucrose for 3h at room temperature, embedded in OCT compound (Sakura Finetek, Thatcham, UK) and frozen using liquid nitrogen. 60 μm sections were cut using a cryotome and dried on Polysine slides. The sections were then blocked in 1% BSA, 0.3% Triton x-100, 0.01 M glycine in PBS at 4°C overnight and stained with a 7.5 μg/ml DyLight 488-conjugated ER-TR7 Fibroblast antibody (Novus Biologicals, Littleton, Colorado, USA) solution for 2h at room temperature. The sections were washed, dried, and mounted in ProLong Gold medium (Thermo Fisher Scientific, Life Technologies). Isotype controls were carried out using rat IgG2a isotype control KLH/G2a-1-1 (Novus Biologicals) and were negative.

4.3.3 2-photon microscopy and image processing

This is described in the Methods sections of previous 2 chapters, subsections 2.3.3 and 3.3.1. Final processing of the FRC network images was performed using Imaris and GIMP 2.6 (GNU Image Manipulation Program, http://www.gimp.org). It is important to note that the FRC network and T cell movement were imaged in separate experiments, as to visualise the FRC network required the tissue to be fixed and frozen.

4.3.4 T cell motility data processing

The pre-processed data were imported to R statistical language and environment (R Development Core Team, http://www.r-project.org/), where all further analysis was undertaken as described in chapter 3, section 3.3.2. I measured the apparent step lengths and turning angles between consecutive microscope scans, as illustrated in chapter 3 in Fig. 3.1. Note that the measured values of these parameters depend on the scanning interval, which I discuss and analyse in detail in chapter 3.

4.3.5 FRC network representation

Manual curation was needed to correct false positive or negative FRC fibre joining points and to add points where fibres changed direction. For further reference, I summarily term all these points 'nodes'. Connections (edges) between nodes were then recorded manually, corresponding to fibres visible in the original image. Thus, a FRC network representation was generated consisting of nodes representing turns or joints of FRC fibres, connected by edges representing straight network segments. I found this time-consuming procedure to be the most accurate one currently available, after trying various automatisations. The process was greatly assisted by the Compiz compositing window manager for Linux (http://www.compiz.org/, free and open-source) and the rgl package for R, to enable transparency and accurate overlaying and rotation of the 3D network model and the original image. The LN contained areas of high FRC network density, probably where the network enwraps blood and lymphatic vessels. These were densely filled with FRC nodes and connected with edges in the model, as closely as possible to the image. I consider this the most appropriate treatment of these areas, as presumably T cells have little constraint in moving on these structures, which is well approximated by dense, heavily connected networks. Again, all steps of the procedure were performed independently of treatment - the file names were changed to random automatically and an annotation file stored, and files were again linked to treatment using the annotation file after manual processing was done.

4.3.6 Network metric measurements

It is desirable to measure all metrics that could potentially affect T cell movement. Network angles (values between 0° and 180°) were measured between each pair of edges joining one node. This represents all the possible turns a hypothetical T cell could take when moving along the network. All edge lengths were measured. Connectivity for each node was calculated as the number of edges joining the node. Density of nodes was calculated for each image as the total number of nodes recorded divided by the volume of the imaged area. Note that the metrics will be biased due to boundary effects, i.e. a bias created by imaging only a part of the FRC network. This is not a simple problem to deal with in 3D images [63], but would have to be addressed if the real values were of interest. As the boundary effects can be expected to be equal for both naive and primed networks, it should not affect the comparison undertaken here.

4.3.7 Statistical comparison of network metrics

To examine potential differences between naive and primed networks, I tested whether the measured metrics are better described by the same statistical distribution for networks for both treatments or by a different distribution for each. As the fit of the whole distribution is tested, this is more sensitive to differences than statistical tests for the shift of the location parameter (such as a t-test for the mean of the normal distribution). Distributions were chosen according to the nature of these metrics and were checked for good fit visually and using the likelihood values of different candidate distributions. I chose the normal distribution for node density, the negative binomial distribution for connectivity, the gamma distribution for fibre lengths and the truncated normal distribution on the interval $(0, 2\pi\rangle$ for angles. Likelihood-ratio tests (LRT) were used to determine when two separate distributions were required to distinguish between treatments. Values of $p < 0.05$ were regarded as indicating significant differences.

4.3.8 Estimation of T cell instantaneous speed

The instantaneous speed v is the limit of apparent speed v_a (apparent distance moved during one sampling period T divided by the value of T) as T approaches 0. Therefore, the correct estimation can be obtained by extrapolating the function of v_a versus T to $T = 0$. To measure v_a for different T, I temporally sub-sampled T cell movement imaging data to higher sampling periods. This was done by an integer factor of values 2 to 11 (sub-sampling periods T_2 to T_{11}) – for higher sub-sampling, the data set was too small. For the extrapolation, we have to assume that the trend continues outside the observed data range, so it is critical to find the correct model to fit the data. I therefore derive the theoretical function for the dependence of v_a on T for all types of movement with finite step lengths, i.e. both network movement and random walk with persistence time (RWPT). For movement following diffusion, displacement is proportional to square-root of time, so step lengths measured for scanning period T are proportional to $sqrt(T)$. This also holds for network movement or any movement with finite step length between turns for larger time ($T > L/v$) (e.g. [15]), and has specifically been shown to hold for T cell imaging data at times longer than a few minutes [17, 9, 20]. The apparent speed v_a for a given T is step length divided by T, therefore:

$$v_a \sim \sqrt{T}/T$$

This is a reasonably good fit to our data for larger T. For small T ($T < L/v$), where the extrapolation is to be performed, the dependence of v_a on T is linear, as the probability of a cell making a turn between consecutive scans is proportional to the distance travelled during one scanning period. I show this more rigorously below, referring to Fig. 4.4 for illustrating the argument.

With a certain frequency f, the cell will make a turn between two consecutive scans. In those cases, the apparent distance travelled and the apparent speed will be smaller than the real values (multiplied by a factor of K, where $0 < K < 1$). In the rest of the cases (frequency $1 - f$), when the cell makes no turn between consecutive scans, the apparent speed and distance travelled will correspond to

the real values, that is v and $l = Tv$, respectively. The apparent mean distance travelled l_a will be determined by these two outcomes and their frequencies:

$$l_a = fKl + (1 - f)l$$

The frequency f of cells turning between consecutive scans is the ratio of the number of turns on a given trajectory to the total number of imaging intervals per that trajectory. As on average, the imaged section of a trajectory with N turns will have the total length of N step lengths L, the total number of imaging intervals can be expressed as $N(L/l)$. Therefore:

$$f = N/N(L/l) = l/L$$

Combining the last two equations:

$$la = \frac{K-1}{L}l^2 - l$$

Substituting $l = Tv$ and $l_a = Tv_a$:

$$Tv_a = \frac{K-1}{L}(Tv)^2 + Tv$$

Substituting $K - 1 = -C$ (where C is a positive number as $K < 1$):

$$v_a = v - \frac{C}{L}Tv^2$$

Which is a linear function of T with intercept term equal to the instantaneous speed v. This equation could also be used to calculate L directly, conditional on inferring the value of C.

For this reason, I used a natural spline fit, where interpolation is polynomial and extrapolation is linear using the slope of the interpolating curve at the nearest data point (i.e. the point closest to $T = 0$ for extrapolating the instantaneous speed). This data point in this case corresponds to $T = 45$ s, which fulfils the condition $T < L/v$ for the current estimates of T cell persistence time, mean T cell speed and T cell step (persistence) length [1, 4].

As a check, I performed an FRC network-bound movement simulation and a RWPT simulation (details below). Both simulations closely resembled the data in terms of the dependence of v_a on T and the instantaneous speed estimation method was accurate for these simulations.

4.3.9 FRC network movement model

The FRC network movement simulation was constructed using the imaging data of the real FRC networks. As described above, I converted the images of FRC networks into a computational model represented by a set of nodes connected by line segments. Example images of this geometric representation of the networks can be seen in Fig. 4.1c, d. The movement of individual T cells on these networks was then simulated as a simple agent-based model, implemented in R. The simulated T cells, represented by 3D coordinates, were allowed to move along network segments and upon reaching a node, they followed one of the joining edges randomly with equal probabilities. This model allows double-backing of cells on the same fibre when they reach a node, but whether this is allowed or not does not matter for our purpose: as double-backing is equivalent to turning on the node, it does not change the step length between turns. When no other edges joined the node (a dead-end), the T cell reversed direction on the same edge. I used the estimated instantaneous speeds for naive and primed cells and simulated their movement on corresponding networks structures (measured from naive and primed LN). As noted earlier, the FRC network metrics are biased due to boundary effects, but as this can be expected to be equal for both naive and primed networks, it should not affect the comparison. A total of 70,000 T cell steps were simulated for each scanning period to ensure that error is negligible.

4.3.10 Random walk with persistence time (RWPT) model

This is based on a previously published [39] model of random walk with 'free time' t_{free} (sometimes also termed 'persistence time'), during which cells move with a constant speed of v_{free}. This results in constant step lengths $l = t_{free}v_{free}$, so could also be called a random walk with fixed step. Between steps of length l,

T cells turn randomly so that new step vectors come from a uniform distribution on a sphere around the current location. This was achieved by drawing the azimuthal angle ϕ from uniform distribution on $(0, 2\pi]$ and the polar angle θ from a distribution with probability density $1/2\sin(\theta)$ on $(0, \pi]$ for each step, same as in [39]. I used the previously estimated speeds for naive and primed cells to set the values of v_{free}. The persistence time was set to 2 minutes for both populations (consistent with [17, 20, 39], although the exact value is not important for the inference of step length ratio. I do not implement a pause time between turns like in [39]; as this makes no difference to the cell trajectory (shape), therefore it makes no difference to the analysis I perform. A total of 70,000 T cell steps were simulated for each scanning period to ensure that error is negligible. The model is spatially unbounded, meaning there is no observation boundary effect and no limitation on the physical volume for movement (like the LN anatomy in real data). This presents no problem for this purpose as we are only evaluating the ratio of step lengths (i.e. indirectly the spatial frequency with which turns occur on the trajectory). However, neither the FRC network movement nor the RWPT model are suitable for other analyses generally (e.g. calculating motility coefficients).

4.3.11 Model and data comparison based on step (persistence) length

Consider a movement with finite step (persistence) lengths L between turns and its observation in discrete time (Fig. 4.4. For small imaging period ($T < L/v$), cell locations will be repeatedly recorded along the same step, and therefore the turning angle observations will be zero-inflated and the mean apparent turning angle ta will be underestimated. As imaging period increases, ta approaches the real value t, up to a certain point ($T \sim L/v$), where cells are recorded on average once per step and zero-inflation is minimal. As T further increases, the dependence between consecutive cell locations decreases (the effect of network structure or persistence time decreases) and the apparent angles will approach the values for a random walk, i.e. ta will asymptotically approach $\pi/2$ (90°). If the real value t is sufficiently large, a maximum will appear before the

asymptotic part of the ta versus T function (as can be seen in Fig. 4.5). In such case the maximum ta would be the closest value to the real value of t. The shorter the step length between turns, the earlier the curve approaches the asymptote and the earlier the maximum appears. I evaluated the dependence of the apparent turning angle τ_a on scanning period T in T cell movement imaging data. To achieve this, I used the same temporal sub-sampling as described above for estimating T cell instantaneous speed. On the x-axes of the presented graphs, I plot the product of T and the estimated instantaneous cell speed v, as I aim to estimate the step length ratios (distances) and Tv is the estimated distance travelled by cells during period T. For τ_a vs Tv functions in the FRC network model and the RWPT model, I used an arctangent fit:

$$\tau_a = c \arctan(bT^a) + d$$

as it exhibits a good fit and has a horizontal asymptote (equal to $a\pi/2 + d$), which is the expected theoretical behaviour. I located a maximum departing from the theoretical arctangent fit for both models using a spline fit and used it as a characteristic point on the curves to estimate the ratio of naive and primed cell step lengths. The functions for the dependence of ta on T in imaging data exhibited a more complex behaviour than those for the FRC and RWPT simulations, which is not surprising and is probably caused by various sources of noise in the data. However, as the functions exhibited distinct maxima inside the data range, I used spline fits to estimate the locations of these maxima.

4.4 Results

4.4.1 Comparison of FRC network structure in naïve and primed lymph nodes

Here I present a detailed analysis of the FRC network geometry in both naive and primed mice. I tried to capture all the parameters of the network geometry which might affect T cell movement, and report the measurements of fibre length, network angle, connectivity (number of fibres per node) and node density. Fig. 4.1a, b presents an example of *ex vivo* MPLSM images of ER-TR7 antibody-stained FRC networks in the naive and primed (post-immunisation) states. Fig. 4.1c, d shows images of the corresponding geometric representations of the networks, used for structural measurements and for subsequent T cell movement simulations. Network nodes were defined as points at which the FRC strands join or change direction. Connections between nodes were then recorded, corresponding to fibres in the original image. This was accomplished by examining the 3D image from different angles, so some connections do not visually match for the perspective in the presented MPLSM images. I measured the lengths of FRC fibres (strands between two nodes), angles between joining fibres, connectivity expressed as the number of fibres joining a node and network density as the spatial density of the nodes. The measurements comprise a total of 1136 vertices and 1849 edges for naive networks; and 885 vertices and 1482 edges for primed networks.

Likelihood-ratio tests (LRT) were employed to calculate p-values determining whether the measured network metrics are better described by the same statistical distribution for both treatments (naive and primed) or by a different distribution for each treatment. As the fit of the whole distribution is tested, this is more sensitive to potential structural differences than statistical tests only for the shift of the location parameter (such as a t-test). Fig. 4.2 shows the comparison of these parameters, plotted as beanplots to visualise the shapes of the entire distributions. A beanplot consists of a one-dimensional scatter plot with one horizontal line per data point, the length of which represents the number of occurrences of a given value; the estimated density of the distribu-

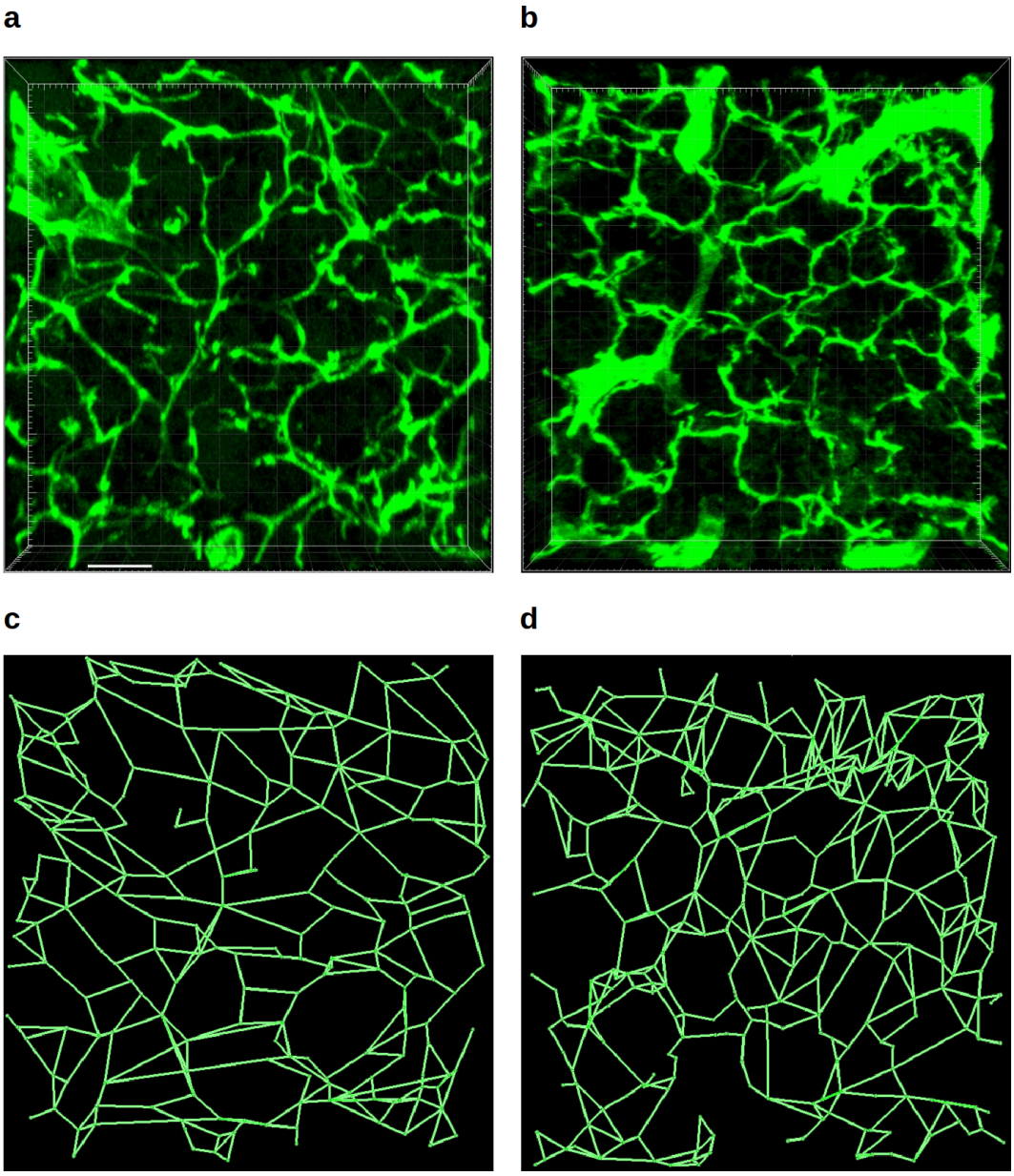

Figure 4.1: **FRC network structure in naive and primed lymph nodes** Presented here are examples of the naive **(A)** and primed **(B)** FRC network MPLSM images. The lower panel displays sections of the generated geometric representations of the naive **(C)** and primed **(D)** FRC networks, corresponding to **A** and **B**, respectively. The geometric representations were then used to measure network metrics. Scale bar 20 μm.

tion (purely to aid interpretation and not corresponding to the distributions used to perform statistical comparisons); and lines for averages of individual groups (thick) and an overall average for the whole plot (dotted). I found the distributions of fibre lengths in primed and naive networks to be significantly different ($p < 0.00$, Fig. 4.2a), although the means do not differ greatly, with the mean fibre length of 12.00 ± 0.14 μm in primed and 13.48 ± 0.13 μm in naive networks, respectively (mean ± standard error of the mean). The network (node) density distributions were also significantly different (p = 0.01, Fig. 4.2b) and the mean density higher by 40% in primed compared to naive networks. The mean angles between adjoining fibres were 91.9° for primed and 92.4° for naive networks and the distributions did not differ significantly (p = 0.14, Fig. 4.2c), suggesting that the real T cell turns (unbiased by discrete-interval scanning) should also be roughly equal for primed and naïve cells. The mean network connectivity (the average number of fibres joining a node) was 3.35 for primed and 3.26 for naive networks and the distributions did not differ significantly ($p = 0.43$, Fig. 4.2d).

The node connectivity of 3.35 for primed and 3.26 for naive networks correspond to those obtained from electron micrographs of lymphoid stroma in [31] and to the idea on which a previous modelling study was based [60] that nodes form when growing FRC fibres branch in two, giving a predicted connectivity of 3. The numbers are slightly higher than 3, as presumably the process of FRC network formation is more complex and new fibres can probably grow from FR cells and join existing fibres – consistent with the hypothesis that this happens in priming when the LN expand. As the boundary effect results in a negative bias of connectivity, the real values are probably higher.

Further studies can be carried out utilising the methods used here to investigate the structure of FRC networks in larger samples, more detail and in different contexts.

4.4.2 Estimation of instantaneous T cell speed

The presented method to estimate instantaneous cell speeds (Fig. 4.3b) illustrates the possible magnitude of bias and discrepancy in estimating instanta-

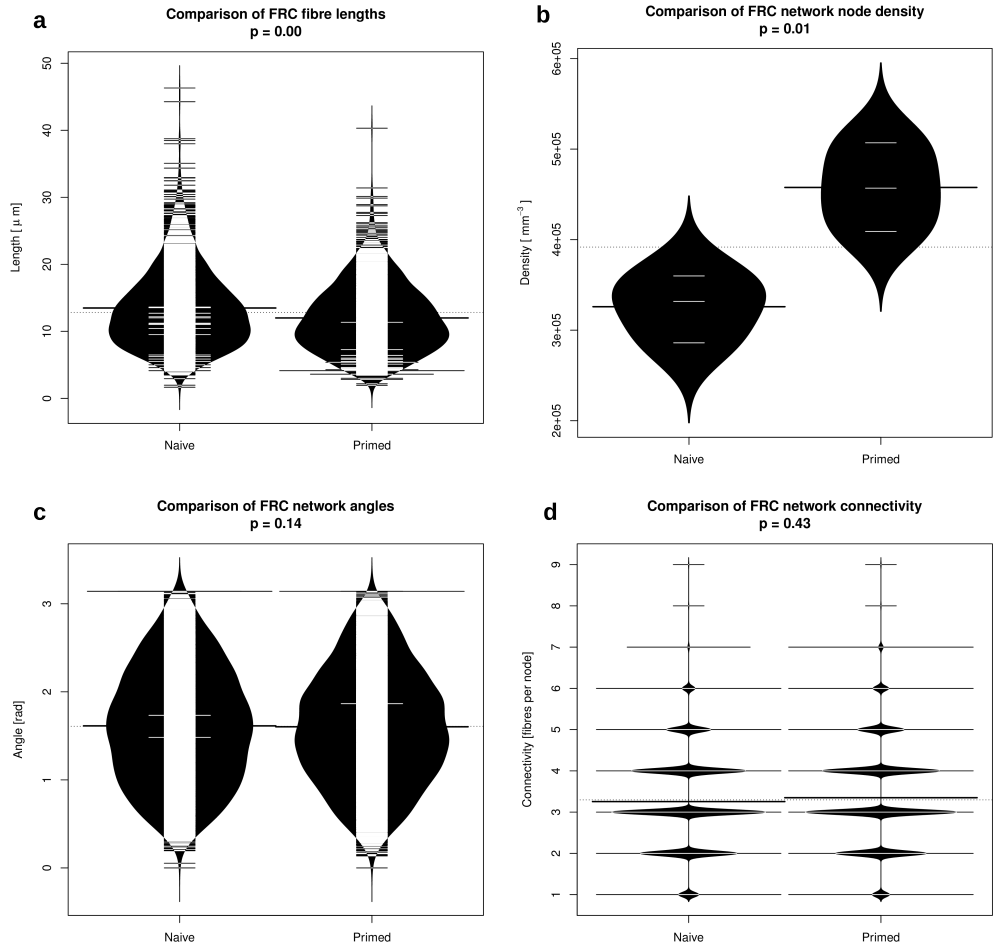

Figure 4.2: **Comparison of FRC network structure in naive and primed lymph nodes**
A. Fibre lengths differ, but not by a large factor (13.48 μm for naive and 12.00 μm for primed networks). The difference is in the opposite direction than would be expected if the network simply expanded after priming.
B. The density of FRC network nodes is higher in primed networks. This could be the reason for shorter fibre length in primed networks.
C. and D. No significant difference in network angles and connectivity.
Values were pooled for all detected FRC nodes and fibres from three imaging fields (three animals) per treatment. Likelihood-ratio tests (LRT) were used to determine when two distributions were required for a given metric to distinguish between treatments and to calculate the corresponding p-values.

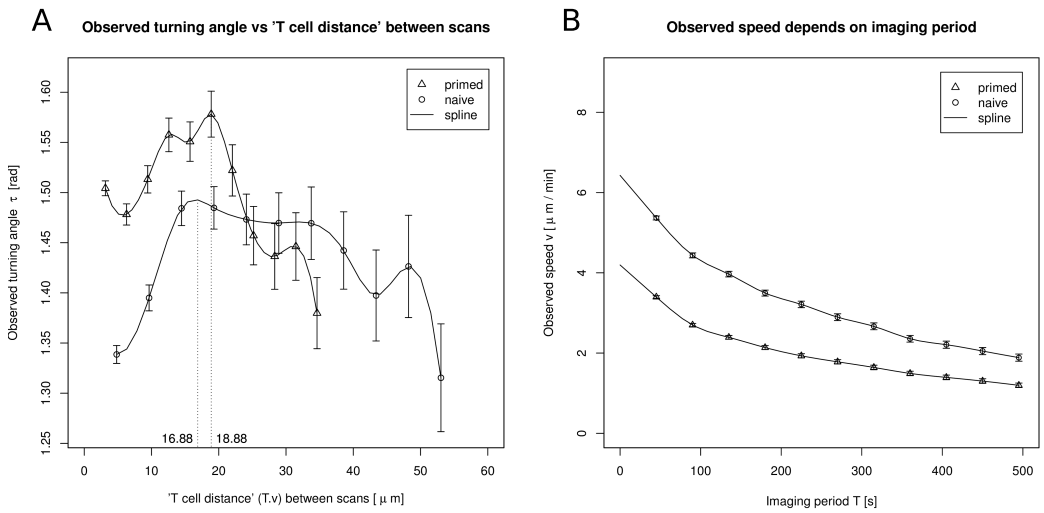

Figure 4.3: **The dependence of observed (apparent) turning angle and instantaneous speed on imaging period.**
A. Apparent turning angle and the estimation of naive/primed cell step length ratio.
I examined the dependence of the mean apparent cell turning angle τ on the estimated distance travelled by cells during period T (the product of the imaging period T and cell speed v). The x-axis locations of the τ maxima are proportional to the T cell step (persistence) lengths between turns (explanation in Methods 4.3.11)
B. Instantaneous and apparent cell speed and imaging period.
This plot shows the substantial effect of imaging period T on the apparent T cell speed. I used natural spline (dotted lines) extrapolation to $T = 0$ to estimate the real instantaneous T cell speed. This extrapolation was verified to perform well for both the 'random walk with persistence time (fixed step)' and the FRC network walk models.
All error bars show the standard error of the mean.

neous T cell speed simply by dividing step length by the corresponding imaging period. It is important to be aware of this when making comparisons of studies that were done with different scanning periods. It is also important to note that apparent T cell speeds might differ between two cell populations solely due to their different turning behaviour, even if their actual speeds are equal. For example if a cell has a bias towards returning to it's previous location rather than moving away from it (i.e. low displacement rate), the estimated speed will be lower as the cell will on average displace less in a given time interval that a cell with the same instantaneous speed which has higher tendency to move away from the original location. By performing a natural spline fit of the dependence of observed speed v_a on imaging period T and extrapolating to $T = 0$, I estimated the instantaneous speeds to be approximately 6.43 μm/min for naive cells and 4.20 μm/min for cells in priming.

The method can be further developed and perfected by analysing larger volumes of imaging data and setting up imaging experiments with very high scanning frequency by sacrificing resolution and imaging volume. This might allow to infer the dependency of apparent speed on the imaging period at very low T and compare this to my extrapolation. However, for the purpose of this study, it is the ratio of naive/primed speed that matters, which I show to be roughly conserved for the two estimation methods I tested and across different imaging frequencies.

4.4.3 Naive/primed cell step length ratio estimated from imaging data, and expected for FRC-guided versus RWPT movement

Next I used the imaging data of the FRC network structure and T cell motility in LNs combined with a mathematical and computational approach to test the hypothesis that T cells move along the FRC network. When movement is confined to a network, the network fibre length determines T cell step length (straight step between turns, i.e. persistence length). By contrast, if T cells perform random walks with turns made after a given persistence time, perhaps governed by an internal clock, step lengths are proportional to cell speed, as they

are the product of the persistence time and the instantaneous speed. Fig. 4.4 presents a diagram comparing these 'extrinsic' (network-dictated) and 'intrinsic' models of motion. Therefore, I developed a method to infer the ratio of step lengths between T cells in naive and immunised state from imaging data, to compare this to the step length ratios expected for the two competing movement hypotheses.

Fig. 4.3a shows the estimation of naive/primed cell step length ratio from imaging data by investigating the dependence of the mean apparent turning angle τ_a on the product (Tv) of the imaging period T and cell speed v.If the time between successive image frames (the sampling period) is short compared to the typical time between major changes in direction, the mean turning angle will be heavily biased towards very small values, because cell locations are captured multiple times between major turns. For longer sampling periods, information about the cell trajectory will be lost and the measured angles will tend to random values with a mean of 90°. If cells move at speed v between major turns, then for a certain (intermediate) sampling period T, where the product T_v is close to the cell step length, a local maximum will appear in the plot of mean turning angle (y-axis) and the product T_v (x-axis). The location of this maximum is proportional to the T cell step (persistence) length (see Methods for a detailed explanation).

This allows us to estimate the naive/primed step length ratio, which is 0.89 – close to 1. In a movement on a network, it is the network fibre length which determines T cell step (persistence) length. In a movement following a RWPT, step lengths are proportional to cell speed (distance travelled between turns is a product of t_{free} and v_{free}). Therefore, from my measurements of FRC network fibre lengths, the step lengths should be roughly equal for primed and naive cells in case they move on the FRC network, as the ratio of naive/primed fibre lengths is 13.48 μm / 12 μm $\approx$ 1.12. In case T cells follow a RWPT, the step length ratio would be v_{naive} / v_{primed} = 6.43 μm/min / 4.20 μm/min $\approx$ 1.53. These results support the hypothesis that T cells move on the FRC network rather than following a random walk with persistence (free) time.

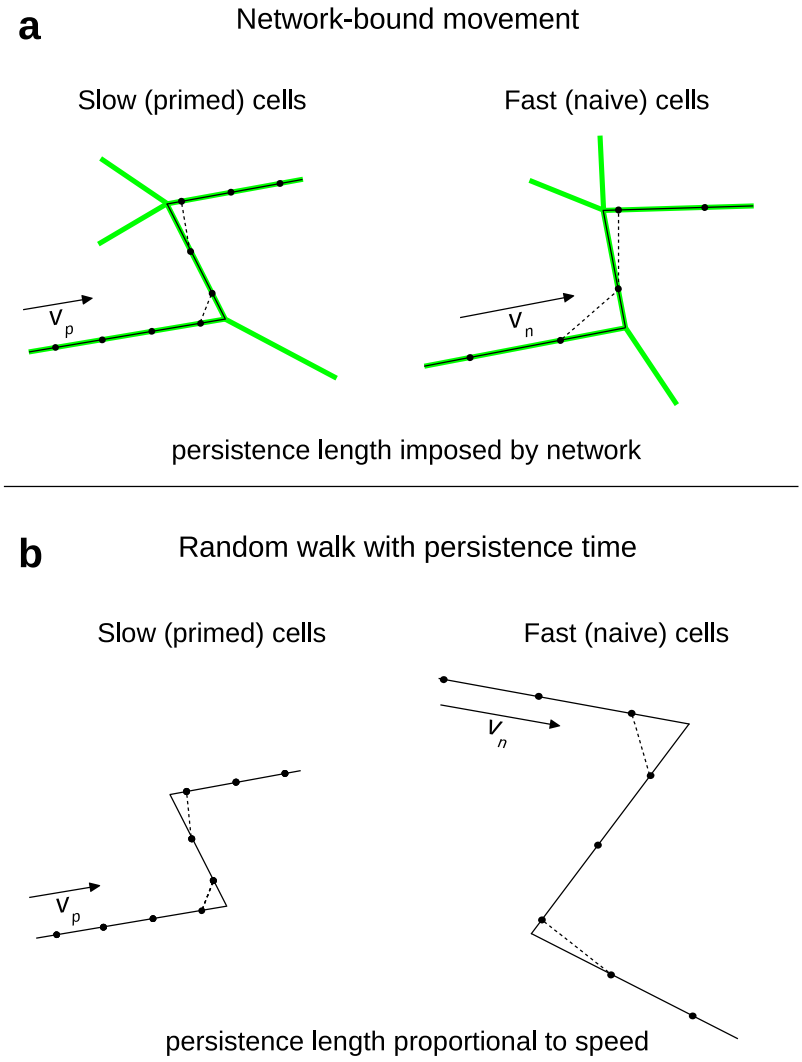

Figure 4.4: **Diagram of a network-bound movement and a random walk with persistence time (RWPT).**
The diagram illustrates two different types of movement with finite step length; a network-bound movement and a RWPT, for two different cell speeds vn > vp, all observed at the same imaging frequency. **A. Network-bound movement. B. RWPT.** In a network-bound movement, the distance travelled between turns (step or persistence length) is imposed by the network fibre length. In a RWPT, persistence length is proportional to cell speed. This diagram also illustrates the bias of the instantaneous speed and turning angle measurements introduced by the discrete scanning process (dotted line).

4.4.4 Estimation of naive/primed cell step length ratio for movement simulations, and comparison to data

While the argument for comparing FRC network movement to the RWPT model based on step (persistence) length supports the FRC-bound movement hypothesis over RWPT, it is by no means conclusive. The simulation models carried out and analysed below serve to further illustrate and support this point.

I built agent-based simulation models of FRC network-bound movement and of RWPT. To parameterise these models, geometric representations of the measured FRC networks and the instantaneous speeds of naive and primed cells, both estimated above, were utilised. The FRC network movement model was run 6 times, one for each imaged and reconstructed FRC network, and the results then pooled. I employed the same method as in the previous section to infer the step length ratio between naive and primed T cells in the simulations. However, as it is feasible to perform a very large number of individual simulations, the error of the model output can be minimised so that it is negligible.

As can be seen by examining Fig. 4.5, the naive/primed cell step length ratio for the FRC network movement model is 1.22, which roughly corresponds to the ratio of naive/primed FRC fibre lengths (1.12). The same analysis of the RWPT model gives naive/primed cell step length ratio of 1.54, which corresponds to the naive/primed cell speed ratio (1.53). This is in agreement with the reasoning and conclusions above. A model of T cell movement like the RWPT, where cell persistence is driven by an intrinsic persistence time is therefore not supported by my results. It is more likely that this persistence is imposed by the FRC network structure. Of course this is not a definitive proof of the FRC network movement, as other alternative modes of movement might account for this. However, the two compared models are the most popular and both have a mechanistic biological basis – and there is currently no known biological basis for alternative models.

Unexpected discrepancies occur between both models and the real T cell movement data, when the shapes of the curves in Fig. 4.3a and Fig. 4.5 are compared. In Fig. 4.3a, the asymptotic behaviour was not detected within the

given Tv (x-axis) range investigated (or rather, it is difficult to say whether it can be detected due to the large statistical error for the real data). Note that the range on the x-axis is much smaller for the data (Fig. 4.3a) compared to the simulations (Fig. 4.5), due to the limited imaging duration. It is unclear why there appears to be a pronounced drop in Fig. 4.3a and why the values remain below the expected long-term value of 90°. While this behaviour is interesting, and is probably worth a more detailed investigation in the future, I believe that this is not relevant for the specific point made here. That is because I only seek to compare the general behaviour in therms of the $x - scale$ of characteristic points on the curves and these should linearly proportional to the characteristic scales of the movement (e.g. the persistence length). In this case I chose to compare the first local maxima for primed and naive cells – but other characteristic points on the curves along the $x - axis$ could be chosen for this comparison. Therefore, the exact shape of the curves is likely not relevant to this specific analysis. The fact that the curves differ between the data models is not entirely surprising, as these cell movement models are very simple and intended to capture only certain characteristics of interest of the real T cell movement, which is undoubtedly a much more complex process. Note that a pronounced global maximum only appears if the real turns are on average higher than 90°, as is the case for the FRC-bound model but not the RWPT model due to double-backing on the network – this only reflects the mean value of the turning angles and is not an effect particular to the network movement.

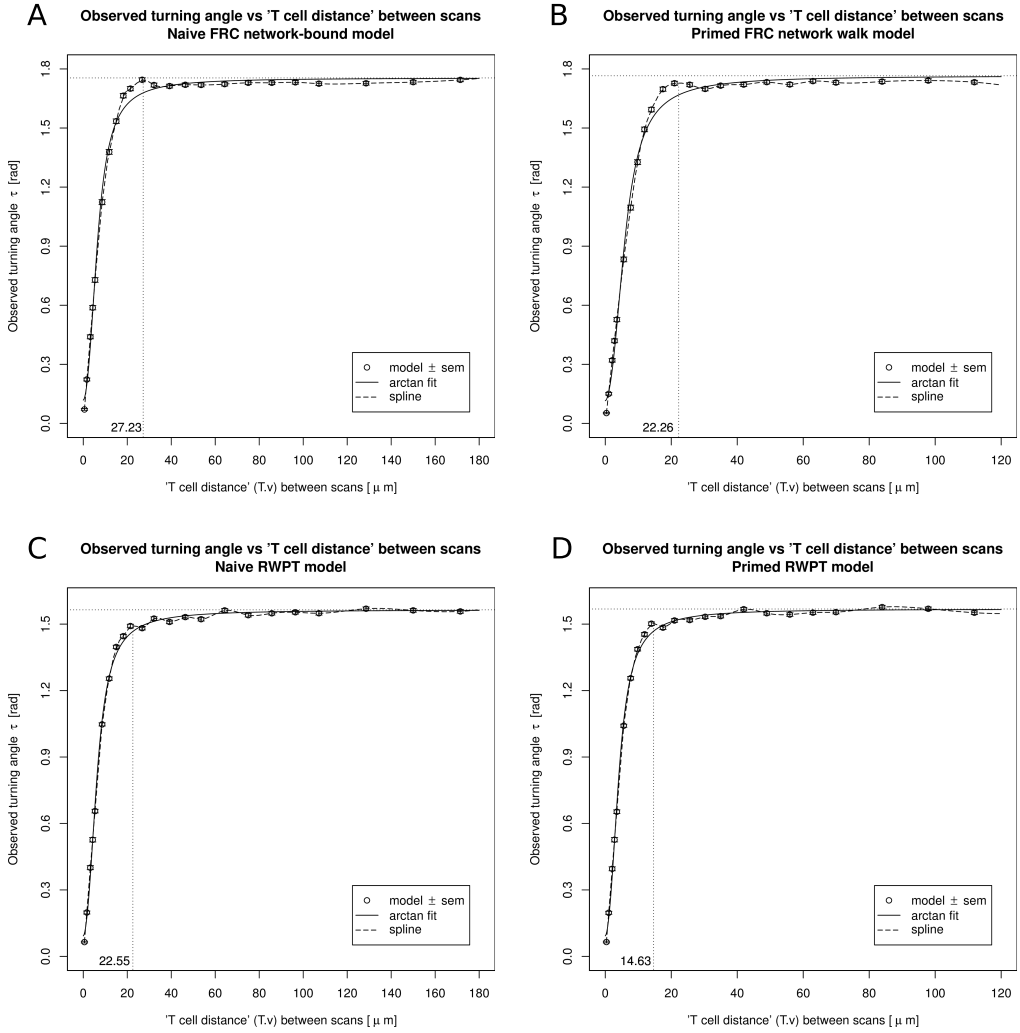

Figure 4.5: **Estimation of naive/primed cell step length ratio for movement models**
The local maxima where data points stray from the theoretical (arctangent) fit are used as characteristic points for the estimation of step length ratios.
A. and B. naive and primed FRC network movement model. The step length ratio is 1.22, which roughly corresponds to the ratio of FRC fibre lengths (1.12).
C. and D. naive and primed 'random walk with persistence time (fixed step)' (RWPT) model. The step length ratio is 1.54, which corresponds to the speed ratio (1.53).
These results in conjunction with Fig. 4.2B support the reasoning that FRC network walk is a more likely model than 'random walk with persistence time (fixed step)'. All error bars show the standard error of the mean.

4.5 Discussion

The major contribution of this chapter is that it answers, or goes some way to addressing, the following biological questions: Do T cells move along the FRC network or follow a random walk with persistence (free) time, what is the fine-scale structure of the FRC network, does it differ between naive and primed states and what is the effect of scanning frequency on the observed speed and turning angles and how to make more realistic estimates of these two parameters? Measuring the fine-scale spatial metrics of the FRC network structure and T cell movement in naive and primed states provides a new insight in a controversial area of immunology.

I found that there is little difference in the FRC network structure between naïve and primed states. This is perhaps surprising, as LN expand in volume shortly after priming [54, 55]. This expansion alone would lead to a 'stretched', spatially less dense network with lower node density and longer FRC fibres. This could be hypothesised to serve the function of making the T cell movement in the densely-packed LN environment more efficient, although the increased total number of cells might counter this effect. Also, lower-density networks were found to decrease T cell-DC search time in a model of movement on a hypothetical network [60], due to a decrease in the total size of the network that the T cells have to search. However, it was not made clear how this would translate to the phenomenon of LN expansion in priming and would probably be countered by the increased volume of the LN. On the other hand, it is possible that the FRC network is highly responsive to this expansion and new fibres are formed in a short time, increasing the node density and decreasing the mean fibre length, having the opposite effect to the spatial stretching.

The changes in FRC mean fibre length and network density I observed are actually in the opposite direction than would be expected if the network simply stretched when the LN increases in volume following immunisation. These results suggest that the FRC network adapts rapidly (within 20 h post-immunisation) to the expansion in LN volume by remodelling, rather than simply stretching. This appears to contradict a recent conclusion that the FRC network stretches following immunisation [56]. However, the lengths of fibres

were not measured directly in that study and the conclusion was based on the diameters of circles that could be fitted into 'gaps' between network branches and on the average area occupied by individual FRC in 2D slices, which were both larger upon immunisation. My direct observations of a decrease in mean fibre length and an increase in network node density are compatible with the increase in gap size and area per FRC after immunisation. The mean distance between original network nodes may increase due to LN expansion, increasing gap sizes; but if simultaneously FRC increase in volume or divide and cluster together, or the connections between FRC thicken and contort, the effective number of nodes increases and so the mean fibre length can decrease (as can be seen in Fig. 4.1). Indeed, Yang et al. [55] described increases of FRC size within 20 h and proliferation within 40 h of immunisation.

The FRC network angles in both primed and naive LN were close to the value of 90°, which would correspond to angles between consecutive steps in a random walk. The naive and primed networks did not differ in terms of the distribution of turning angles, suggesting there is no remodelling in this sense and T cells should exhibit the same turning angles in the naive state and during priming. An assumption that network nodes form when growing FRC fibres bifurcate [60] predicts a network connectivity (number of fibres per node) of three. As my connectivity measurements are higher, presumably the process of FRC network formation is more complex with new fibres growing from FRCs and joining existing fibres, which is also consistent with the hypothesis that new fibres form during the expansion of LN following immunisation.

An alternative explanation which appears much less likely, is that although the whole LN expands in priming, the volume of the FRC areas remains unaffected. I would suggest that this phenomenon should be further investigated experimentally by imaging sections of the entire LN.

As mentioned earlier, there are areas of very high FRC network density, probably where the network enwraps blood and lymphatic vessels, which result in a high number of short fibres. This is unlikely to result in any differences between naïve and primed networks however, as these areas seem to occupy the same relative proportion in naive and primed networks. Also, as I point out in the Methods, section 4.3.6, the boundary effect will result in bias of

the measured parameters, except for the density of nodes. The measured connectivity and edge length will be lower than the actual values, and some bias can also be expected for the measured angles. There are methods for correcting such biased data, but this is not a simple problem in 3D images [63], especially with one dimension of the measured volume very small (the thickness). I tried to correct for this effect by including a buffer zone and discarding measurements close to edges where edge effect is most marked, but due to the limited imaging volume, the remaining sample size was small and the effect of this correction was not clear. This issue would have to be addressed if the accurate values were of interest. Advanced imaging studies of larger volumes – especially thicker sections – would be desirable. However, as the boundary effect can be expected to be equal for both naive and primed networks, it should not pose a problem for merely comparing these.

I have then taken a quantitative, data-based approach to show that an FRC network-bound movement model is more consistent with T cell movement imaging data than the random walk with persistence time (RWPT) model. I verified this by running simulations of the two different movement models, utilising the directly observed FRC network structures for the FRC-bound network movement simulation. These simulations support these conclusion.

It is experimentally extremely difficult to image the FRC network and live T cells at the same time. The most direct observations were performed in [35], where GFP chimeras reconstituted with non-fluorescent hematopoietic cells were used to visualise the LN stroma (i.e. not FRC exclusively). It is not yet possible to image FRC specifically in a physiological system like the one I used, i.e. in intact lymph nodes. The advantage of the quantitative method developed here is that performing such experiments is not required – it allows the separate measurements of the FRC network structure and T cell movement to be made in the most suitable experimental setups.

Although the analysis supports the FRC network movement model over the RWFT model, there might be alternative mechanisms to the FRC network movement that could result in T cells having a constant persistence length rather than persistence time. However, this seems unlikely as there seems to be no known cellular or molecular mechanism in lymph node T cell movement

to explain this, e.g. different persistence times in such a ratio that would compensate for different speeds. Of course, T cell movement also will be affected by interactions with DCs and possibly other cells, which might constitute another source of T cell turning and periodicity in T cell movement. Another drawback is the relatively large magnitude of error for apparent turning angle measurements (Fig. 4.3a), resulting in uncertainty of the persistence length estimates. Analysing more data using the method presented here, which is now straightforward, should address this problem. As the support for the FRC-bound movement over RWPT relies on the uncertain estimate of the step length ratio inferred from T cell imaging data, based on multiple measurements of the same quantity at different scanning frequencies (resulting in autocorrelation between these datapoints), and on an extrapolation using splines, it is not statistically feasible to calculate confidence intervals. To be statistically rigorous, one approach to address this would be to analyse a massive dataset and perform a bootstrap to generate confidence intervals, which I think would be very worthwhile in the future.

In analysing the T cell movement data for the purpose of this comparison, I showed how direct estimates of turning angle and instantaneous speed from imaging data are biased and how this bias can be corrected. My speed estimates differ from those obtained by dividing the apparent distance travelled during one imaging period T by the value of T, which is a conventionally utilised method, and Fig. 4.3b illustrates the extent of possible bias and discrepancy between studies carried out for different imaging periods. It is also important to note that apparent T cell speed might differ between two cell populations solely due to their different turning behaviour. For example if a cell has a bias towards returning to its previous location (low displacement rate), the estimated speed will be lower than for a cell with the same instantaneous speed and a higher displacement rate. My estimate of 6.43 μm/min for naive T cell speed is lower than in some other studies, e.g. 10.8 μm/min [17] and 10.7 μm/min [20], which were performed at a scanning period of 10 s. However, discrepancies in T cell motility parameter estimates between imaging studies are common and are probably due to differences in the experimental set-up and methods used to track cells (and also whether 3D speeds or 2D projections of speeds

were estimated) and the likely high natural variation in cell motility parameters. For example, [23] report speeds of about 16 μm/min for naive and 11 μm/min for primed T cells (naive/primed cell speed ratio of 1.45, corresponding to my estimate of 1.53) at scanning periods of 18 s and [25] reported speeds of about 4 μm/min for primed cells at scanning periods of 18–38 s, in this case corresponding to our data (Fig. 4.3b).

It could be argued that for very short imaging intervals, which were utilised in some studies (i.e. 10s), so that for example the cells do not move more than their diameter in each interval, the bias of estimating instantaneous speed by simply dividing observed step length by T is likely very small. However, it is also possible that my approach is better than even imaging at such a fine time interval (low T) as there will then be a large relative error due to the uncertainty of T cell centroid location determination (due to limited spatial resolution of imaging and the constant movement of T cell membrane). In any case, imaging is a trade-off between duration, volume, resolution and the scanning interval, so we are often limited in the experimental scanning frequency achievable. Also, the presented method allows to correct previous estimates and make comparisons between studies performed at different scanning intervals.

An important point to address is that T cells might stop periodically, which has an effect on the average speed and might also affect the naive/primed speed ratio, especially when the pause times differ between these two cases – due to different T cell-DC interaction times in naive and immunised states, where T cells will interact for longer times if DCs carry a cognate antigen. Therefore, it is possible that the naive/primed speed ratio that I estimated (which includes pausing) does not correspond to the ratio when T cell speeds excluding pausing are considered. As the latter (speeds between pauses) will relate to persistence lengths in the RWPT model, we need to make sure that the ratio of these speeds corresponds to the ratio for my estimates. Importantly, the above-mentioned study [23] excluded cells in clusters, which were presumably interacting to DCs. Although this can not guarantee the exclusion of absolutely all interacting T cells, the naive/primed speed ratio for this study of approx. 1.45 corresponds to my estimate of 1.53. Therefore, it seems that T cell pausing behaviour does not play an important role in terms of my conclusions. The phenomenon is worth

of further study though and it is generally important when talking about T cell speed to distinguish whether this is the instantaneous speed in intervals when T cells are moving between pauses, or whether pausing is included. For example, instantaneous speed estimates when including pausing might differ between two cell populations, but this could be because the pausing times differ, while the speeds between pauses might be equal. So, ultimately, the exact determination of instantaneous speed when moving between pauses is of interest in studies where this distinction is relevant.

I have shown that estimates of turning angles can also differ between studies as a result of the discrete-time imaging (Fig. 4.3a). Apparent T cell turning angles might differ between two populations solely due to their different speed, as cells moving slower will more often be captured between turns. This issue cannot be resolved by simply imaging at high frequency – this would possibly provide a good estimate of instantaneous speed, but turning angle measurements would be even more heavily biased. Here, I presented a method for finding the optimal sampling period at which a more realistic estimate of turning angle is obtained.

Same as for estimating instantaneous cell speed, the issue of scanning period-introduced bias in turning angle measurements is important for making comparisons of studies that were performed with different scanning periods. Also, T cell turning angles might differ between two populations solely due to their different speed, even if the actual turning angles are equal, as cells moving slower will more often be captured between turns, increasing the proportion of zero turns. This could lead to misinterpreting turning angle analysis; for example when directly comparing apparent turning angles between naive and primed cells, the differences could wrongly be attributed to changes in cell behaviour or in the surrounding environment. As the FRC network angles do not differ between these two scenarios, then if T cells do move on the network, the actual turning angles should not differ either.

There are some discrepancies in literature between persistence lengths and FRC fibre lengths reported by different studies. The observed average distance 'between intersections of FRC strands' of about 17.3 μm in [35] was pointed out to correspond to T cell persistence length from an imaging study [17]. The

latter study reports T cell speed of 10.8 μm/min and movement in a consistent direction for 1-3 min periods; taking 2 min as the mean persistence time gives persistence length 21.6 μm. Another study [20] reports that T cell movement is linear for periods of about 3 min with mean speed 10.7 μm/min, giving mean free path of about 30 μm. These discrepancies should be addressed, as the accurate inference of cell persistence lengths under different conditions might shed more light on both the FRC structure and other mechanisms affecting T cell migration in LN. For example in [39], the authors report that the distance moved between turns is about twice the distance between intersections in the fibroblastic reticular cell network, and propose that this indicates that at an intersection, a T cell will turn onto a new fibre $\sim 50\%$ of the time. This is based on an assumption that fibres run continuously in a straight fashion, and are joined by other fibres that cross their course, rather than that they branch out; there are possibly other, more likely explanations for this. The presented method currently does not allow the exact value of the persistence length, only persistence length ratios for different datasets. However, it might be feasible to further develop this methodology – for example the inference of coefficient C on page 123 in the Methods section 4.3.8 would allow to calculate persistence lengths directly.

In summary, these results strongly suggest that major changes in T cell movement during priming do not derive from alterations to the FRC network structure as this changes relatively little with immunisation. This narrows down the possible explanations to effects such as chemokine action, intrinsic changes in T cell movement behaviour and differences in T cell-DC interaction behaviour. The small change to the FRC network structure following immunisation might also serve to allow continued unaltered surveillance of other T cell clones for self and foreign antigens even during immune response. I believe this warrants further study – the network structural changes upon immunisation could be further investigated by measuring the structure of the FRC network and the dimensions of the whole LN in both states at different time points.

In terms of potential practical applications, these findings are relevant to the study of T cell-APC search and its role in the adaptive immune response, for which the mechanism of T cell movement through the LN environment

forms an underlying basis. My model expands on previous studies [37, 60, 64] by utilising experimental data on the FRC network structure and provides a platform to further build upon in order to make more realistic estimations of the antigen-search efficiency, for example in the context of infectious disease. Specifically in the infectious disease context, it has been hypothesised that fibrosis accompanying HIV infections causes CD4+ T cell depletion by disrupting the LN tissue architecture, thus limiting T cell access to self-antigen/MHC signals and the survival factor IL-7 on the FRC network [65], the latter of which has been recently shown experimentally in HIV-1 [66]. Also, the persistent lymphocytic choriomeningitis virus (LCMV) infection in mice has been shown to target FRCs and disrupt the FRC network structure in spleen, which was linked to consequent immunosuppression [67]. These results highlight the fact that targeting lymphoid stroma directly affects the immune response, and might also prove to be clinically tractable as an efficient way of manipulating the immune response for therapeutic purposes or enhancing the efficiency of vaccines.

Chapter 5

Synthesis and Future Directions

5.1 Summary of results

This section contains a summary of findings from all data chapters and discusses the possible implications for future studies in this area.

5.1.1 Chapter 2

In chapter 2, I presented a quantitative study of the static spatial arrangement of T cells and DCs in lymph nodes (LN), based on a large dataset of 2-photon microscopic images in naive and primed (immunised) state. Previous studies were largely descriptive, or used very simple quantitative comparisons and equivocal assumptions. I performed statistical analyses of spatial clustering and over-dispersion of cells using pair-correlation function (PCF), counts of cells in contiguous spatial quadrats (using the variance and mean of the counts to assess departure from spatial randomness) and developed a scale- and density-independent statistic to assess the cell spatial patterns. This allowed a novel formal statistical analysis of cell spatial patterns.

Using pair correlation functions to explore the clustering or overdispersion of cells, both T cells and DCs in both naive and immunised state were found to be clustered in some cases over a certain spatial range. This was highly variable across datasets, but significant clustering generally occurred at ranges between 20 and 50 μm, and was more pronounced for T cells compared to DCs. This scale is of interest as it should correspond to the spatial scale of the processes underpinning the mechanism of T cell and DC behaviour in LN – possibly the range of action of the DC dendrites, or the spatial scale of the FRC network. We can roughly compare this to the spacing ('gap size') of the FRC networks – in chapter 4, where the FRC network geometry was quantified, the mean length of FRC fibre was found to be around 12-13.5 μm. This included areas of very high FRC density, which were approximated by a dense mesh of short fibres - therefore the length of FRC fibres outside these dense areas, which more closely corresponds to the characteristic 'gap size' in the FRC network, will be somewhat higher than this. These measurements are roughly in agreement with the observed clustering range of T cells and DCs, as it is likely that these are confined to the FRC network. More accurate comparisons of the FRC geometry,

or the geometry of DC dendrites, to the spatial arrangement of T cells and DCs are likely a worthwhile future endeavour. It would be possible, for example, to study the intervals of spacing of the FRC fibres, or the clustering of FRC network nodes (where fibres intersect or branch out), and correlate these to the spatial patterning of lymphocyte distribution.

Further, and more formal spatial analyses, did not support the hypothesis that T cells cluster more during priming compared to the naive state. T cells are significantly clustered in both naive and primed setting, but no significant difference was detected between these cases. I also further studied the spatial arrangement of DCs, as this too might reflect the immunological state. For example, an overdispersed spatial pattern of DCs could serve to increase the efficiency of T cell search for cognate antigen, by making T cell-DC encounters more likely than if DCs were clustered. However, when pooling all the dataset together, I did not detect a significant departure of DC spatial patterns from complete spatial randomness (CSR) – it appears that in both naive and primed state, the DCs occupy the imaged areas of LN in a random spatial pattern (i.e. indistinguishable from a Poisson point process). The conclusion based on the best models is that T cells are significantly more departing from CSR compared to DCs, although this is undetectable when the interaction between treatment and cell type is taken into account (i.e. when we try to differentiate this effect between treatments).

Cell type and cell diameter were found to be collinear variables (linearly dependent) in our data, and were equivalently good explanatory variables for the measured spatial effects. Therefore it is not possible from this analysis to determine whether the cause for the difference in spatial patterns between T cells and DCs is simply driven geometrically by differences in cell diameters or by other differences between these cell types. Distinguishing between the effect of these two variables by performing a more detailed measurement of individual cell diameters could be the focus of future studies.

In my analyses, I accounted for two 'nuisance' variables which can bias the results; the cell diameter and cell spatial density, and I also develop a method which is not sensitive to cell spatial density. I highlight the need to account for these variables in future studies - cell diameter should be measured in addition

to cell movement characteristics, and should then be accounted for in further analyses.

These findings are in contrast to conclusions of some of the previous studies, where T cells were generally considered to be clustered in the primed state more than in the naive state. This was attributed to the aggregation of T cells around antigen-bearing DCs. Many of the studies where clustering is reported utilised the *in vitro* route of immunisation, where DCs are labelled and incubated in a concentrated antigen *in vitro* prior to transfer. This likely results in a very high concentration of antigen on the surface of these DCs, which then form centres of intense attraction for T cells. Here I show that in a system using *in vivo* immunisation, such an effect is undetectable even for the relatively large dataset used. This leads us to a conclusion that the cellular interactions accompanying immunisation are too subtle to detect significant changes in T cell spatial patterns when immunisation is performed *in vivo*, at physiological or nearly-physiological (or naturally occurring pathological) concentrations of antigen or antigen-bearing DCs. If T cell-DC search times are long relative to their interaction duration, then only a few small clusters will be present at any given time, insufficient to create a detectable increase in T cell spatial clustering. This suggests that rather than quantifying spatial clustering at a larger scale, effort should be made to quantify smaller (cell) scale effects like the temporal duration of individual T cell-DC interactions, where more notable differences might be detected between different immunological states.

If spatial clustering needs to be evaluated, the pair correlation function is a relatively straightforward quantitative method which provides a clear graphical summary of the spatial patterns, and should be used as a primary means of evaluating cellular spatial patterns, rather than qualitative descriptions or arbitrarily defined *ad-hoc* metrics. The scale- and density-independent statistic which I developed (based on quantiles of cell distances compared to a random (Poisson) spatial patterns) then provides a suitable tool to further quantitatively assess the departure from randomness at a spatial range of interest.

5.1.2 Chapter 3

In chapter 3, I studied the dynamic behaviour of T cells – their migration through LN in relation to DCs. There has been considerable interest in inferring the mode of T cell movement, particularly whether this is a random walk or exhibits some form of taxis. I addressed the question directly, within a rigorous formal statistical framework, using T cell and DC multi-photon imaging data.

I developed a set of Bayesian state-space models of the movement of T cells in naive and primed lymph nodes. This is the first time that this highly flexible statistical framework has been applied in this field. I formulated and tested several alternative mechanistic models of T cell movement behaviour – comparing a model where T cells 'become aware' of the nearest DC only at a certain threshold distance (interaction model) to a model where T cell migration behaviour gradually changes with proximity to the nearest DC (gradient taxis model), possibly as the T cell follows a gradient of chemokines. This was performed using the data on both cell step lengths and turning angles.

It appears that there is no detectable chemotaxis or other attractive action at distance between T cells and DCs in the sense of a continuous functional dependence of T cell speed or turning angles on the distance to the nearest DC, and that T cells only change their movement parameters once they interact with a DC. Undirected movement through LN is therefore likely to be a sufficient physiological mechanism for T cells to locate antigen-bearing DCs. As there is a fairly high density of DCs in a LN in the sense that there are usually several DCs at a similar distance to a T cell, the concentration of potential chemokines might be fairly uniform throughout most of the LN. Chemotaxis towards one of the DCs would then only occur at a very short distance, when this DC becomes the 'dominant' attractor for a given T cell. Therefore, if such a chemotaxis does occur, it might be possible to detect it through imaging at a much finer temporal resolution (and possibly also spatial) than currently performed. However, for the same reason (relatively high DC density), it is likely that there is no need for chemotaxis as an undirected movement is a sufficiently efficient mechanism for T cells to encounter DCs with sufficient frequency.

By distinguishing between two movement states of T cells: 'interacting' and

'freely migrating', I could also clarify how much of the observed decrease in average T cell speed during priming compared to naive scenario is due to a proportion of T cells interacting with DCs and how much actual slowing down occurs when cells are 'freely migrating'. It is obvious from my results that the observed reduction in mean speed in primed compared to naive scenario (down by approx. 37%) is caused not only by the increased proportion of T cells interacting with DCs, but also by the exploring, non-interacting cells slowing down their rate of migration (down by approx. 33%). The reason for this slowing down is currently unknown. It is possible that these slow cells are the ones that have previously undergone an interaction with DCs and have become activated, or that this serves to prolong the T cell transit time through inflamed lymph nodes, preventing their premature exit. It would be of interest to infer whether this observed decrease in speed has such a specific function in the adaptive immune response, or how it affects the efficiency of antigen search, or whether it is simply a consequence of the changes in the LN environment following immunisation - e.g. the increased total density of cells.

It was also unclear what the detected differences in turning angle distributions for the two distinct states mean mechanistically. The apparent directional persistence in both naive and primed cells in the 'freely migrating state' could be conceivably driven by two alternative mechanisms. First, there might be an intrinsic T cell program – an internal timer driving the T cell persistence time. Alternatively, this persistence could be driven by the physical structure of the fibroblast reticular network (FRC), in case that T cell movement is constrained to it. This was investigated in detail in chapter 4.

If cells are constrained to an FRC network, and therefore the values of turning angles are imposed by this network and not driven by an intrinsic movement program, there is a possible mode of taxis that would evade this analysis. This would occur if the cells preferentially chose FRC fibres leading towards a nearby DC. Such a form of taxis might remain undetected by the presented analysis, as the values of the turning angles would be unaffected (being fixed - dictated by the network). To address this in the future, a model incorporating the bearing towards the nearest DC (angle between movement direction and straight line towards the DC) as a response variable, instead of

the absolute turning angle, could be employed to test for this type of taxis.

The analysis highlights the complexity of the system and the need to for using large datasets and rigorous statistical analyses. The Bayesian state-space models are a very suitable tool for this analysis. These models allow the analysis of T cell step lengths and turning angles simultaneously to detect different movement types, which is a conceptual improvement to analysing these two measured properties of the cell movement in isolation. The models I performed are certainly not exhaustive, and the framework could be further applied in this field. For example, taxis models where cells are moving along the FRC network could be formulated and tested using imaging structural data on the FRC network geometry. Models can also be formulated in which behavioural states of cells depend on other variables such as location within tissue, concentrations of cytokines, or the proximity to other cell types, and more than two behavioural states can easily be modelled. An inherent advantage of the Bayesian approach is that information about a certain system can easily be updated iteratively - by utilising the results of one study as prior information for a later study - which is certainly advantageous in a field where large amount of data have been collected. These models are also suitable for making predictions. This could be done for a set of models to perform so-called 'posterior predictive checks' to see which of the models generates the most realistic outcome based on comparison to the data, ideally using a feature of the data that wasn't explicitly addressed in the model. Or, these models could be used to make novel predictions or extrapolate beyond the limitations of the experimental technique used to generate the data – for example to extrapolate spatially and temporally beyond the possibilities of multi-photon *ex vivo* LN imaging. This would be useful in studying the larger-scale and longer-term aspects of the process like the transit time of a T cell through a naive versus inflamed LN, the probability of finding a specific antigen-presenting DC, and the resulting long-term immune response outcomes.

5.1.3 Chapter 4

In chapter 4, I employed mathematical models to combine measurements of T cell movement and fine-scale FRC network structure in both naive and

immunised states. Although the fibroblast reticular cell (FRC) network has been shown to influence the movement of naive T cells in LN to some degree, the exact mechanism remains unclear.

I show that differences between FRC network structure in naive state and following immunisation are minimal, contrary to what would be expected given that the LN expand in volume substantially after immunisation. Strikingly, this suggests a very substantial and rapid (within 20 h) network growth and remodelling upon immunisation, compensating for the increase in LN volume, rather than simple stretching.

I hypothesise that T cell step lengths are proportional to FRC fibre lengths and not to cell speed, as would be the case if cells followed a popular alternative model of a 'random walk with persistence (free) time'. I imaged and measured the fine-scale characteristics of FRC networks and T cell movement in both naive and immunised mice and found that this matches a model of FRC network-bound movement better than the alternative 'intrinsically-driven' movement with a persistence time. I then built the first simulation of T cell movement on directly observed FRC network structures and compared this to the alternative random walk with persistence time (RWPT) model. The results add to the accumulating indirect evidence of T cell movement on the FRC network, however, it still is not possible to make an unequivocal conclusion due to the high level of noise present in the data, even when using a relatively large set of T cell movement data. Also, unexpected discrepancies occur between both models and the real T cell movement data, which warrants future investigation.

The unexpected and significant finding that there is little change in FRC network structure in priming rules out a possible explanation for changes in T cell movement after antigen exposure as a result of changes to the network structure. This narrows down the possible explanations to other effects like chemokine gradients (which are an unlikely mechanism, as shown in Chapter 3), intrinsic changes in T cell movement behaviour and differences in T cell-DC interaction behaviour. It would also be interesting to investigate whether the fact that the FRC network structure is relatively conserved after immunisation serves a specific function – i.e. whether the constant structure is required for an efficient functioning of the organ.

In analysing the T cell movement data for the purpose of the comparison of the two alternative modes of movement, I have also shown how direct estimates of turning angle and instantaneous speed from imaging data are biased due to the discrete nature of multi-photon imaging. I investigated this bias quantitatively, demonstrated a dramatic dependence of these metrics on the imaging frequency used in imaging experiments, and presented a method to correct this bias. This bias also means that apparent T cell turning angles may differ between two cell populations solely due to their different speed, as cells moving slower will more often be captured between turns, increasing the proportion of measured zero turns. Conversely, apparent T cell speed might differ between two cell populations solely due to their different turning behaviour. For example if a cell has a bias towards returning to its previous location (low displacement rate), the estimated speed will be lower than for a cell with the same instantaneous speed and a higher displacement rate. It is therefore important in similar future studies, and when making comparisons between different studies, to account for this effect – and perhaps to estimate the characteristic step (persistence) length of T cells under different conditions, rather than compare the direct (biased) estimates of turning angle and speed.

The accurate inference of cell persistence lengths under different conditions might shed more light on both the FRC structure and other mechanisms affecting T cell migration in LN. The presented method currently does not allow the exact value of the persistence length, only persistence length ratios for different datasets. However, it might be feasible to further develop this methodology – for example, the inference of coefficient C (page 123 in the Methods section 4.3.8) would enable the calculation of persistence lengths directly, which should prove worthwhile in the future.

As the support for the FRC-bound movement over RWPT relies on the uncertain estimate of the step length ratio inferred from T cell imaging data, based on multiple measurements of the same quantity at different scanning frequencies (resulting in autocorrelation between these datapoints), and on an extrapolation using splines, it is not statistically feasible to calculate confidence intervals. To be statistically rigorous, one approach to address this would be to analyse a very large dataset and perform a bootstrap of the estimates to

generate confidence intervals. In the past, this involved a laborious and costly generation of imaging data, but with the improving practice of sharing data in published studies, it should now be possible to collect this historic data for the purpose of such a quantitative study.

5.2 Conclusions and outlook

The quantitative methods used and developed here can be employed to further investigate cell behaviour as captured by modern microscopic methods and to rigorously and reproducibly analyse cell behaviour in different contexts. This shows that it is important to use careful rigorous approaches, relatively large datasets and to account for potential confounding variables and effects. Similar conclusions have been made previously in [36], where some of the potential biasing factors and pitfalls in the interpretation of imaging data have been discussed, and I show quantitatively some of the less discussed potential sources of bias and propose practical solutions. Specifically, the analysis points out that confounding variables like cell diameter and cell density can affect the results, and – perhaps more importantly – how the apparent cell speed and turning angles can be very heavily influenced by the chosen imaging frequency, and I present methods to address these biases.

Given the intense interest in this field in the recent years, an uptake of some of the methods presented here should be relatively rapid and should prove fruitful. The state-space modelling approach is perhaps a more advanced method and is not commonly used in biomedical research, but is exceptionally suitable to address the type of problems common to this area. Most of the other methods and concepts are not novel and are relatively accessible, and should be more readily up-taken in this field.

I have, quite surprisingly, failed to detect some of the frequently claimed or proposed effects, even when using a relatively large imaging dataset. This highlights some of the complex methodological issues that must be reconciled and overcome before asserting unqualified conclusions. This is not a novel or uncommon problem, nor are the causes for this unknown, and is discussed for example in an article ”Research: increasing value, reducing waste” [68]: ”A

focus on publication of reports in journals with high impact factors and success in securing of funding leads scientists to seek short-term success instead of cautious, deliberative, robust research."

This probably leads to a general tendency to keep collecting more data and find novel variations on the applications of the experimental methods available, instead of a more careful approach and rigorous analysis of the already present, yet under-exploited, data. This is especially pronounced when it comes to new technologies like multi-photon imaging, which naturally leads to an 'applications arms race' for the primacy in the use of a particular technique in a particular field. While this is understandable, and while such pilot studies do have an important value, a more rigorous research following from these primary studies might then never even be performed, as novel technologies prompt even further perpetuation of this short-term goal-driven approach.

According to [69], 85% of all the money invested in biomedical research is wasted in an unjustified and largely avoidable manner. While the exact number is debatable, as it is impossible to infer exactly the future potential of findings that may currently seem to have little value, this analysis and the underlying overwhelming evidence of avoidable wastage of research funding are certainly worrying. This is especially so given that resources are a severely limiting factor, especially in the current atmosphere of economic austerity.

I believe that some of the of reasons for this inefficiency is directly linked to the relative scarcity of theoretical and quantitative approach. This in turn leads to flaws in the analysis and reporting of results and their irreproducibility, and to the preference for moving on to new exciting applications of experimental methods before the previous data have been appropriately analysed and fully exploited. Only so much progress can be achieved by pure observation and by correlative and comparative studies. To make fundamental advancements in our understanding of the system and our ability to make predictions based on the observations, we need to determine mechanisms and establish predictive potential, and creating rigorous mathematical and statistical models and frameworks facilitating the fitting of such models to data is essential to be able to do this.

Perhaps this tendency is unsurprising as at a certain point in any scientific

discipline, little further progress can be made without the development of an underlying quantitative theory, and this generally requires mathematics beyond the level accessible to most practitioners at that time. Hopefully, biomedical research is moving beyond this critical point and we are approaching the end of this 'stationary phase' in theoretical development in immunology. There certainly seems to be an increasing tendency to address these issues – both by revisiting the standard biomedical curriculum and the scientific publication culture and standards, and by tightening interdisciplinary collaborations. This should lead to an establishment of a well-working iterative cycle of experimental and theoretical research, leading to fundamental scientific advancements.

Chapter 6

References

[1] R. N. Germain and M. K. Jenkins. In vivo antigen presentation. *Curr Opin Immunol*, 16(1):120–125, February 2004.

[2] J. B. Huppa and M. M. Davis. T-cell-antigen recognition and the immunological synapse. *Nat Rev Immunol*, 3(12):973–983, December 2003.

[3] D. J. Campbell, C. H. Kim, and E. C. Butcher. Chemokines in the systemic organization of immunity. *Immunol Rev*, 195(1):58–71, 2003.

[4] J. Banchereau, F. Briere, C. Caux, J. Davoust, S. Lebecque, Y.-J. Liu, B. Pulendran, and K. Palucka. Immunobiology of dendritic cells. *Annu Rev Immunol*, 18(1):767–811, April 2000.

[5] D. M. Catron, A. A. Itano, K. A. Pape, D. L. Mueller, and M. K. Jenkins. Visualizing the first 50 hr of the primary immune response to a soluble antigen. *Immunity*, 21(3):341–347, September 2004.

[6] M. L. Dustin. Stop and go traffic to tune T cell responses. *Immunity*, 21(3):305–314, September 2004.

[7] G. Shakhar, R. L. Lindquist, D. Skokos, D. Dudziak, J. H. Huang, M. C. Nussenzweig, and M. L. Dustin. Stable T cell-dendritic cell interactions precede the development of both tolerance and immunity in vivo. *Nat Immunol*, 6(7):707–714, July 2005.

[8] M. Lee, J. N. Mandl, R. N. Germain, and A. J. Yates. The race for the prize: T-cell trafficking strategies for optimal surveillance. *Blood*, 120(7):1432–1438, 2012.

[9] T. Riggs, A. Walts, N. Perry, L. Bickle, J. N. Lynch, A. Myers, J. Flynn, J. J. Linderman, M. J. Miller, and D. E. Kirschner. A comparison of random vs.

chemotaxis-driven contacts of T cells with dendritic cells during repertoire scanning. *Journal of Theoretical Biology*, 250(4):732 – 751, 2008.

[10] C. L. Willard-Mack. Normal structure, function, and histology of lymph nodes. *Toxicologic Pathology*, 34(5):409–424, 2006.

[11] K. C. Panchal. Schematic of lymph node showing lymph sinuses. *https://en.wikipedia.org/wiki/File: Schematic_of_lymph_node_showing_lymph_sinuses.svg*, 2008.

[12] T. Katakai, T. Hara, J.-H. Lee, H. Gonda, M. Sugai, and A. Shimizu. A novel reticular stromal structure in lymph node cortex: an immuno-platform for interactions among dendritic cells, T cells and B cells. *International Immunology*, 16(8):1133–1142, 2004.

[13] M. J. Pittet and R. Weissleder. Intravital imaging. *Cell*, 147(5):983–991, November 2011.

[14] C. Scheinecker. Application of in vivo microscopy: evaluating the immune response in living animals. *Arthritis Res Ther*, 7(6):246–252, 2005.

[15] S. Stoll, J. Delon, T. M. Brotz, and R. N. Germain. Dynamic imaging of T cell-dendritic cell interactions in lymph nodes. *Science*, 296(5574):1873–1876, 2002.

[16] T. R. Mempel, S. E. Henrickson, and U. H. von Andrian. T-cell priming by dendritic cells in lymph nodes occurs in three distinct phases. *Nature*, 427(6970s):154–159, January 2004.

[17] M. J. Miller, S. H. Wei, I. Parker, and M. D. Cahalan. Two-photon imaging of lymphocyte motility and antigen response in intact lymph node. *Science*, 296(5574):1869–1873, June 2002.

[18] E. Ingulli, A. Mondino, A. Khoruts, and M. K. Jenkins. In vivo detection of dendritic cell antigen presentation to CD4+ T cells. *The Journal of Experimental Medicine*, 185(12):2133–2141, 1997.

[19] P. Bousso and E. Robey. Dynamics of CD8+ T cell priming by dendritic cells in intact lymph nodes. *Nat Immunol*, 4(6):579–585, June 2003.

[20] M. J. Miller, S. H. Wei, M. D. Cahalan, and I. Parker. Autonomous T cell trafficking examined in vivo with intravital two-photon microscopy. *Proceedings of the National Academy of Sciences*, 100(5):2604–2609, 2003.

[21] S. Hugues, L. Fetler, L. Bonifaz, J. Helft, F. Amblard, and S. Amigorena. Distinct T cell dynamics in lymph nodes during the induction of tolerance and immunity. *Nat Immunol*, 5(12):1235–1242, December 2004.

[22] M. J. Miller, O. Safrina, I. Parker, and M. D. Cahalan. Imaging the single cell dynamics of CD4+ T cell activation by dendritic cells in lymph nodes. *The Journal of Experimental Medicine*, 200(7):847–856, 2004.

[23] B. H. Zinselmeyer, J. Dempster, A. M. Gurney, D. Wokosin, M. Miller, H. Ho, O. R. Millington, K. M. Smith, C. M. Rush, I. Parker, M. Cahalan, J. M. Brewer, and P. Garside. In situ characterization of CD4+ T cell behavior in mucosal and systemic lymphoid tissues during the induction of oral priming and tolerance. *J Exp Med*, 201(11):1815–1823, June 2005.

[24] S. Celli, F. Lemaître, and P. Bousso. Real-time manipulation of T cell-dendritic cell interactions in vivo reveals the importance of prolonged contacts for CD4+ T cell activation. *Immunity*, 27(4):625–634, October 2007.

[25] C. M. Rush, O. R. Millington, S. Hutchison, K. Bryson, J. M. Brewer, and P. Garside. Characterization of CD4+ T-cell–dendritic cell interactions during secondary antigen exposure in tolerance and priming. *Immunology*, 128(4):463–471, 2009.

[26] O. R. Millington, V. B. Gibson, C. M. Rush, B. H. Zinselmeyer, R. S. Phillips, P. Garside, and J. M. Brewer. Malaria impairs T cell clustering and immune priming despite normal signal 1 from dendritic cells. *PLoS Pathog*, 3(10):e143–, October 2007.

[27] T. Kobezda, S. Ghassemi-Nejad, T. T. Glant, and K. Mikecz. In vivo two-photon imaging of T cell motility in joint-draining lymph nodes in a mouse model of rheumatoid arthritis. *Cellular Immunology*, 278(1–2):158 – 165, 2012.

[28] L. R. Taylor. Aggregation, variance and the mean. *Nature*, 189(4766):732–735, March 1961.

[29] L. R. Taylor and R. A. J. Taylor. Aggregation, migration and population mechanics. *Nature*, 265(5593):415–421, February 1977.

[30] J. K. Horne and D. C. Schneider. Spatial variance in ecology. *Oikos*, 74(1):pp. 18–26, 1995.

[31] T. Ushiki, O. Ohtani, and K. Abe. Scanning electron microscopic studies of reticular framework in the rat mesenteric lymph node. *The Anatomical Record*, 241(1):113–122, 1995.

[32] M. D. Gunn, S. Kyuwa, C. Tam, T. Kakiuchi, A. Matsuzawa, L. T. Williams, and H. Nakano. Mice lacking expression of secondary lymphoid organ chemokine have defects in lymphocyte homing and dendritic cell localization. *The Journal of Experimental Medicine*, 189(3):451–460, 1999.

[33] J. E. Gretz, C. C. Norbury, A. O. Anderson, A. E. Proudfoot, and S. Shaw. Lymph-borne chemokines and other low molecular weight molecules reach high endothelial venules via specialized conduits while a functional barrier limits access to the lymphocyte microenvironments in lymph node cortex. *The Journal of Experimental Medicine*, 192(10):1425–1440, 2000.

[34] S. A. Luther, H. L. Tang, P. L. Hyman, A. G. Farr, and J. G. Cyster. Coexpression of the chemokines ELC and SLC by T zone stromal cells and deletion of the ELC gene in the plt/plt mouse. *Proceedings of the National Academy of Sciences*, 97(23):12694–12699, 2000.

[35] M. Bajénoff, J. G. Egen, L. Y. Koo, J. Laugier, F. Brau, N. Glaichenhaus, and R. N. Germain. Stromal cell networks regulate lymphocyte entry,

migration, and territoriality in lymph nodes. *Immunity*, 25(6):989 – 1001, 2006.

[36] J. Textor, A. Peixoto, S. E. Henrickson, M. Sinn, U. H. von Andrian, and J. Westermann. Defining the quantitative limits of intravital two-photon lymphocyte tracking. *Proceedings of the National Academy of Sciences*, 108(30):12401–12406, 2011.

[37] J. B. Beltman, A. F. Marée, J. N. Lynch, M. J. Miller, and R. J. de Boer. Lymph node topology dictates T cell migration behavior. *The Journal of Experimental Medicine*, 204(4):771–780, 2007.

[38] V. Baldazzi, P. Paci, M. Bernaschi, and F. Castiglione. Modeling lymphocyte homing and encounters in lymph nodes. *BMC Bioinformatics*, 10(1):387, 2009.

[39] C. Beauchemin, N. M. Dixit, and A. S. Perelson. Characterizing T cell movement within lymph nodes in the absence of antigen. *The Journal of Immunology*, 178(9):5505–5512, 2007.

[40] F. Castellino, A. Y. Huang, G. Altan-Bonnet, S. Stoll, C. Scheinecker, and R. N. Germain. Chemokines enhance immunity by guiding naive CD8+ T cells to sites of CD4+ T cell-dendritic cell interaction. *Nature*, 440(7086):890–895, April 2006.

[41] T. H. Harris, E. J. Banigan, D. A. Christian, C. Konradt, E. D. T. Wojno, K. Norose, E. H. Wilson, B. John, W. Weninger, A. D. Luster, A. J. Liu, and C. A. Hunter. Generalized Lévy walks and the role of chemokines in migration of effector CD8+ T cells. *Nature*, 486(7404):545–548, June 2012.

[42] G. H. Pyke. Understanding movements of organisms: it's time to abandon the Lévy foraging hypothesis. *Methods in Ecology and Evolution*, 6(1):1–16, 2015.

[43] A. M. Edwards, R. A. Phillips, N. W. Watkins, M. P. Freeman, E. J. Murphy, V. Afanasyev, S. V. Buldyrev, M. G. E. da Luz, E. P. Raposo, H. E. Stanley, and G. M. Viswanathan. Revisiting Lévy flight search patterns of

wandering albatrosses, bumblebees and deer. *Nature*, 449(7165):1044–1048, October 2007.

[44] E. J. Banigan, T. H. Harris, D. A. Christian, C. A. Hunter, and A. J. Liu. Heterogeneous CD8+ T cell migration in the lymph node in the absence of inflammation revealed by quantitative migration analysis. *PLoS Comput Biol*, 11(2):e1004058, 02 2015.

[45] T. A. Patterson, L. Thomas, C. Wilcox, O. Ovaskainen, and J. Matthiopoulos. State-space models of individual animal movement. *Trends Ecol Evol*, 23(2):87–94, February 2008.

[46] J. M. Morales, D. T. Haydon, J. Frair, K. E. Holsinger, and J. M. Fryxell. Extracting more out of relocation data: building movement models as mixtures of random walks. *Ecology*, 85(9):2436–2445, September 2004.

[47] B. T. McClintock, R. King, L. Thomas, J. Matthiopoulos, B. J. McConnell, and J. M. Morales. A general discrete-time modeling framework for animal movement using multistate random walks. *Ecological Monographs*, 82(3):335–349, April 2012.

[48] I. L. Grigorova, M. Panteleev, and J. G. Cyster. Lymph node cortical sinus organization and relationship to lymphocyte egress dynamics and antigen exposure. *Proceedings of the National Academy of Sciences of the United States of America*, 107(47):20447–20452, November 2010.

[49] J. B. Beltman, A. F. M. Maree, and R. J. de Boer. Analysing immune cell migration. *Nat Rev Immunol*, 9(11):789–798, November 2009.

[50] S. J. Turley, A. L. Fletcher, and K. G. Elpek. The stromal and haematopoietic antigen-presenting cells that reside in secondary lymphoid organs. *Nat Rev Immunol*, 10(12):813–825, December 2010.

[51] M. Sixt, N. Kanazawa, M. Selg, T. Samson, G. Roos, D. P. Reinhardt, R. Pabst, M. B. Lutz, and L. Sorokin. The conduit system transports soluble antigens from the afferent lymph to resident dendritic cells in the T cell area of the lymph node. *Immunity*, 22(1):19 – 29, 2005.

[52] A. Link, T. K. Vogt, S. Favre, M. R. Britschgi, H. Acha-Orbea, B. Hinz, J. G. Cyster, and S. A. Luther. Fibroblastic reticular cells in lymph nodes regulate the homeostasis of naive T cells. *Nat Immunol*, 8(11):1255–1265, November 2007.

[53] S. Chyou, F. Benahmed, J. Chen, V. Kumar, S. Tian, M. Lipp, and T. T. Lu. Coordinated regulation of lymph node vascular–stromal growth first by CD11c+ cells and then by T and B cells. *The Journal of Immunology*, 187(11):5558–5567, 2011.

[54] K. A. Soderberg, G. W. Payne, A. Sato, R. Medzhitov, S. S. Segal, and A. Iwasaki. Innate control of adaptive immunity via remodeling of lymph node feed arteriole. *Proceedings of the National Academy of Sciences of the United States of America*, 102(45):16315–16320, 2005.

[55] C.-Y. Yang, T. K. Vogt, S. Favre, L. Scarpellino, H.-Y. Huang, F. Tacchini-Cottier, and S. A. Luther. Trapping of naive lymphocytes triggers rapid growth and remodeling of the fibroblast network in reactive murine lymph nodes. *Proceedings of the National Academy of Sciences*, 111(1):E109–E118, 2014.

[56] S. E. Acton, A. J. Farrugia, J. L. Astarita, D. Mourao-Sa, R. P. Jenkins, E. Nye, S. Hooper, J. van Blijswijk, N. C. Rogers, K. J. Snelgrove, I. Rosewell, L. F. Moita, G. Stamp, S. J. Turley, E. Sahai, and C. Reis e Sousa. Dendritic cells control fibroblastic reticular network tension and lymph node expansion. *Nature*, 514(7523):498–502, October 2014.

[57] T. Katakai, T. Hara, M. Sugai, H. Gonda, and A. Shimizu. Lymph node fibroblastic reticular cells construct the stromal reticulum via contact with lymphocytes. *The Journal of Experimental Medicine*, 200(6):783–795, September 2004.

[58] S. P. Preston, S. L. Waters, O. E. Jensen, P. R. Heaton, and D. I. Pritchard. T-cell motility in the early stages of the immune response modeled as a random walk amongst targets. *Phys. Rev. E*, 74:011910, Jul 2006.

[59] G. Bogle and P. R. Dunbar. Simulating T-cell motility in the lymph node paracortex with a packed lattice geometry. *Immunol Cell Biol*, 86(8):676–687, August 2008.

[60] G. M. Donovan and G. Lythe. T-cell movement on the reticular network. *Journal of Theoretical Biology*, 295(0):59 – 67, 2012.

[61] R. Pankov, Y. Endo, S. Even-Ram, M. Araki, K. Clark, E. Cukierman, K. Matsumoto, and K. M. Yamada. A Rac switch regulates random versus directionally persistent cell migration. *The Journal of Cell Biology*, 170(5):793–802, 2005.

[62] E. Van Vliet, M. Melis, J. M. Foidart, and W. Van Ewijk. Reticular fibroblasts in peripheral lymphoid organs identified by a monoclonal antibody. *Journal of Histochemistry & Cytochemistry*, 34(7):883–90, 1986.

[63] A. J. Baddeley, R. A. Moyeed, C. V. Howard, and A. Boyde. Analysis of a three-dimensional point pattern with replication. *Journal of the Royal Statistical Society. Series C (Applied Statistics)*, 42(4):pp. 641–668, 1993.

[64] F. Graw and R. R. Regoes. Influence of the fibroblastic reticular network on cell-cell interactions in lymphoid organs. *PLoS Comput Biol*, 8(3):e1002436, 03 2012.

[65] J. D. Estes, A. T. Haase, and T. W. Schacker. The role of collagen deposition in depleting CD4+ T cells and limiting reconstitution in HIV-1 and {SIV} infections through damage to the secondary lymphoid organ niche. *Seminars in Immunology*, 20(3):181 – 186, 2008.

[66] M. Zeng, A. J. Smith, S. W. Wietgrefe, P. J. Southern, T. W. Schacker, C. S. Reilly, J. D. Estes, G. F. Burton, G. Silvestri, J. D. Lifson, J. V. Carlis, and A. T. Haase. Cumulative mechanisms of lymphoid tissue fibrosis and T cell depletion in HIV-1 and SIV infections. *The Journal of Clinical Investigation*, 121(3):998–1008, 3 2011.

[67] S. N. Mueller, M. Matloubian, D. M. Clemens, A. H. Sharpe, G. J. Freeman, S. Gangappa, C. P. Larsen, and R. Ahmed. Viral targeting of

fibroblastic reticular cells contributes to immunosuppression and persistence during chronic infection. *Proceedings of the National Academy of Sciences*, 104(39):15430–15435, 2007.

[68] M. R. Macleod, S. Michie, I. Roberts, U. Dirnagl, I. Chalmers, J. P. A. Ioannidis, R. A.-S. Salman, A.-W. Chan, and P. Glasziou. Biomedical research: increasing value, reducing waste. *The Lancet*, 383(9912):101–104, 2014.

[69] I. Chalmers and P. Glasziou. Avoidable waste in the production and reporting of research evidence. *The Lancet*, 374(9683):86–89, 2009.